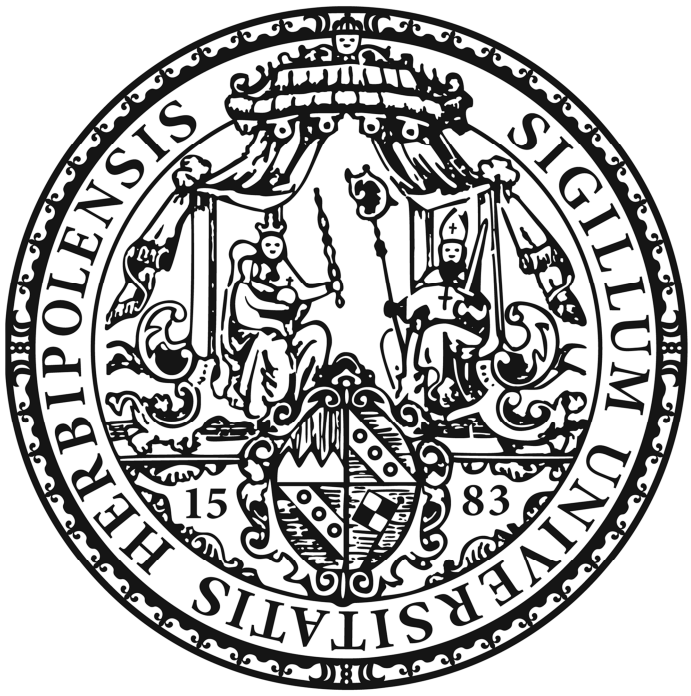

The Vessel Wall and Beyond: Characterization of Myeloid Progenitors in the Adult Mouse Brain

Die Gefäßwand und darüber hinaus:
Charakterisierung myeloider Vorläufer im adulten Mäusehirn

Doctoral thesis for a doctoral degree
at the Graduate School of Life Sciences,
Julius-Maximilian University Würzburg,
Section Neuroscience

submitted by

Tobias Königer

from

Würzburg

Würzburg, April 2019

Submitted on: ……..……..

Office stamp

Members of the *Promotionskomitee*:

Chairperson: Prof. Dr. med. Manfred Gessler

Primary Supervisor: Prof. Dr. med. Stefanie Kürten

Supervisor (Second): Prof. Dr. rer. nat. Rudolf Martini

Supervisor (Third): Prof. Dr. med. Paul V. Lehmann

Date of Public Defence: ……..……

Date of Receipt of Certificates: …….

List of Abbreviations

AGM	Aorta-Gonad-Mesonephros
AMPC	Adventitial macrophage progenitor cell
APC	Allophycocyanin
BBB	Blood-brain barrier
BFU-E	Burst-forming unit-erythroid
BM	Bone marrow
BrdU	5-bromo-2'-deoxyuridine
CCR2	C-C chemokine receptor type 2
CD	Cluster of differentiation
CFU	Colony-forming unit
CFU-C	Colony-forming unit-culture
CFU-G	Colony-forming unit-granulocyte
CFU-GM	Colony-forming unit-granulocyte/macrophage
CFU-M	Colony-forming unit-macrophage
CFU-Mk	Colony-forming unit-megakaryocyte
CFU-S	Colony-forming unit-spleen
CLP	Common lymphoid progenitor
CMP	Common myeloid progenitor
CNS	Central nervous system
CSF	Colony-stimulating factor
CSF-1	Colony-stimulating factor-1
CSF-1R	Colony-stimulating factor-1 receptor
CW	Circle of Willis
CWFA	Circle of Willis fragment assay
Cx3xr1	C-X-3-C motif chemokine receptor type 1
EHT	Endothelial-to-hematopoietic transition
EMP	Erythro-myeloid progenitor
FLK-1	Fetal liver kinase-1
FLT3	Fms-like tyrosine kinase 3
FOV	Field of view
FSC	Forward scatter
GFP	Green fluorescent protein
GM-CSF	Granulocyte-macrophage colony-stimulating factor
GMP	Granulocyte/macrophage progenitor
HSC	Hematopoietic stem cell
HSPCs	Hematopoietic stem and progenitor cells
IBA1	Ionized calcium-binding adapter molecule 1
IF	Immunofluorescence staining
IHC-fr	Immunohistochemistry with frozen sections
IHC-P	Immunohistochemistry with paraffin sections
IL-3	Interleukin-3
IL-34	Interleukin-34
IV-CD45$^+$	Stained by intravenous anti-CD45 antibody
LIN	Lineage marker
LT-HSC	Long-term HSC
MDP	Macrophage/dendritic cell progenitor
MEP	Megakaryocyte/erythrocyte progenitor
MPP	Multipotent progenitor
MSC	Mesenchymal stem cell
MyP	Myeloid progenitor
NSC	Neural stem cell
PB	Peripheral blood
P-Sp	Para-aortic splanchnopleura
SCA-1	Stem cell antigen-1
SCF	Stem cell factor
SD	Standard deviation
SP	Side population
SSC	Side scatter
ST-HSC	Short-term HSC
TAM	Tamoxifen
Tmem119	Transmembrane protein 119
TPO	Thrombopoietin
VEGF	Vascular endothelial growth factor
VW-P	Vascular wall progenitor
WBC	White blood cell
YFP	Yellow fluorescent protein
YS	Yolk sac

Abstract

After almost two decades of extensive research, some controversy has remained regarding the self-renewal of resident macrophages of the central nervous system (CNS). Concurrently, the vessel wall has emerged as a potentially ubiquitous niche for stem and progenitor cells, including committed macrophage precursors. It is conceivable that their occurrence in the CNS might explain the brain-resident hematopoietic potential, which has repeatedly been observed but not yet characterized in detail. In this work, the presence of hematopoietic progenitors inside and outside the vessel wall was studied in the adult mouse brain, as well as their possible contribution to the resident macrophage pool.

An immunohistological analysis did not corroborate $CD45^+$ $SCA\text{-}1^+$ macrophage progenitors, which have been characterized in peripheral arteries, in the circle of Willis. Accordingly, the *ex vivo* culture of CNS vessels did not provide evidence for *de novo* formation of macrophages, but for the extensive proliferative capacity of mature cells. However, when analyzing whole brain suspensions in colony-forming unit (CFU) assays, rare *Iba1*$^-$ *Cx3cr1*$^-$ (immature) clonogenic cells were detected, which were enriched at the cerebral surface/meninges and differentiated into macrophages in culture. Intravenous antibody injection and cell sorting confirmed their residence behind the blood-brain barrier. Intriguingly, brain-derived CFUs produced a unique pattern of colony types compared to cells from bone marrow (BM) or blood. Still they displayed the same immunophenotype as BM-resident myeloid progenitors ($CD45^{lo}$, LIN^-, $SCA\text{-}1^-$, $IL7R\alpha^-$, $c\text{-}KIT^+$) and could be further stratified into a progenitor hierarchy giving rise to all erythro-myeloid cell types *in vitro*. This similarity was substantiated by labeling of their progeny in *Flt3*^{Cre} x *Rosa26*$^{mT/mG}$ mice, which indicated a descendance from hematopoietic stem cells. While forced repopulation of brain macrophages using the CSF-1R inhibitor PLX5622 did not point to a role of progenitors in *in vivo* microglia/macrophage maintenance, recent advances in hematology imply that they might be involved in CNS immunosurveillance.

In conclusion, though there was no evidence for adventitial macrophage precursors in the CNS, this study confirms the presence of myeloid progenitors in the adult brain and provides the anatomical and phenotypical details necessary to elucidate their relevance in neuroinflammation.

Zusammenfassung

Nach fast zwei Jahrzehnten intensiver Forschung wird der Selbsterhalt residenter Makrophagen im zentralen Nervensystem (ZNS) immer noch kontrovers diskutiert. Gleichzeitig hat sich die Gefäßwand als eine potentiell ubiquitäre Nische für Stamm- und Vorläuferzellen herausgestellt, einschließlich determinierter Vorläufer für Makrophagen. Dass diese auch im ZNS vorhanden sind, könnte die wiederholten Berichte über hämatopoetisches Potenzial im Gehirn erklären, welches bisher nicht genau charakterisiert wurde. In der vorliegenden Arbeit wurde daher die Existenz hämatopoetischer Vorläuferzellen sowohl innerhalb als auch außerhalb der Gefäßwände des Gehirns erwachsener Mäuse untersucht. Weiterhin wurde deren Beitrag zu residenten Makrophagen-Populationen überprüft.

Eine immunhistologische Analyse konnte $CD45^+$ $SCA\text{-}1^+$ Makrophagen-Vorläufer, wie sie in peripheren Arterien beschrieben wurden, im *Circulus arteriosus Willisii* nicht bestätigen. Entsprechend lieferte die Kultur von ZNS-Gefäßen keine Hinweise auf eine Neubildung von Makrophagen, zeigte aber ein hohes Teilungsvermögen reifer Zellen auf. Allerdings wurden in *colony-forming unit assays* mit Hirnzellsuspensionen seltene *Iba1*$^-$ *Cx3cr1*$^-$ (unreife) klonogene Zellen detektiert, die im Bereich der Hirnhaut angereichert waren und in Kultur zu Makrophagen differenzierten. Eine intravenöse Antikörperinjektion und Zellsortierung belegten, dass sie sich hinter der Blut-Hirn-Schranke befanden. Klonogene Zellen des Hirns erzeugten ein eigentümliches Muster an Kolonietypen, welches sich von dem des Knochenmarks und des Blutes unterschied. Trotzdem glichen sie in ihrem Immunphänotyp myeloiden Vorläuferzellen des Knochenmarks ($CD45^{lo}$, LIN^-, $SCA\text{-}1^-$, $IL7R\alpha^-$, $c\text{-}KIT^+$) und konnten weiter in eine Hierarchie von Vorläufern aufgespalten werden, die *in vitro* alle erythro-myeloiden Zelltypen hervorbrachte. Diese Ähnlichkeit wurde dadurch unterstrichen, dass ihre Nachkommen in *Flt3*^{Cre} x *Rosa26*$^{mT/mG}$ Mäusen markiert wurden, was eine Abstammung von hämatopoetischen Stammzellen anzeigte. Während die induzierte Repopulation von Hirn-Makrophagen mit Hilfe des CSF-1R Inhibitors PLX5622 keine Vorläuferbeteiligung beim Erhalt von Mikroglia/Makrophagen *in vivo* vermuten ließ, deuten neue Erkenntnisse im Bereich der Hämatologie darauf hin, dass die beschriebenen Vorläufer in die immunologische Überwachung des ZNS involviert sein könnten.

Wenngleich keine Anhaltspunkte für adventitielle Makrophagen-Vorläufer im ZNS gefunden wurden, bestätigt diese Arbeit die Existenz myeloider Vorläufer im adulten Hirn und liefert notwendige anatomische und phänotypische Informationen, um deren Bedeutung im Rahmen entzündlicher Prozesse des ZNS aufzuklären.

Table of Contents

1 Introduction

1.1 Hematopoiesis

1.1.1 Adult hematopoiesis: stem cells, progenitors, and their niches

Hematopoiesis describes the formation of blood cellular components, including leukocytes, erythrocytes and platelets. As most blood cells have a limited lifespan, they must be constantly replaced in the adult organism.[1]

Hematopoietic stem cells (HSCs) are considered the base of adult hematopoiesis. HSCs are rare cells that mostly exist in a quiescent state. They have the exclusive ability to self-renew and give rise to a hierarchy of increasingly commited progenitors via asymmetric cell division, which eventually differentiate into all mature blood cell types (Fig. 1). Experimentally, HSCs are defined by their robust long-term and multi-lineage hematopoietic repopulating potential, meaning that a single cell is able to permanently regenerate the entire blood system after serial transplantation into myeloablated hosts.[1]

Progenitors, on the other hand, have lost this ability. They display a limited lifespan and become more and more lineage-restricted as they differentiate towards mature cells. Their hallmark is the ability for rapid and extensive proliferation. That way, progenitors amplify the rare divisions of HSCs in order to satisfy the high demand for mature cells. In specific culture assays, progenitors can therefore be identified by their capacity to produce a large number of differentiated progeny within short periods of time.[1]

Terminally differentiated cells eventually carry out specific functions in the organism. They usually divide no further and often die after several days or weeks. Given the limited lifespan of progenitors and mature cells, both compartments ultimately depend on constant replenishment by stem cells[1]. However, even though most hematopoietic cells in the adult organism descent from

HSCs, there are some exceptions, such as certain tissue macrophages or B-1 cells, which originate from different sources already during the embryonal/fetal period[2].

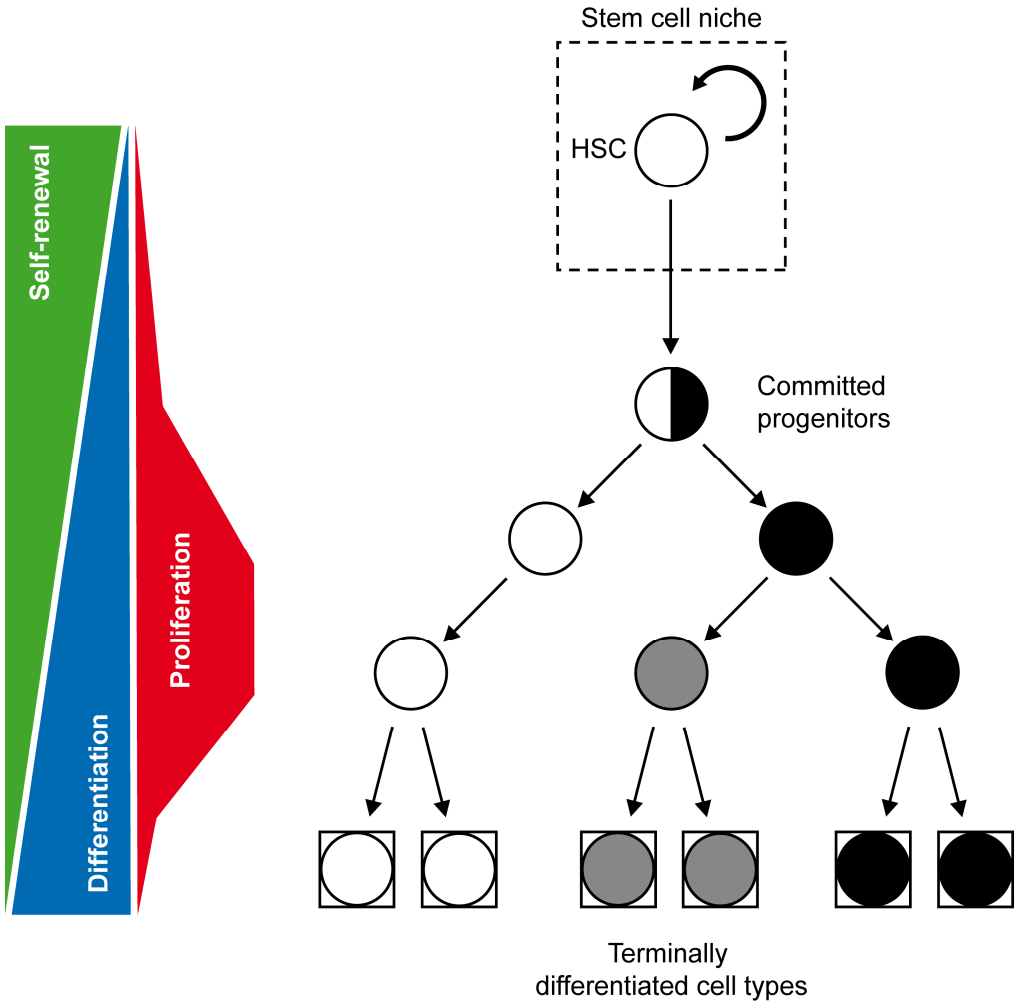

Figure 1 | The hierarchical organization of adult hematopoiesis. HSCs that reside in the stem cell niche mature in a stepwise process via various committed progenitor stages towards terminally differentiated blood cell types, while gradually losing the capacity for self-renewal. The rare cell divisions of HSCs are amplified via extensive proliferation of the progenitor compartment. Terminally differentiated cells mostly lose the ability to enter the cell cycle.

The main site of adult hematopoiesis is the bone marrow (BM), which is densely populated by a mixture of developing blood cells and their precursors, supported by stromal cells and the extracellular matrix they produce. Newly generated cells are discharged into abundant fenestrated sinusoidal blood vessels[1]. Most HSCs reside adjacent to these sinuses in a special micro-environment called "the stem cell niche", which extrinsically orchestrates their fate including quiescence, proliferation, and differentiation[3–5]. It is composed of a collection of secreted and cell-bound molecules provided by stromal cells (e.g. endothelial cells, macrophages, osteoclasts, fibroblasts, and neurons), as well as a specific physicochemical environment[1,3,4].

Hematopoiesis is a flexible process that reacts to disturbances such as infections or hypoxia due to blood-loss or high altitude exposure with the selective increase of appropriate blood cell types[1]. The emerging concept of "trained immunity" has brought even more depth into this regulation, as it has been shown that hematopoiesis does not only adpat the composition of cells that it produces after a pathological stimulus, but also differently equips innate immune cell progeny via epigenetic configuration to become more potent effectors[6,7].

1.1.2 The hematopoietic tree: focus on myeloid progenitors and their identification

In the classical model of hematopoiesis, blood cell production follows a unidirectional program of gradual lineage restriction via multiple discrete progenitor steps, which is reminiscent of a hierarchical family tree (Fig. 2). Multipotent HSCs are the origin of this tree and sustain hematopoiesis. They can be separated into perpetually self-renewing long-term HSCs (LT-HSC) and short-term HSCs (ST-HSC), which only reconstitute the hematopoietic system for several weeks upon transplantation before they end their productive lifespan. ST-HSCs subsequently differentiate into multipotent progenitors (MPP). These can still produce all blood cell lineages, but their self-renewal potential is short and difficult to detect under transplant conditions[8].

Following the loss of self-renewal, multipotency is abandoned during an important fate decision, which takes place at the level of MPPs. The latter can enter one of two main branches: the lymphoid differentiation pathway, eventually giving rise to e.g. T cells, B cells, and natural killer cells, or the erythro-myeloid pathway, which produces erythrocytes, megakaryocytes/ platelets, granulocytes, monocytes/macrophages, and dendritic cells[1,2]. Lineage choice is expressed by MPP conversion into either the common lymphoid progenitor (CLP)[9] or the common myeloid progenitor (CMP)[10]. There is a strong differentiation bias towards the myeloid lineage. For every CLP generated, about 180 CMPs are produced in mice[11]. This is consistent with many short-lived myeloid cell types in contrast to the long-lived lymphocytes, which may even show hallmarks of self-renewal[12,13].

During myeloid differentiation, oligopotent CMPs, which can still adopt a few different fates, are gradually restricted towards unipotent progenitors, eventually maturing into only a single, terminally differentiated cell type. Throughout this process, fate decisions are influenced by growth factors[14], often termed “colony-stimulating factors” (CSF), as many of these molecules

have been discovered in clonogenic culture assays. In these assays, a progenitor-containing cell preparation is cultured within a semisolid matrix in the presence of various growth factors that stimulate progenitor survival, proliferation, and differentiation[1]. As the matrix inhibits cell migration, the progeny of every progenitor clusters together as a distinguishable colony, which may consist of one or multiple cell types, depending on the potential of the original colony-initiating cell[1]. By sorting whole BM cells into different fractions and analyzing their corresponding colony-forming potential, many different myeloid progenitor (MyP) stages have been elucidated in conjunction with their surface phenotype (also summarized in Fig. 2). Among them are further oligo- or bipotent progenitors beneath CMPs, such as the granulocyte/ macrophage progenitor (GMP)[10], the macrophage/dendritic cell progenitor (MDP)[15], and the megakaryocyte/erythrocyte progenitor (MEP)[10].

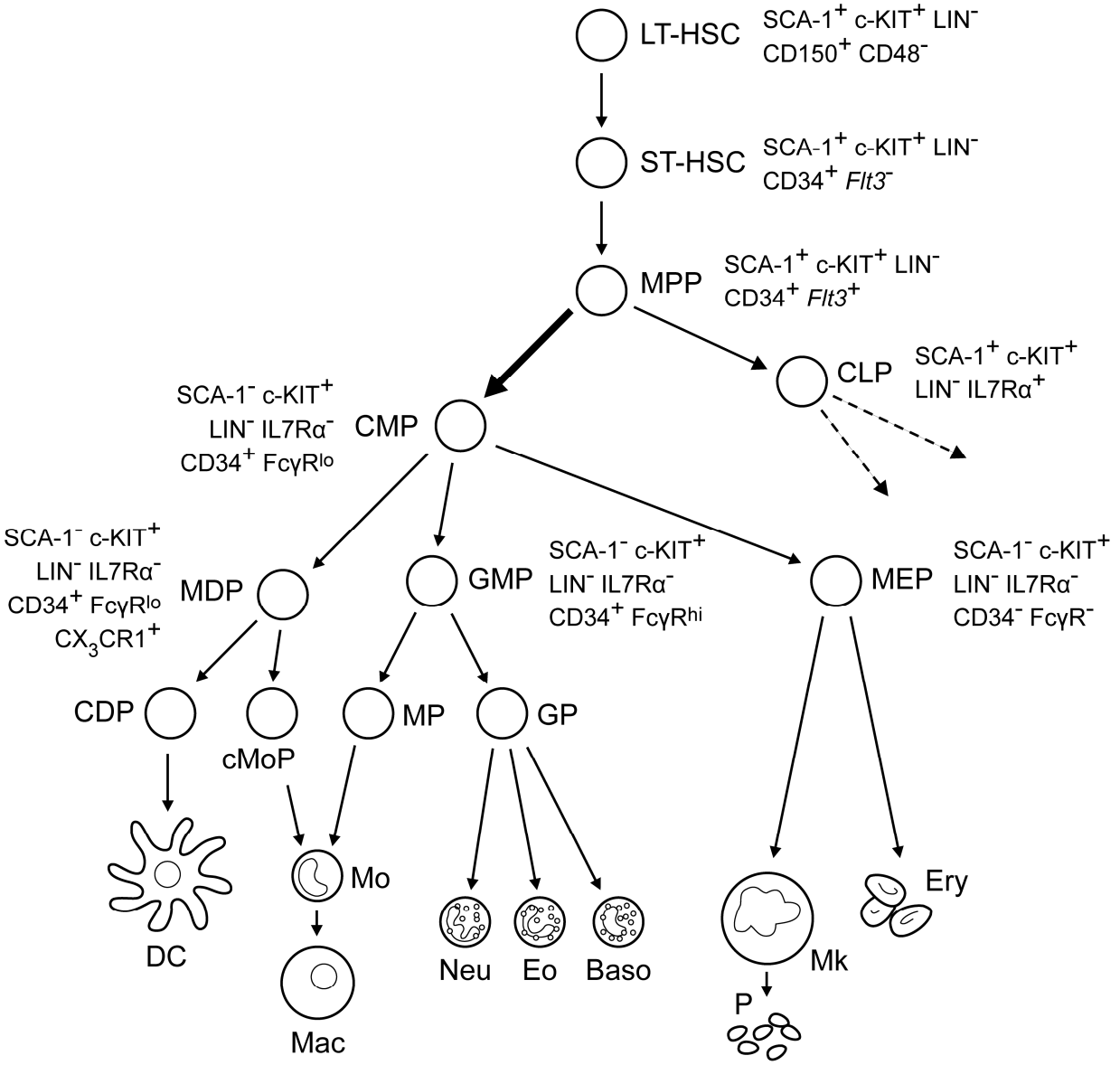

Figure 2 | Overview of adult mouse myelopoiesis (simplified). Stem cell-derived MPPs differentiate into CMPs, which become further restricted while passing through multiple progenitor stages, eventually giving rise to all erythro-myeloid cell types. Selected progenitor phenotypes are shown[15–17]. LT-HSC: long-term hematopoietic stem cell; ST-HSC: short-term hematopoietic stem cell; MPP: multipotent progenitor; CMP: common myeloid progenitor; CLP: common lymphoid progenitor; MDP: macrophage/dendritic cell progenitor; GMP: granulocyte/macrophage progenitor; MEP: megakaryocyte/ erythrocyte progenitor; CDP: common dendritic cell progenitor; cMoP: common monocyte progenitor; MP: monocyte progenitor; GP: granulocyte progenitor; DC: dendritic cell; Mo: monocyte; Mac: macrophage; Neu: neutrophil; Eo: eosinophil; Baso: basophil; Mk: megakaryocyte; P: platelet; Ery: erythrocyte.

1.1.3 The development of hematopoiesis

Hematopoietic development in the vertebrate embryo follows a wave-like pattern (Fig. 3). These waves are partly overlapping and occur at different sites. While early, unipotent progenitors produce a small set of unique cell types to carry out specific developmental functions, sequential waves give rise to an increasingly diverse and heterogeneous hematopoietic system, eventually culminating in the emergence of mature HSCs[2].

The first embryonic wave is called the primitive wave[2]. In mice, this wave starts around day 7.5 post gestation (also called "embryonic day 7.5", abbreviated: E7.5) in the posterior plate mesoderm of the extra-embryonic yolk sac (YS). Here, hemogenic angioblasts differentiate into clusters of hematopoietic cells within the so called "blood islands" until the YS vasculature is formed[2,18]. The primitive wave generates erythrocytes, macrophages, and megakaryocytes, which are unique compared to their distinctive successors[19,20]. For instance, primitive erythrocytes first emerge as a nucleated form, which enucleates in the circulation between E12.5 and E16.5. Moreover, their hemoglobin has a higher affinity to oxygen than the one expressed by late fetal and adult red blood cells[18]. Primitive megakaryocytes, on the other hand, are diploid in contrast to their polyploid counterparts in the adult BM. They also release platelets that are larger in size[19]. Finally, primitive macrophages have been shown to bypass the monocyte stage and directly emerge from YS precursors[21].

The second embryonic wave is called the pre-definitive or transient definitive wave[2,22]. It starts at E8.5, when erythro-myeloid progenitors (EMP) emerge from hemogenic endothelium in the YS, embryo proper, and allantois via endothelial-to-hematopoietic transition (EHT)[2,20,23]. Next to EMPs, also early lymphocytic progenitors develop around this time point[24]. Importantly, pre-definitive B cell progenitors preferentially differentiate into B-1 cells[25], which are long-lived and persist into adulthood[2]. Likewise, recent lineage tracing approaches have shown that EMPs are the origin of long-lived tissue macrophages[26–28]. Once the blood circulation is established, from E8.5 onward, EMPs migrate into the fetal liver, where they expand and transiently produce definitive erythro-myeloid cell types until at least E16.5[22,27–29].

Almost concomitant with the development of EMPs, the foundation for definitive hematopoiesis is laid at E8.5 with the emergence of HSCs from intraembryonic hemogenic endothelium[30–32]. The definitive wave begins with the generation of immature HSCs in the para-aortic splanchnopleura (P-Sp) region and proceeds to give rise to fetal HSCs in the aorta, gonads, and mesonephros (AGM) regions at E10.5 (which themselves arise from the P-Sp)[22,33,34]. Just like EMPs, HSCs are generated via EHT, which is induced in response to shear stress from circulating blood and depends on the development of a beating heart[35,36]. In addition to the AGM regions, HSC activity has been detected in other embryonic sites, such as the vitelline/umbilical arteries, embryonic head, placenta, and YS[2]. Subsequently, fetal HSCs join EMPs in the fetal liver, which remains the major hematopoietic organ until right before birth[37]. Circulating HSCs then gradually seed the fetal spleen and BM, the latter being the site of permanent adult hematopoiesis[38].

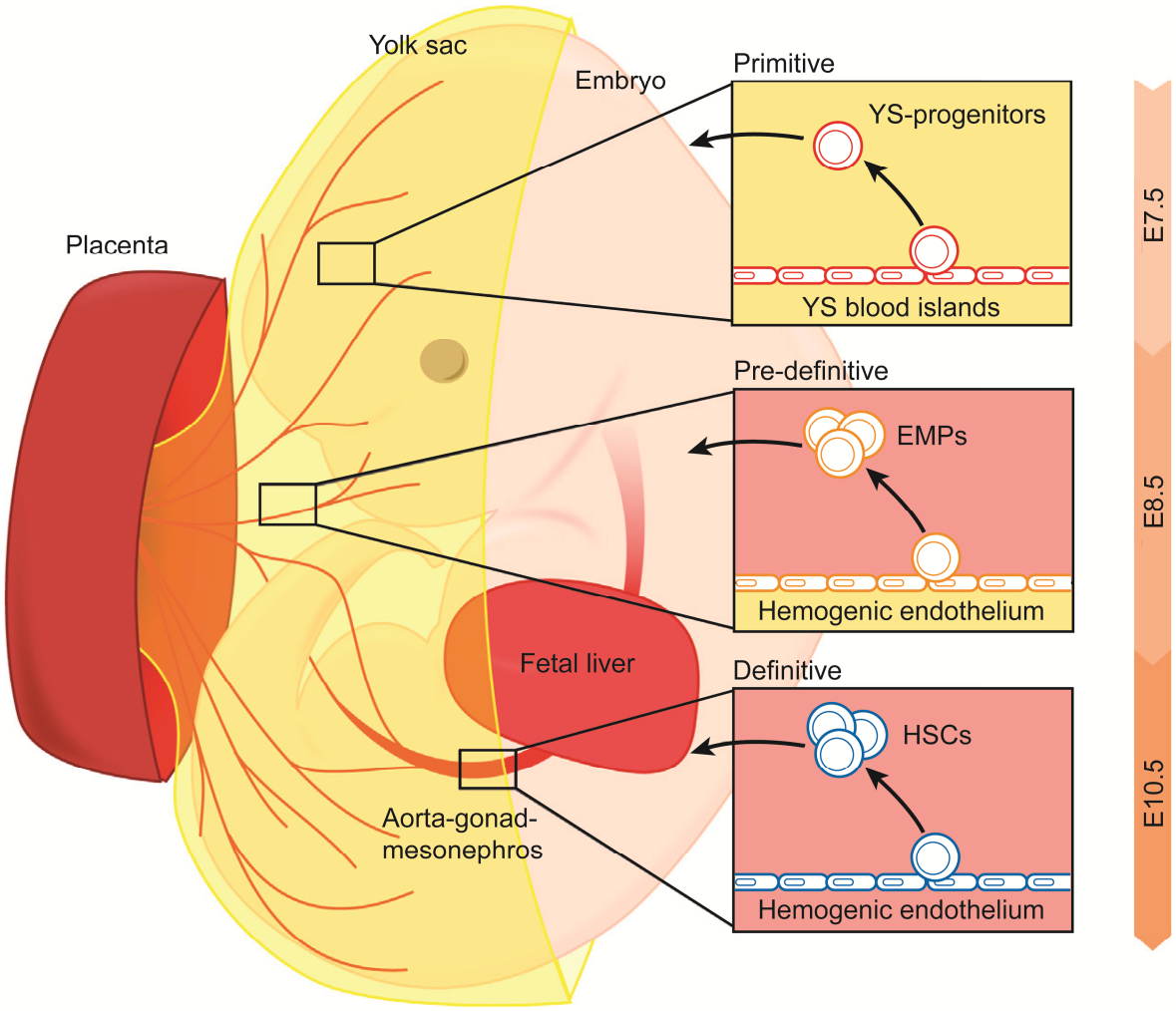

Figure 3 | The development of hematopoiesis in mice. Primitive hematopoiesis starts at E7.5, when first hematopoietic cells arise in the blood islands of the extraembryonic yolk sac from hemogenic angioblasts. At E8.5, hemogenic endothelium (e.g. in the YS) produces early lymphocytic progenitors and erythro-myeloid progenitors (EMP) of the pre-definitive wave, which colonize the fetal liver as soon as blood circulation is initiated. Almost concomitantly, definitive hematopoiesis begins with the generation of immature HSCs from hemogenic endothelium in the P-Sp, which develops into the AGM regions. Here, fetal HSCs arise at E10.5 and later also colonize the fetal liver. The latter remains the main hematopoietic organ until shortly before birth, while HSCs are gradually seeding the BM, which is the site of permanent adult hematopoiesis. (Figure modified from Ginhoux and Guilliams, 2016[22].)

1.1.4 Hematopoietic stem and progenitor cell trafficking

Hematopoietic stem and progenitor cells (HSPCs) do not only change their location during development, but remain migratory in the adult organism. While most HSPCs are retained inside the BM via CXCL12/CXCR4-signaling[39], a small number of stem and progenitor cells circulates within the blood at any time[40]. The latter constantly re-engraft the BM, while being replenished by HSPCs that are newly mobilized[41–43]. The extent of HSPC mobilization follows a circadian rhythm, with maximal release during the resting period[44–46], contracyclically to serum cortisol levels[45,47]. Moreover, the number of circulating progenitors strongly increases in response to stress[48], inflammation, and damage to distant organs such as ischemic stroke[49] or myocardial infarction[50,51]. Apart from peripheral blood, HSPCs can be recovered from multiple solid tissues under physiological conditions such as the spleen[52], liver[53], muscle[54], lungs[55], intestine[55,56], kidneys[55], thymus[57], and aorta[58,59]. It has been shown that BM-derived HSPCs enter these organs from the blood and leave again via the draining lymphatics, eventually returning to the blood through the thoracic duct[41] (Fig. 4). Once in the circulation, HSPCs can either re-engraft the BM or repeat the peripheral migration cycle, which is guided by sphingosine-1-phosphate (S1P) gradients[41,60–62].

HSPCs accumulate at sites of tissue injury[49,63–65]. This is achieved both actively by C-C chemokine receptor type 2 (CCR2)-mediated chemotaxis[66], as well as passively via down-regulation of S1P receptor 1 (S1P1), resulting in prolonged retention of routinely migrating progenitors in the injured tissue[41]. Accordingly, HSPCs have been shown to participate in immune responses and tissue repair. They are able to sense pathogens through pattern recognition receptors[67–69] and react to inflammatory stimuli with proliferation[41,70,71], differentiation into myeloid cells[41,67], as well as extensive secretion of chemokines and cytokines[72].

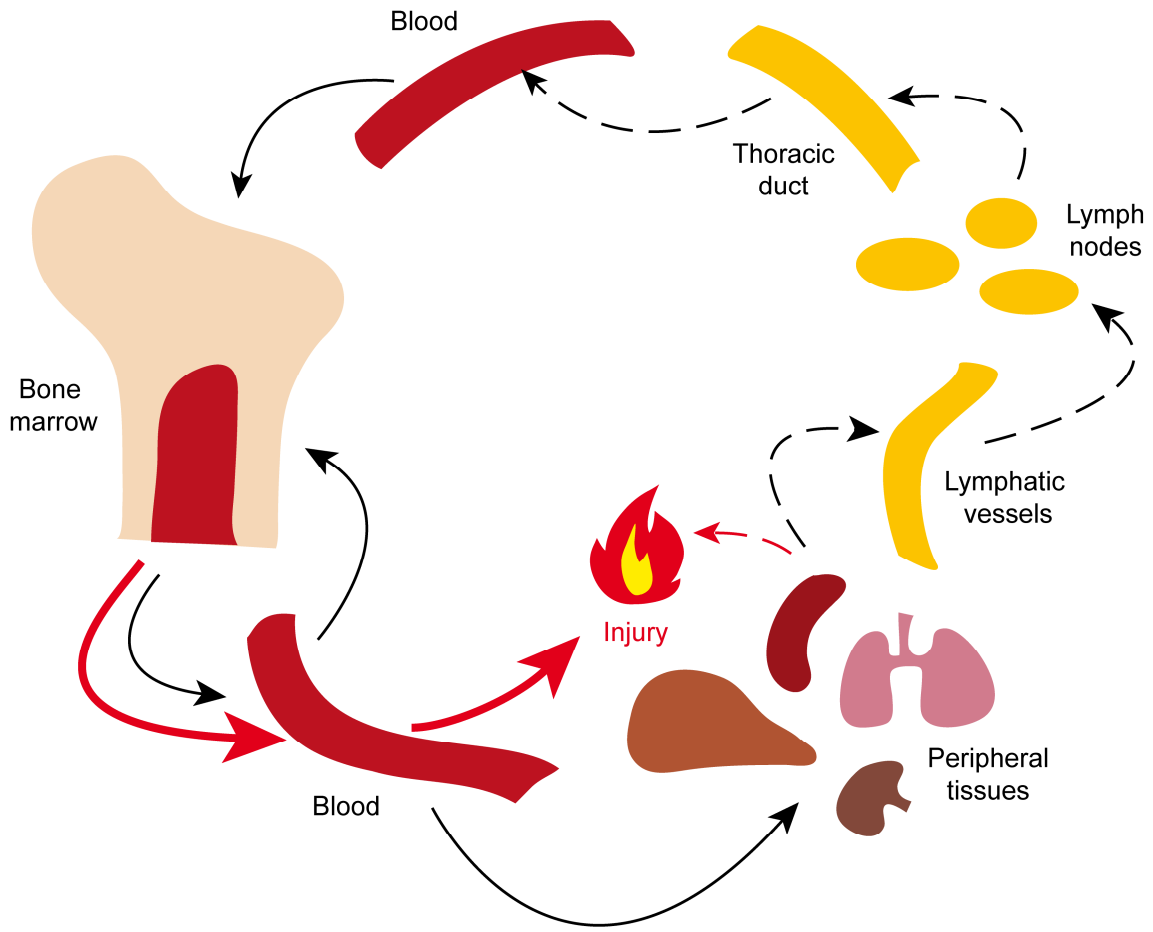

Figure 4 | Hematopoietic stem and progenitor cell (HSPC) trafficking. HSPCs constantly circulate between BM and blood and can enter a peripheral migration cycle through various organs, which they leave via draining lymphatics to re-enter the circulation. In case of tissue injury, HSPCs are released from the BM in increased quantities and are recruited to/retained at the site of the insult. (Figure adapted from Mazo et al., 2011[73].)

1.2 CNS macrophages - the most prominent hematopoietic cells inside the brain

1.2.1 CNS macrophages in health and disease

Like the majority of tissues, the central nervous system (CNS) contains populations of specialized tissue macrophages[74]. The latter represent the primary immune effector cells of the CNS and include the so-called "border macrophages" (perivascular, subdural meningeal, and choroid plexus macrophages), strategically located at CNS interfaces, as well as parenchymal microglia, which are surrounded by neurons, astrocytes and oligodendrocytes[75]. Microglia make up around 5 - 12 % of the total number of glial cells in the mouse brain[76]. They are homogenously distributed throughout the parenchyma and form a cellular grid with their ramified processes (Fig. 5). While microglia generally show a territorial behavior with their cell soma permanently remaining in a fixed position, their processes are highly motile and are continuously sampling the environment. This way, the brain parenchyma is completely screened by microglia once every few hours[77,78].

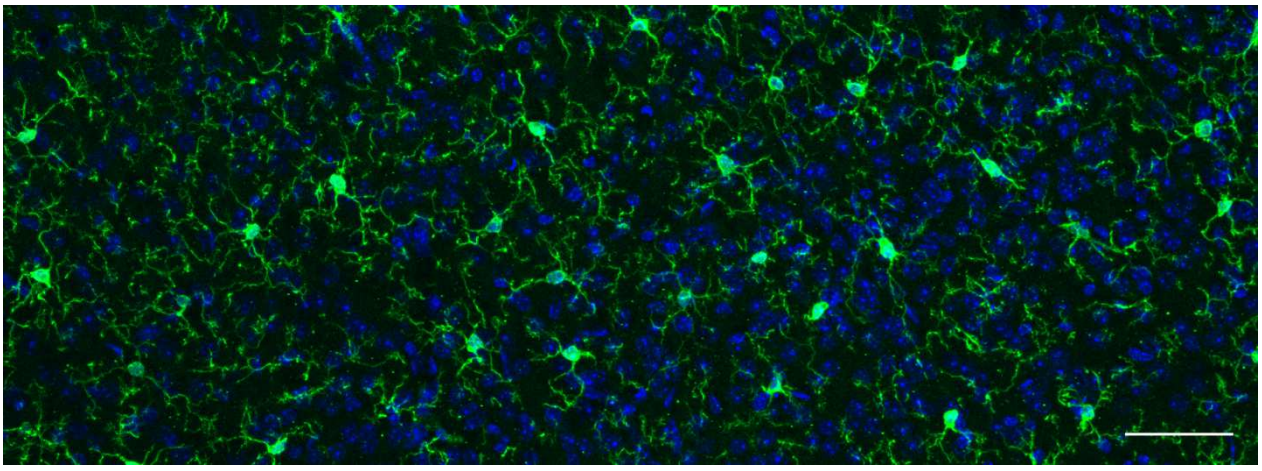

Figure 5 | Microglia in the adult CNS parenchyma. IBA1-staining (green) of microglia within a brain section derived from an adult mouse. Cell nuclei are stained with DAPI (blue). Scale bar: 50 µm.

Like other macrophages, microglia ingest and degrade dead cells, debris, and foreign material[79]. During a pathological challenge, they rapidly transition into an activated state, retract their processes and move to the site of injury in order to phagocytose, release effector molecules and orchestrate inflammatory processes[80].

Microglia exert important functions during CNS development and homeostasis, such as control of developmental neurogenesis[81], wiring[82], synaptic pruning[83], monitoring of synaptic activity[84], and regulation of adult neurogenesis[85]. Due to their exceptional position as the major immune cell population inside the CNS, microglia (and border macrophages) are also involved in the pathogenesis of a multitude of CNS disorders. These include multiple sclerosis[86], amyotrophic lateral sclerosis[87], brain tumors[88], ischemic stroke[89], traumatic brain injury[90], Alzheimer's disease[91], Parkinson's disease[87], prion disease[92], neuropathic pain[93], depression[94], and Huntington's disease[87].

1.2.2 CNS macrophage development

Unlike macroglia (astrocytes, oligodendrocytes, and ependymal cells), which derive from the neuroectoderm, microglia are of myeloid origin. Their colonization of the CNS is evolutionary conserved across vertebrate species and occurs before macrogliogenesis[95].

Microglia originate from EMPs that can be labeled in the YS as early as E7.5 in mice[26-28,96–99]. Their independence of HSCs is corroborated by the fact that microglia develop in the absence of the master transcription factor Myb as well as the Fms-related tyrosine kinase 3 (Flt3)[26,96], both important regulators of fetal and adult hematopoiesis. Importantly, a recent study suggested that border macrophages of the CNS share the same or a similar ontogeny[98].

As soon as the vascular system has been established, EMPs and their progeny disseminate over the embryo via the incipient circulation[29,95,100]. They reach the neuroepithelium by E9.5-10[20,26,101,102], as angiogenic sprouts from the perineural vascular plexus start penetrating into the developing brain[103]. Microglia precursors enter the brain rudiment through the leptomeninges and lateral ventricles[101,104]. They differentiate via a $CD45^+$ *C-X-3-C chemokine receptor type 1* $(Cx3cr1)^-$ stage into $CD45^+$ $Cx3cr1^+$ cells, which eventually evolve into ramified microglia as early as E14[26]. Growing coverage of the CNS is achieved via migration of amoeboid cells as well as their extensive proliferation between E10.5 and postnatal day 0 (P0)[26]. At E13.5, the blood-brain barrier (BBB) is established, presumably sealing the microglia population inside the CNS[105]. This way, YS-derived cells seem to be protected from replacement by fetal monocytes, which infiltrate other tissues around E14.5[28]. Microglia further expand until P14[106], while they continue to show an uneven distribution and activated morphology, pointing to their participation in CNS maturation[100]. In the third postnatal week, their numbers begin to decline to approximately 50 %, eventually reaching adult levels at 6 weeks of age, which are then maintained throughout life[106,107].

Although the YS origin of microglia is widely accepted, it remains controversial whether it is the exclusive and universal source of microglia during development. Recently, Xu et al. suggested an alternative origin of adult microglia based on observations in zebrafish. Here, embryonic microglia that derived from the rostral blood islands, a region analogous to the mouse YS, were later replaced by cells originating from the ventral wall of the dorsal aorta[108]. Importantly, this source was still Myb-independent and therefore not equivalent to HSCs[108]. Another fate mapping study in zebrafish obtained similar results[109]. However, in this study, the second wave replacing primitive microglia was found to originate from Myb-dependent HSCs[109].

Also in mice, the sudden increase of microglia cell numbers during certain time points of development has led to speculations about monocyte influx[104]. Using intra-liver delivery of lentiviral vectors at E14, when the liver is the main hematopoietic organ, Askew et al. actually demonstrated a perinatal infiltration of liver-derived cells into the brain, where they differentiated into a microglia-like phenotype[107]. Yet these cells were short-lived and had largely vanished by P6[107]. This is consistent with conditional lineage tracing studies in mice, which never found evidence for a major contribution of HSCs to the adult microglia pool[27,99,101]. However, an early engraftment of HSC-derived microglia has also been suggested based on non-inducible *Hoxb8*^{Cre} fate mapping[110,111]. Even though Hoxb8 seems to be exclusively expressed in HSPCs, labeled microglia were found in the brains of newborn and adult *Hoxb8*^{Cre} x *Rosa26*^{YFP} mice[110].

1.2.3 CNS macrophage maintenance: a collection of proposed mechanisms

As soon as the CNS macrophage pool is established, there is a constant rate of apoptosis and replacement of mature cells. In mice and humans, the physiological turnover of microglia has been investigated in a multitude of studies using ^{3}H-thymidine labeling[112], pulse-chase labeling with the thymidine analogs 5-bromo-2'-deoxyuridine (BrdU)[107] or iododeoxyuridine[113], Ki67 staining[107,114], retrospective ^{14}C-labeling[113], and chronic intravital two-photon imaging[107,115]. Estimated proliferation rates fall within a range of 0.08 - 2 % in humans[107,113] and 0.1 - 0.8 % in mice[107,112,114,115]. Despite the varying absolute turnover rates they determined, all studies agree on a model of active and slow microglia replacement, which enables few cycles of renewal of the whole population in a lifetime. However, in response to pathology, this rate can be adapted in a spatio-temporal manner: Microglia numbers rapidly and transiently increase surrounding lesion sites, a reaction that is collectively termed "microgliosis"[116].

Several mechanisms for the maintenance and expansion of microglia have been postulated over time (Fig. 6), which are going to be addressed in the following chapter:

1. Infiltration of circulating precursors (e.g. monocytes)
2. Differentiation from pericytes or pericyte-like stem cells
3. Differentiation from NESTIN^{+} parenchymal progenitors
4. Division of terminally differentiated cells

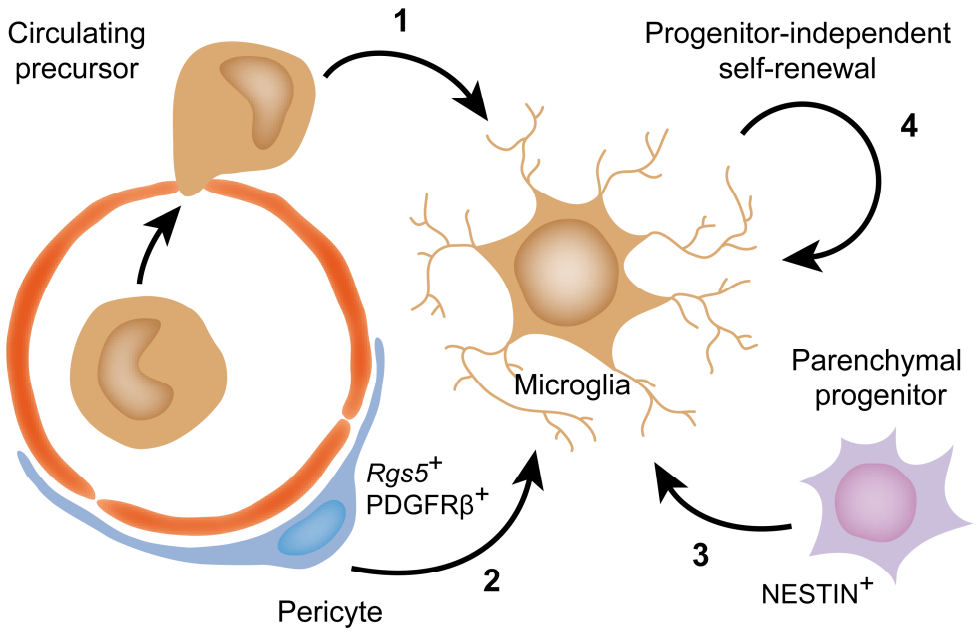

Figure 6 | Proposed mechanisms of microglia maintenance and expansion in health and disease. Microglia have been suggested to be replenished via CNS infiltration of circulating precursors, such as monocytes (1), to differentiate from *Rgs5*$^{+}$/PDGFRβ^{+} pericytic (2) or NESTIN^{+} parenchymal (3) progenitors, and to self-renew via division of mature cells (4).

1.2.3.1 Infiltration of circulating precursors

In his original model of the mononuclear phagocyte system, Van Furth proposed that HSC-derived monocytes are released into the circulation from the BM and continuously immigrate into tissues, where they differentiate and replace resident macrophages[117]. A plethora of studies has supported this view also with regard to microglia[118–124]. However, what was common to all of these studies was the use of BM chimeras that relied on preconditioning of the recipient animal via whole body irradiation[118–124]. In 2007, Ajami et al. tested these findings in a model of parabiosis, which is based on the surgical joining of two animals in order to create a shared circulation. To their surprise, green fluorescent protein (GFP)-labeled cells from the donor animal engrafted into the spleen and liver of the wild-type recipient, but did not contribute to the microglia pool even after 5 months[125]. In a follow-up study, they found that although monocytes

massively infiltrated the inflamed CNS and differentiated into macrophages, the latter were short-lived and did not persist in the normal CNS environment[126]. In support of this hypothesis, no change in microglia number was observed in *Ccr2*$^{-/-}$ mice[107,127], which show reduced levels of circulating monocytes due to their deficient egress from the BM[128]. Also, microglia remained unlabeled in *Flt3*^{Cre} x *Rosa26*^{YFP} mice, which trace the fate of fetal/adult HSCs and their progeny including monocytes[27].

Mildner et al. resolved the discrepancy between BM chimeras and parabionts, as they blocked the engraftment of BM-derived cells into the CNS by simply shielding the head of the BM recipient during irradiation[127]. Similar results were obtained when BM was transplanted without preconditioning into *Rag2*$^{-/-}$ x $y_c^{-/-}$ mice[127]. It is now appreciated that whole body irradiation damages the BBB[129–133], induces cytokine release in the CNS[127], and injures resident microglia[134,135]. Yet irradiation alone did not induce recruitment of physiologically circulating precursors (e.g. monocytes) into the CNS[125]. It has been suggested that upon intravenous injection of BM cells, especially stem and early progenitor cells, which usually do not enter the bloodstream in high quantities, are able to efficiently engraft the wounded CNS and differentiate into long-lasting microglia-like cells[126,136,137]. Clearance of the microglial niche by certain depletion systems, however, even induced monocyte influx and persistance[138,139]. Nevertheless, it seems as if these artificially seeded cells cannot acquire the full microglial phenotype[139–142].

Over the last years, new lineage tracing approaches (based on the mouse lines *Runx1*^{CreER}, *Tie2*^{CreER}, *Csf-1r*^{CreER}, and *Cx3cr1*^{CreER}, crossed to inducible fluorescent reporter strains) consistently demonstrated that many tissue macrophage populations in mice self-renew locally throughout life[27,28,98,101]. Microglia seem to be particularly independent of peripheral sources, as after their establishment from YS precursors, no influx of circulating cells at all was indicated in these models[27,28,101].

The *Cx3cr1*^{CreER} mouse line has proven particularly useful to study microglia maintenance[143,144]. Here, the cre-estrogen receptor fusion protein is expressed in *Cx3cr1*$^{+}$ cells, which comprises several tissue macrophage populations including microglia, as well as late MyPs and CCR2^{-} Ly6C^{lo} patrolling monocytes. Application of tamoxifen (TAM) specifically induces a stable recombination event in all of these cell types, so that they start e.g. expressing a fluorescent reporter. Importantly, over time, only long-lived cells (such as microglia) will continue to carry the cre-mediated mutation, while short-lived cells (such as monocytes) will be replaced by non-recombined stem and progenitor cells in the BM[143,144]. Using this model, which achieved unprecedented specificity as well as high targeting efficiency of CNS macrophages, it was shown that during forced repopulation as well as under physiological conditions microglia and most border macrophages (especially subdural meningeal and perivascular macrophages) regenerated from a CNS-internal pool[98,142,145].

While it is widely acknowledged that BM-derived cells do not cross the BBB to become microglia under physiological conditions, the discussion continues. In 2018, Fehrenbach et al. claimed a dependence of adult microglia on definitive hematopoiesis after observing decreased microglial numbers in the non-inducible *Vav1*^{Cre} x *dicer*$^{fl/fl}$ mouse model, which shows impaired blood cell generation[146]. However, the study lacked a detailed proof that the *Vav1* promoter is never active in mature microglia. The latter would be important, as a conditional dicer knock-out in adult microglia led to a similar decrease in their cell number[147].

1.2.3.2 Differentiation from pericytes or pericyte-like stem cells

Pericytes, which cover capillary endothelial cells, have long been believed to possess stem cell-like capabilities[148,149]. Most observations that support a possible differentiation of pericytes into CNS macrophages stem from experimental models of ischemic stroke[150,151]. Here, microglia-like cells concomitantly expressing the pericyte markers regulator of G-protein signaling 5 (*Rgs5*) or platelet-derived growth factor receptor-β (PDGFRβ) have repeatedly been reported in perivascular regions of the infarct area[150,151]. Intriguingly, also primary brain pericytes of mouse and human origin acquired a microglia-like morphology and marker expression *in vitro*, which seemed to depend on the exposure to hypoxic conditions[150,151]. The latter have already been described to drive brain pericyte differentiation towards neuronal and vascular lineages[148]. Likewise, pericytes from the brains of transgenic Alzheimer mice were reported to spontaneously differentiate into a $CD11B^+$ microglial-like cell type *in vitro*[152].

Recently, the question of pericyte stemness was addressed in an exhaustive study that made use of an inducible *Tbx18*^{CreER} system to trace the fate of pericytes in multiple organs *in vivo*[153]. The investigators found that although *Tbx18*$^+$ pericytes displayed a mesenchymal stem cell (MSC)-like behavior *in vitro*, they did not contribute to other cell types, including microglia, in the living animal[153]. While the study made clear that pericytes do not replenish the microglia pool under homeostatic conditions, their differentiation into microglia-like cells during pathology still cannot be excluded. As suggested previously[150,151], specific conditions such as hypoxia could be necessary to induce the stem cell-like character of pericytes *in vivo*, which might not have been reached in the cortical stab wounds assessed in the *Tbx18*^{CreER} system[153]. Unfortunately, a model of cerebral ischemia was not tested.

1.2.3.3 Differentiation from NESTIN$^+$ parenchymal progenitors

Evidence for the existence of a hidden microglial progenitor within the CNS parenchyma comes from Kim Green's group[154]. He and his co-workers were the first to observe the rapid repopulation of microglia following an almost complete depletion in adult mice due to oral administration of high doses of PLX3397 (Pexidartinib), a potent inhibitor of the receptor tyrosine kinases colony-stimulating factor-1 receptor (CSF-1R), c-KIT, and FLT3[155]. Surprisingly, even after elimination of ~99 % of microglia, the microglial pool returned to normal levels within 7 days, without any obvious contribution from the periphery[154]. Repopulating cells showed transient expression of the stem and progenitor cell markers CD34 and c-KIT, as well as the intermediate filament NESTIN[154].

In the normal CNS, NESTIN is expressed by pericytes[149], NG2$^+$ oligodendrocyte precursor cells[156], and - most characteristically - neural stem cells (NSCs)[157]. Despite its reputation as a neuroectodermal lineage marker, NESTIN is found in a variety of tissues such as embryonic skeletal and cardiac muscle, liver, and kidney[158]. In fact, NESTIN seems to be particularly linked to mitosis, as it is expressed by several proliferative cell types, from reactive astrocytes to vascular endothelial cells[79]. It is also considered a marker for cancer stem cells[158]. Still, the expression of NESTIN surprised the authors and let them suspect the existence of a microglial progenitor apart from the normal hematopoietic lineages[154]. Intriguingly, they noted a sudden emergence of many proliferating NESTIN$^+$ non-microglial cells at the 2 day recovery time point, which appeared to convert into a *Cx3cr1*$^+$ microglial phenotype within the following 24 h[154]. To further support their hypothesis, they estimated that the surviving 1 % of microglia would have to divide every 5 - 6 h to explain the rapid pace of repopulation without an additional progenitor source, which would be highly unlikely[154].

However, this proliferation rate seems exaggerated and has been criticized in a recent study[145]. The concept of NESTIN$^+$ microglia progenitors is further challenged by the notion that lineage tracing of *Nestin*-expressing NSCs has not been reported to label microglia, neither at baseline nor under disease conditons[79]. Accordingly, when forced microglia repopulation was reproduced in the inducible *Nestin*^{CreER} fate mapping model, new microglia did not derive from *Nestin*$^+$ cells that had been tagged in the steady-state or during depletion, even though repopulating microglia transiently expressed NESTIN[145,159]. NESTIN expression indeed seems to be a robust feature of repopulating cells and has also been observed in a genetic microglia depletion model[142]. It is possible that it is induced by specific conditions such as the disruption of population homeostasis or associated changes in the CNS milieu, as proliferating microglia in the steady-state have not been observed to express *Nestin*[107]. Thus NESTIN$^+$ microglia might just reflect a transient repopulating phenotype instead of a bona-fide progenitor[79,155].

1.2.3.4 Division of terminally differentiated cells

Apart from circulating or resident precursors, the idea that tissue macrophages themselves might possess a stem cell-like character has emerged as an alternative explanation for their self-renewal[160]. The prevailing concept of differentiation claims that maturation from stem cells towards specialized cell types is accompanied by a gradual decrease in self-renewal and proliferative activity, until the functional, terminally differentiated cell is eventually securely locked in the G_0 phase. However, in 2009, Aziz and co-workers reported that macrophages are relatively easily reprogrammed to a state of indefinite self-renewal by double knock-out of the transcription factors MafB and c-Maf[161]. Importantly, this was not associated with cellular transformation and mutated macrophages did not alter their immunophenotype and morphology, gene expression profile, or characteristic functions such as phagocytosis[161]. The authors

concluded that self-renewal in the strict sense, without loss of cellular identity, is possible in macrophages and speculated about their transient reprogramming to a stem cell-like state *in vivo*[160]. This concept was supported by a study that examined the repeated genotoxic depletion of lung macrophages[97]. Labeling of proliferating macrophages after the first round of depletion with BrdU and after a second round via Ki67 staining revealed that cells entered the cell cycle after the second round independently of previous proliferative activity, arguing against clonal expansion of a progenitor population[97,160].

The self-renewal capacity of microglia was specifically addressed by Bruttger et al. in 2015 using *Cx3cr1*^{CreER} *x* iDTR *x Rosa26*$^{-stop-YFP}$ mice[142]. In this model, *Cx3cr1*$^{+}$ macrophages in the CNS (and other tissue macrophages) specifically expressed the diphtheria toxin receptor (DTR) as well as yellow fluorescent protein (YFP) after an initial TAM pulse. Following microglia depletion via administration of diphtheria toxin, the CNS was rapidly repopulated by YFP^{+} cells, suggesting that repopulation was solely driven by the local proliferation of *Cx3cr1*$^{+}$ cells[142]. Meanwhile, this result has been reproduced in models of microglia depletion/repopulation using pharmacological CSF-1R inhibition[145,159]. It is further supported by the fact that the microglia pool remained stably labeled in the *Cx3cr1*^{CreER} x *Rosa26*^{YFP} model even 9 months after TAM administration[98].

As *Cx3cr1* in the CNS is thought to be exclusively expressed in mature microglia/ macrophages, these observations were interpreted as proof for their self-renewal capacity. However, it is difficult to completely rule out the existence of a rare population of *Cx3cr1*$^{+}$ precursors. In an attempt to do so, Tay et al. refined the *Cx3cr1*^{CreER} lineage tracing model by crossing it to the "confetti" reporter strain[162]. In the resulting "microfetti" mice, microglia randomly expressed one of four possible fluorophores after induction. By choosing a low TAM dose, a relatively modest labeling efficiency of about 14 % was achieved to provide sufficient

spatial resolution while following the fate of individual, labeled cells. This way, the authors were able to observe the turnover of *Cx3cr1*$^{+}$ microglia in different brain regions, but found no evidence for a designated proliferative niche. A "drift towards clonality" was also not observed, meaning large clusters of same-color cells after prolonged observation periods, which should occur if a rare *Cx3cr1*$^{+}$ proliferative precursor would have been labeled by chance[162]. Consistently, mathematical modeling of microglial turnover in the human brain using retrograde ^{14}C labeling agreed with the homogeneous proliferation of mature microglia, but not with the proliferation of a subpopulation of quiescent, long-lived progenitor cells[113].

Recently, direct evidence for the physiological self-renewal of microglia was obtained by chronic two-photon imaging of mature cells through a cranial window in living mice[107,115]. Here, ramified *Cx3cr1*$^{+}$ microglia were observed in real-time giving rise to daughter cells that migrated apart and integrated into the microglia network[107,115]. These results suggest that, at least under steady-state conditions, all microglia have the ability to self-renew.

1.3 The vascular wall as a niche for stem and progenitor cells

1.3.1 The vascular architecture

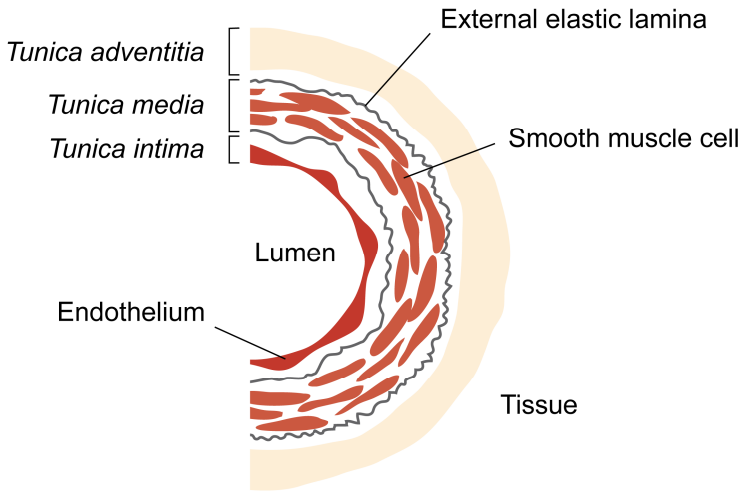

Figure 7 | The structure of an artery. The vascular wall is composed of three layers: the *tunica intima* (inner layer), the *tunica media* (middle layer), and the *tunica adventitia* (outer layer). Each layer is composed of different cell types and exerts diverse tasks to enable functionality of the whole vessel.

Apart from capillaries and venules, which constitute the microvasculature, all blood vessels are composed of three layers (Fig. 7). The *tunica intima* is the vessel's inner layer and in direct contact with blood. It is mainly composed of a thin endothelial lining, which provides a frictionless pathway for the movement of the blood and restricts the passage of molecules and cells, plus a small subendothelial zone. The *tunica media* is the middle layer. It consists of contractile smooth muscle cells and elastic fibers that regulate the internal diameter of the vessel and absorb the fluctuating pressure within the vascular system. The *tunica adventitia* is the outer layer, conferring additional stability to the vessel and embedding it into its surrounding. It is built up of fibrous tissue and includes a variety of cell types such as fibroblasts and immune cells. In case of larger vessels such as the aorta, the adventitia holds so called *vasa vasorum*, microvessels that supply the thick vessel wall with oxygen and nutrients.[163]

1.3.2 Stem and progenitor cell subsets in the vascular wall

Blood vessels are more than a mere ductwork throughout the body. For instance, the vasculature is an integral component of stem cell niches, such as the HSC niche in the BM or the NSC niche in the subventricular and subgranular zones of the CNS[164]. More importantly, vessels themselves have attracted the attention of stem cell research, as they seem to harbor a broad spectrum of cells with stem and progenitor cell characteristics. Vascular wall progenitors (VW-Ps) have been reported within all three mural layers in several species, including mice, rats, and humans[165].

The inner adventitia, adjacent to the external elastic lamina, has emerged as the prime candidate for the vascular stem cell niche[165]. It has therefore also been termed the "vasculogenic zone"[166] (Fig. 8). In human and animal vessels, this region contains prominent expression of markers for stemness (CD34, c-KIT, STRO-1, NOTCH-1, OCT-4, SCA-1, and FLK-1) and cell proliferation[165]. Most research on VW-Ps so far has been done by selecting cells based on these markers and studying their differentiation potential *ex vivo* or after reintroduction into living animals[165]. However, recent studies have also demonstrated *in vivo* activity of VW-Ps via genetic fate mapping, including their contribution to pathology[167,168]. Intriguingly, lineage tracing even suggested that vessels bear the intrinsic potential to populate the "vasculogenic zone" via Klf4-dependent reprogramming of vascular smooth muscle cells into a progenitor phenotype[169].

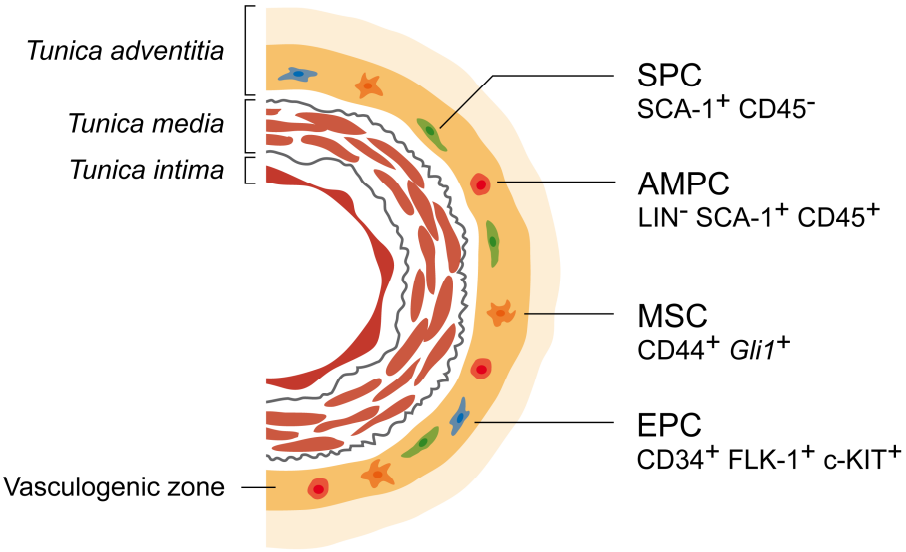

Figure 8 | The tunica adventitia is a niche for stem and progenitor cells. Presented is a simplified view of the vessel wall and its "vasculogenic zone", which harbors most of the vascular wall progenitors (VW-Ps) described so far. Different types of VW-Ps are shown, combined with a selection of markers most commonly used for their identification. AMPC: adventitial macrophage progenitor cell; EPC: endothelial progenitor cell; MSC: mesenchymal stem cell; SPC: smooth muscle progenitor cell.

Among the best studied VW-Ps are lineage-committed endothelial progenitor cells[170] and smooth muscle progenitor cells[171,172] as well as MSCs, which show trilineage differentiation capability towards chondrocytes, osteoblasts, and adipocytes *in vitro*[173,174]. MSC-like cells inside the adventitia and in pericyte niches across major organs have been shown to be marked by sonic hedgehog signaling[167]. Recently, genetic fate mapping based on the hedgehog mediator glioma-associated oncogene homolog 1 (Gli1) revealed that these cells replace vascular smooth muscle cells after injury and differentiate into osteoblast-like cells or myofibroblasts under pathological conditions[167,168]. Importantly, also progenitors with hematopoietic potential have been reported in the adventitia, including circulation-derived HSPCs as well as adventitial macrophage progenitor cells (AMPCs)[59,175].

Inherent potential for the generation of macrophages has been noted in early studies with arteries from mice, rats, and humans[166,176]. However, these mainly relied on observations in aortic cultures and transplantation assays. As the self-renewal and proliferative capacity of mature macrophages[160] had not been elaborated yet, focus was mainly on excluding a contribution of circulating cells, such as monocytes. Importantly, *in vivo Cx3cr1*^{CreER} fate mapping demonstrated that a least part of the aortic macrophage population seems to self-renew during adulthood[177], leaving it ambiguous whether the observed macrophage expansion in previous studies resulted from proliferation of resident progenitors or mature cells.

The presence of vessel-resident hematopoietic progenitor cells had been suggested before by Montfort and colleagues, who showed that vessel grafts protected lethally irradiated mice by contributing to the recipient's hematopoiesis[58]. Although the grafts failed to establish long-term multilineage reconstitution, their radioprotective activity pointed at least towards the presence of myelo-erythroid progenitors inside the transplanted vessels[178]. Psaltis et al. confirmed these findings by demonstrating a rare population of circulation-derived HSPCs in mouse aorta[59]. Surprisingly, the authors also detected a markedly enriched content of macrophage-committed progenitors in aortic cell disaggregates compared to other hematopoietic or non-hematopoietic tissues[59,175]. These were not diminished in osteopetrotic (*op*/*op*) mice, which show reduced macrophage numbers due to CSF-1 deficiency[179], and were only scarcely exchanged following transplantation of GFP-labeled BM[175]. Progenitor activity was traced back to an undifferentiated lineage marker $(LIN)^-$, $CD45^+$, stem cell antigen-1 $(SCA\text{-}1)^+$ population that resided in the adventitia of multiple peripheral arteries, a surface phenotype that excluded mature macrophages, monocytes, or MyPs from the BM[59,175].

1.4 Hematopoietic potential inside the adult CNS

Although the brain is not regarded as hematopoietic organ, cells with hematopoietic potential have repeatedly been described in the CNS. It has been claimed that adult NSCs are highly plastic and can even adopt a hematopoietic fate under specific conditions. This was established by their putative ability to repopulate the hematopoietic system following transplantation into lethally irradiated hosts[180,181]. Although primary NSC isolates and clonal cultures neither expressed hematopoietic markers nor formed hematopoietic colonies in CFU assays, they appeared to shift towards an HSC-like phenotype *in vivo*, as indicated by long-term and multi-lineage reconstitution[180]. However, in an extensive study comprising 128 transplanted animals, Morsehead et al. could not reproduce a hematopoietic competence of NSCs[182]. Based on their observations, the authors suspected a transformation of NSCs in long-term culture or a contamination with HSPCs to be the reason for the blood cell potential observed in earlier studies[182].

In fact, HSPC-like cells have repeatedly been observed among preparations from the adult mouse brain[41,183–186]. Their first report stems from Perry F. Bartlett, who observed hematopoietic colony-formation in spleens of irradiated mice following intravenous injection of brain homogenates[184]. He noted a distinct colony pattern compared to transplanted BM cells as well as a slightly different surface phenotype of colony-forming units-spleen (CFU-S) from BM and brain. In contrast to BM, CFU-S frequencies in the brain were not reduced in anemic W^f/W^f mice, leading him to speculate that the brain harbors an independent population of hematopoietic stem or progenitor cells[184].

While looking for microglia progenitors, Alliot et al. later described a cell population of similar size within adult brain suspensions that extensively proliferated in coculture with D19 astrocyte layers and progressively acquired a F4/80$^+$ macrophage-like phenotype[185]. However, as the study relied on feeder cells that prominently produced CSF-1 for progenitor stimulation[185], it might have missed a broader hematopoietic differentiation potential. By a comparable setting, Nataf et al. demonstrated the presence of MyPs in the rat choroid plexus[186]. It is conceivable that both groups were actually investigating the progenitor population already described by Perry F. Bartlett. The latter was further supported by a study of Asakura et al., who examined the so-called "side population" (SP) in cell preparations from multiple organs. The SP is defined by efflux of the dye Hoechst 33342 via multi-drug resistance transporters, a characteristic feature of stem and progenitor cells. All organs tested, including the brain, contained such a population, which produced hematopoietic colonies in CFU assays[183].

2 Significance and Aim

There is ever-growing interest in brain macrophages, which constitute the interface between neuroscience and immunology and have been identified as major players in virtually every CNS disorder. Even though much progress has been made in elucidating CNS macrophage ontogeny and maintenance, there are still questions that remain to be resolved. Different lines of evidence indicate that mature microglia and border macrophages are capable of self-renewal in the steady-state and do not rely on input via a progenitor compartment. However, it is not entirely clear whether additional sources can contribute to the brain macrophage pool during pathology. One such source might be the vessel wall, which has emerged as a versatile niche for stem and progenitor cells. As vessels span the whole organism, this niche is potentially ubiquitous and might harbor macrophage/microglia progenitors also in the CNS. Concurrently, it might be the source of hematopoietic potential, which has repeatedly been described in the brain, but up to date remains insufficiently characterized.

In this study, four main objectives were set as follows:

1. To revisit the mouse CNS vasculature in the light of current knowledge about VW-Ps.
2. To establish the *ex vivo* culture of mouse CNS vessels for the functional assessment of macrophage/microglia potential within the vessel wall.
3. To better characterize the hematopoietic potential within the CNS.
4. To revisit CSF-1R inhibitor-mediated CNS macrophage depletion and repopulation in living mice with a focus on possible precursor contribution.

3 Results

3.1 No evidence for AMPCs within the CNS vasculature of adult mice

3.1.1 No CD45$^+$ SCA-1$^+$ cells were detected in sections of the mouse circle of Willis

As CD45$^+$ SCA-1$^+$ AMPCs have been described in the aortic wall as well as in femoral and carotid arteries[59,175], the presence of cells with a similar phenotype was examined in CNS-associated vessels. Therefore, female C57BL/6 mice at the age of 8 weeks were sacrificed and their aortae and brains processed for immunohistological analysis. Transversal 10 µm paraffin sections were prepared from the ventral side of the brain in order to obtain cross-sections of the circle of Willis (CW), the largest arterial structure of the mouse brain (Fig. 9*a*).

Like in the aorta, markers for stemness (CD34 and fetal liver kinase-1 [FLK-1]) were present in the adventitia of the CW, which only comprised a 1 - 2 cell layer (Fig. 9*b* and Fig. S1). However, the staining pattern of SCA-1 markedly differed in both vascular structures. In the aorta, strong SCA-1 reactivity was detected throughout the adventitia (Fig. 9*c*). Weaker staining was observed on endothelial cells. At the media-adventitia interface, regularly spaced adventitial cells could be observed that dimly stained for CD45, while also appearing positive for SCA-1. Conversely, while endothelial cells of the CW stained more intensely for SCA-1, the staining was hardly detectable within the adventitia (Fig. 9*d*). Still CD45$^+$ cells were regularly encountered within this layer, which most likely represented adventitial macrophages or extravasated leukocytes patrolling the vascular space. Nevertheless, in contrast to the aorta, CD45$^+$ SCA-1$^+$ cells were not detected in the CW.

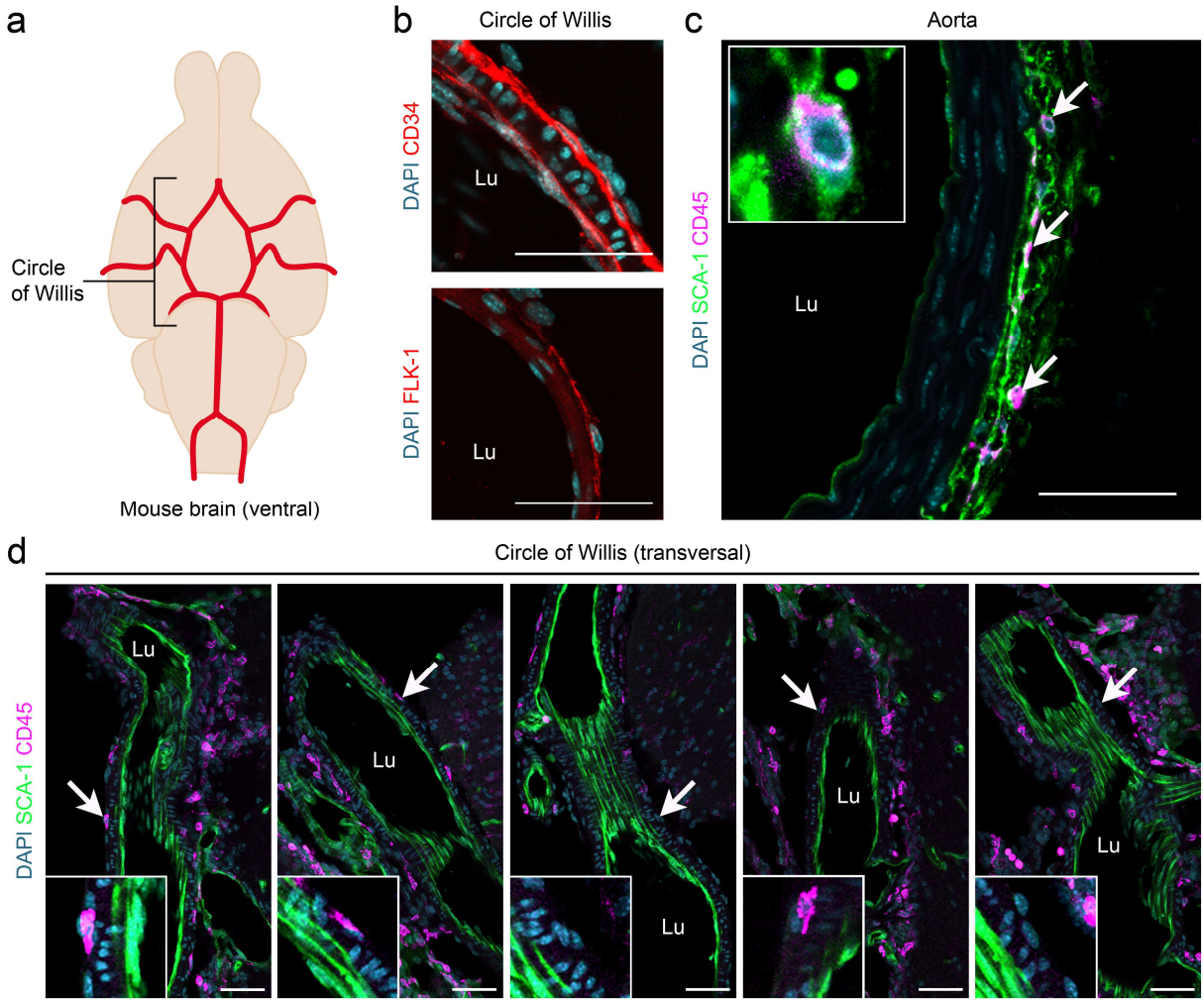

Figure 9 | No SCA-1$^+$ CD45$^+$ AMPC-like cells were detected in histological sections of the mouse circle of Willis (CW). (**a**) Schematic representation of the CW at the ventral aspect of the mouse brain. (**b**) Markers for stemness were present within the adventitia of the CW, as demonstrated by CD34 and FLK-1 immunostaining. (**c**) Representative image of an aortic cross-section, immunostained for SCA-1 and CD45. Double positive cells were located in the inner adventitial layer of the vessel (arrows). (**d**) Representative images of transversal sections through the CW, immunostained for SCA-1 and CD45. Some cells within the thin adventitial layer were CD45$^+$, but did not stain for SCA-1. Arrows indicate details that are presented in higher magnification in the inlay. All images are maximal projections of multiple Z-planes spanning a 10 µm paraffin section that had been acquired using a confocal microscope. A total of 10 cross-sections per animal were analyzed from n = 4 mice. Scale bars: 50 µm. Lu: vessel lumen.

3.1.2 The CWFA is a tool to study CNS-associated AMPCs *in vitro*

Progenitors are best described not by markers, but by their ability to extensively proliferate and differentiate. Therefore, the "circle of Willis fragment assay" (CWFA) was established to study possible AMPCs *in vitro* (Fig. 10*a*). The protocol was based on the aortic ring assay[187]. In brief, C57BL/6 mice at the age of 8 - 12 weeks were sacrificed and transcardially perfused with PBS to remove circulating cells from the vasculature. The CW was dissected from the brain and cut into 2 - 3 mm long fragments, which were embedded into a collagen type I matrix and cultured under hypoxic conditions, in the presence of VEGF and additional macrophage-stimulating factors.

Histological analysis of collagen-embedded fragments demonstrated that complete vessels including all vascular layers were obtained via dissection (Fig. 10*b*). Starting around the fourth day of culture, single cells with a thin, fibroblast-like morphology emigrated from the vessel into the surrounding collagen matrix, accompanied by capillary-like sprouts (Fig. 10*c*). However, only ~50 % of vessels showed detectable cell growth during the observation period of 7 - 10 days. Between days 5 and 6, a homogenous population of round cells, clearly distinct from the aforementioned fibroblast-like cells, started to emerge. At day 7, these cells were scattered around the vessel and occasionally formed large, loose clusters. In whole-mount immuno-fluorescence stainings (IF), they stained positive for the pan-myeloid marker CD11B and displayed a macrophage-like morphology (large cell body with a ruffled surface and a small, round nucleus) (Fig. 10*d*).

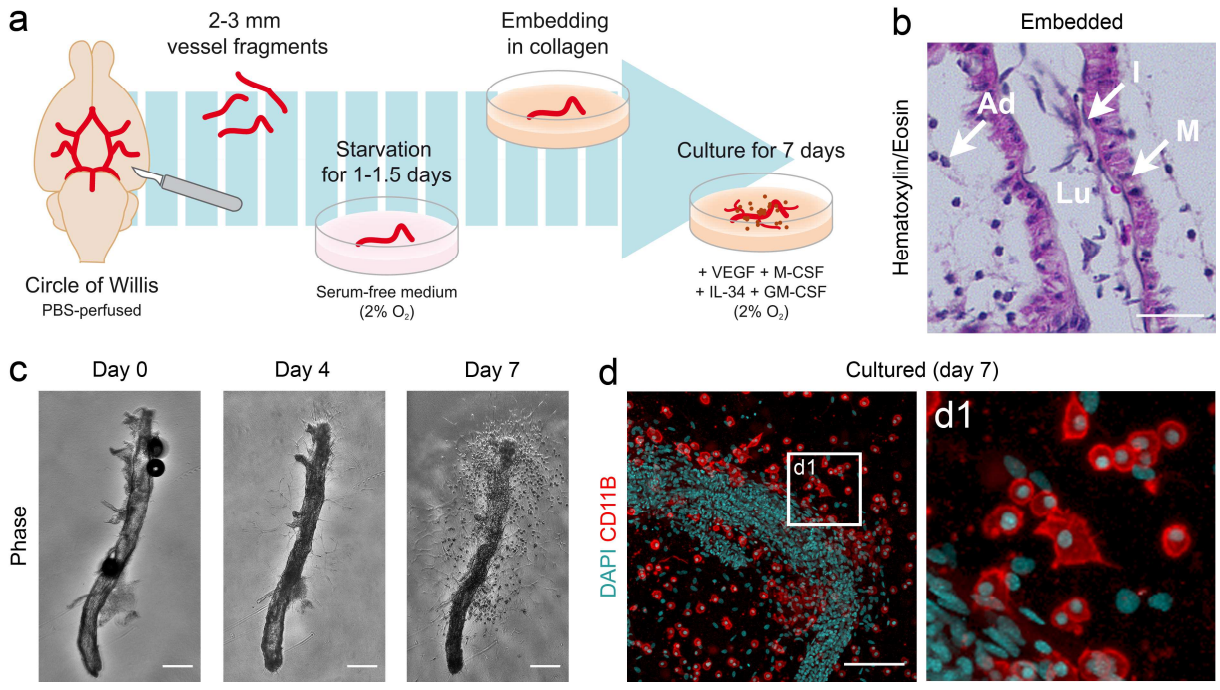

Figure 10 | The circle of Willis fragment assay (CWFA). (**a**) Schematic overview of the experimental procedure. Fragments of the CW were dissected from adult mouse brains after transcardial perfusion with PBS. The fragments were starved in serum-free medium under hypoxic conditions and embedded in a collagen type I matrix. Embedded vessels were cultured in medium supplemented with growth factors for 7 days at hypoxia. (**b**) Hematoxylin and eosin staining of a 10 µm paraffin section through a vessel fragment freshly embedded in collagen. All vascular layers are present including intima (I), media (M), and adventitia (Ad). Blood is mostly cleared from the vessel lumen (Lu). (**c**) CW fragment growing in a collagen matrix for 7 days. Within the first four days of culture, fibroblast-like cells and endothelial cords started to migrate into the surrounding matrix. Until day 7, rapid expansion of round, high-contrast cells occurred, which clustered around the vessel. (**d**) Whole-mount immunofluorescence staining (IF) of an embedded vessel fragment following 7 days of culture. $CD11B^{+}$ cells with macrophage-like morphology (see d1) are prominent, cluster around the vessel, and infiltrate the collagen matrix. Scale bars (b): 25 µm; (c,d): 250 µm.

3.1.3 The CSF-1R inhibitor PLX5622 systemically depleted macrophages *in vivo*

CNS macrophages have been shown to depend on CSF-1R signaling for their survival[154]. To analyze macrophage-depleted vessels in the CWFA, treatment of mice with the CNS-penetrable CSF-1R inhibitor PLX5622 was established. Female C57BL/6 mice at the age of 6 weeks were fed for 7 - 21 days with PLX5622, formulated in AIN-76A standard rodent chow at 300 - 1200 mg kg^{-1}.

Quantification of ionized calcium-binding adapter molecule 1 (IBA1) positive cells in sagittal brain sections (Fig. 11*a*) revealed a dose-dependent decrease in CNS macrophage density already after 7 days of PLX5622 treatment (Fig. 11*b*). The highest PLX5622 dose led to a maximal depletion of ~85 % within 7 days. Depletion varied slightly over different brain regions and appeared least efficient in the olfactory bulb. Longer treatment durations did not enhance depletion efficiency. Outside the CNS, PLX5622 also led to depletion of Kupffer cells in the liver (Fig. 11*c*) and reduced the fraction of monocytes in peripheral blood (PB) (Fig. 11*d*).

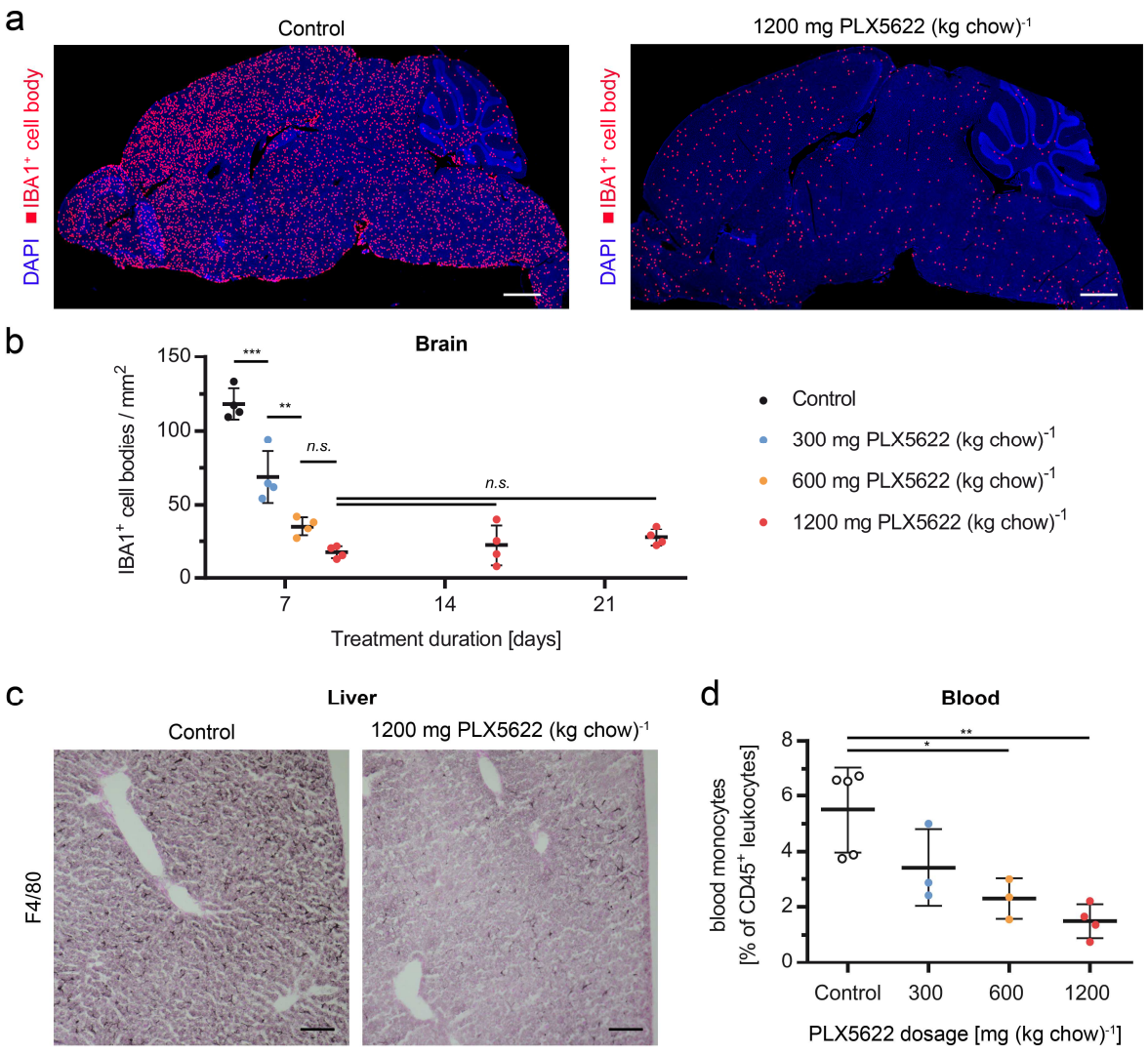

Figure 11 | Systemic monocyte/macrophage depletion in living mice using the orally administered CSF-1R inhibitor PLX5622. (**a, b**) Within 7 days, PLX5622 depleted CNS macrophages in a dose-dependent manner. Longer treatment periods did not increase depletion. (**a**) Representative images of 10 µm sagittal brain slices from mice that had been fed with control or PLX5622-containing chow (shown treatment duration: 7 days). Following immunostaining and image acquisition, IBA1$^+$ cell bodies were automatically selected in ImageJ and replaced by red squares to ensure visibility in low magnification. Scale bars: 1 mm. (**b**) Global CNS macrophage densities within brain slices as shown in **a** following PLX5622 treatment. Area measurements and cell counting was performed automatically using ImageJ. Results represent the means of one preliminary experiment including $n = 4$ mice per treatment group and time point. Error bars indicate SDs. Statistical analysis was performed using successive ordinary one-way ANOVAs with Tukey's multiple comparisons test. $^{**}P < 0.01$, $^{***}P < 0.001$, n.s.: non-significant. (**c**) PLX5622 treatment depleted F4/80$^+$ Kupffer cells in the liver. Shown are DAB-stained 10 µm paraffin

Figure 11 (continued) liver sections of mice that had been fed with control or 1200 mg PLX5622 (kg chow)$^{-1}$ for 7 days. Images are representative of one experiment including $n = 4$ animals per treatment group. Scale bars: 100 µm. (**d**) Blood monocytes were reduced in a dose-dependent manner following PLX5622 treatment. The percentage of monocytes among total CD45$^+$ leukocytes was analyzed via flow cytometry in mixed PB of mice that had been fed with control or PLX5622-containing chow for 7 days. Monocytes were defined as the SSC^{lo} FSC^{hi} CD11B$^+$ fraction of CD45$^+$ white blood cells[188] (for gating see also Fig. S9). Results represent the means of one preliminary experiment including $n = 3$ - 5 mice per treatment group. Error bars indicate SDs. Statistical analysis was performed using ordinary one-way ANOVA with Tukey's multiple comparisons test. *$P < 0.05$, ***$P < 0.01$.

3.1.4 Macrophage-depleted CW fragments failed to produce new macrophages *in vitro*

Terminally differentiated CNS macrophages have been shown to self-renew and extensively proliferate in models of forced repopulation[75,142,145,154]. Therefore, macrophage expansion in vessel cultures does not necessarily imply the presence of progenitors. Instead, proliferation of mature cells already present at the time of explantation might solely account for the observed increase in cell number. To test this hypothesis, macrophage-depleted vessels were analyzed in CWFAs. *In vivo* PLX5622 pre-treatment was combined with transient *ex vivo* incubation with clodronate liposomes to achieve maximal depletion (Fig. 12*a*). Vessels were analyzed via whole-mount IFs for CD11B at day 0 (Fig. 12*b*) and day 7 of culture (Fig. 12*c*).

Freshly isolated vessels already harbored a significant number of CD11B$^+$ cells (92 ± 63 CD11B$^+$ cells / vessel), which were located within the adventitia as well as in residual meningeal tissue. Within 7 days of culture, half of the vessels did not show prominent expansion of CD11B$^+$ cells, while the rest displayed a ~17-fold increase (Fig. 12*d*). This was consistent with the ~50 % growth success of the CWFA, as described earlier. In PLX5622 pre-treated vessels, CD11B$^+$ cells were initially reduced by ~90 %, matching the previously established depletion efficiency of the CSF-1R inhibitor *in vivo*. After 7 days of culture, half of the vessels did not excel the maximal

amount of $CD11B^+$ cells found on day 0 (22 $CD11B^+$ cells / vessel) and therefore were assigned to a "growth failure" group. The rest showed a ~21-fold increase in $CD11B^+$ cells over time, which was comparable to the "growth success" subgroup of control samples. Single treatment with clodronate liposomes did not considerably reduce the amount of $CD11B^+$ cells / vessel at day 0. However, this was probably due to the latency between phagocytosis of liposomes and cell death, as all treated vessels showed a strongly decreased amount of $CD11B^+$ cells at day 7 and thus virtually no macrophage expansion. Accordingly, combinatory treatment (PLX5622 plus clodronate liposomes) started with reduced macrophage content at day 0, which was even further diminished at day 7. Importantly, emigration of fibroblast-like cells as well as vascular sprouting occurred in all treatment groups, arguing against general toxicity of the applied depletion regimens.

In conclusion, reducing mature macrophage input in CWFAs via PLX5622 pre-treatment still allowed macrophage growth at a similar rate as in untreated samples. It thus led to a proportionally diminished number of $CD11B^+$ cells at the end of the culture. Treatment with clodronate liposomes, however, completely abolished macrophage expansion. Assuming that the depletion regimens specifically targeted differentiated cells and not possible progenitors, this suggested that mature cell proliferation solely accounted for the increase in $CD11B^+$ cells.

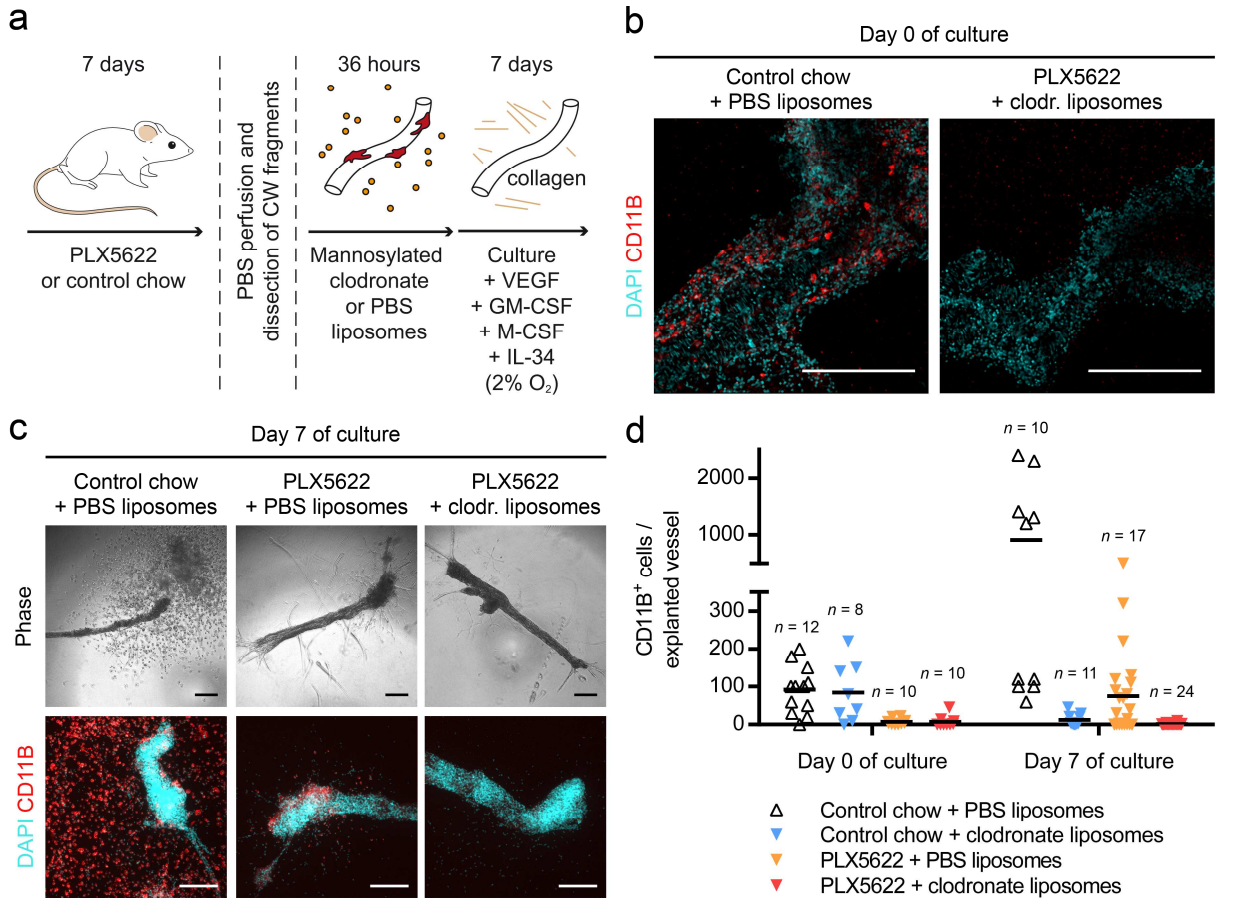

Figure 12 | Macrophage-depleted CW fragments failed to produce new macrophages *in vitro*. (**a**) Schematic overview of the experimental procedure, based on the CWFA protocol. Mice were treated with 1200 mg PLX5622 (kg chow)$^{-1}$ or control diet for 7 days. Intravascular cells were removed via PBS perfusion. Fragments of the CW were dissected and incubated with mannosylated clodronate or PBS liposomes, before embedding in a collagen matrix. Embedded vessels were cultured in the presence of growth factors for 7 days at hypoxia. (**b**) Combining PLX5622 pre-treatment with clodronate-liposomes eliminated CD11B$^+$ cells from vessel fragments. Representative whole-mount IFs of freshly embedded vessels are shown. Images are maximal projections of multiple Z-planes spanning the whole vessel. Scale bars: 250 µm. (**c**) Reduction of residual CD11B$^+$ vascular macrophages via PLX5622 pre-treatment led to respectively lower levels of CD11B$^+$ cells at day 7 of culture, while additional incubation with clodronate liposomes completely abolished macrophage expansion. Representative phase contrast images of cultured vessels as well as epifluorescent images of corresponding whole-mount IFs are shown. Scale bars: 250 µm. (**d**) Quantification of CD11B$^+$ cells in whole-mount IFs as described in **c**. Lines represent the mean. Data were pooled from two independent experiments including a total of n = 8 - 14 mice per group and time point (n in the figure indicate total replicates). Whenever possible, vessel fragments from each mouse were equally distributed among the different treatments.

3.2 Myeloid progenitors within the adult mouse brain

3.2.1 Rare clonogenic cells were detected in brain homogenates

As no evidence was found for macrophage precursors in cultures of CNS-associated vessels, the overall presence of hematopoietic progenitors was examined inside the adult brain. C57BL/6 mice at the age of 10 - 14 weeks were transcardially perfused with heparinized PBS to remove intravascular cells from organs (Fig. 13*a*). Single cell suspensions were prepared from the whole brain and tested for the presence of progenitors in collagen-based CFU assays.

Within 7 days of culture, cellular aggregates of varying size and shape arose from brain cell isolates (Fig. 13*b*), resembling colonies that derived from BM under the same conditions. Colony-forming units-culture (CFU-C) were rare in adult brain (7 ± 4 per 10^5 cells) compared to BM (373 ± 66 per 10^5 cells), but their frequency was within the magnitude of organs known to harbor extramedullary HSPCs, such as liver (12 ± 3 per 10^5 cells) or spleen (15 ± 4 per 10^5 cells) (Fig. 13*c*). Abundance of CFU-Cs among PB leukocytes (4 ± 3 per 10^5 cells) appeared to be slightly lower than in the brain, but the difference did not reach statistical significance. Importantly, adult brain harbored clearly more CFU-Cs than other non-hematopoietic organs tested, as heart cells only gave rise to < 1 CFU-Cs per 10^5 cells and no CFU-Cs were detected in kidney cell suspensions.

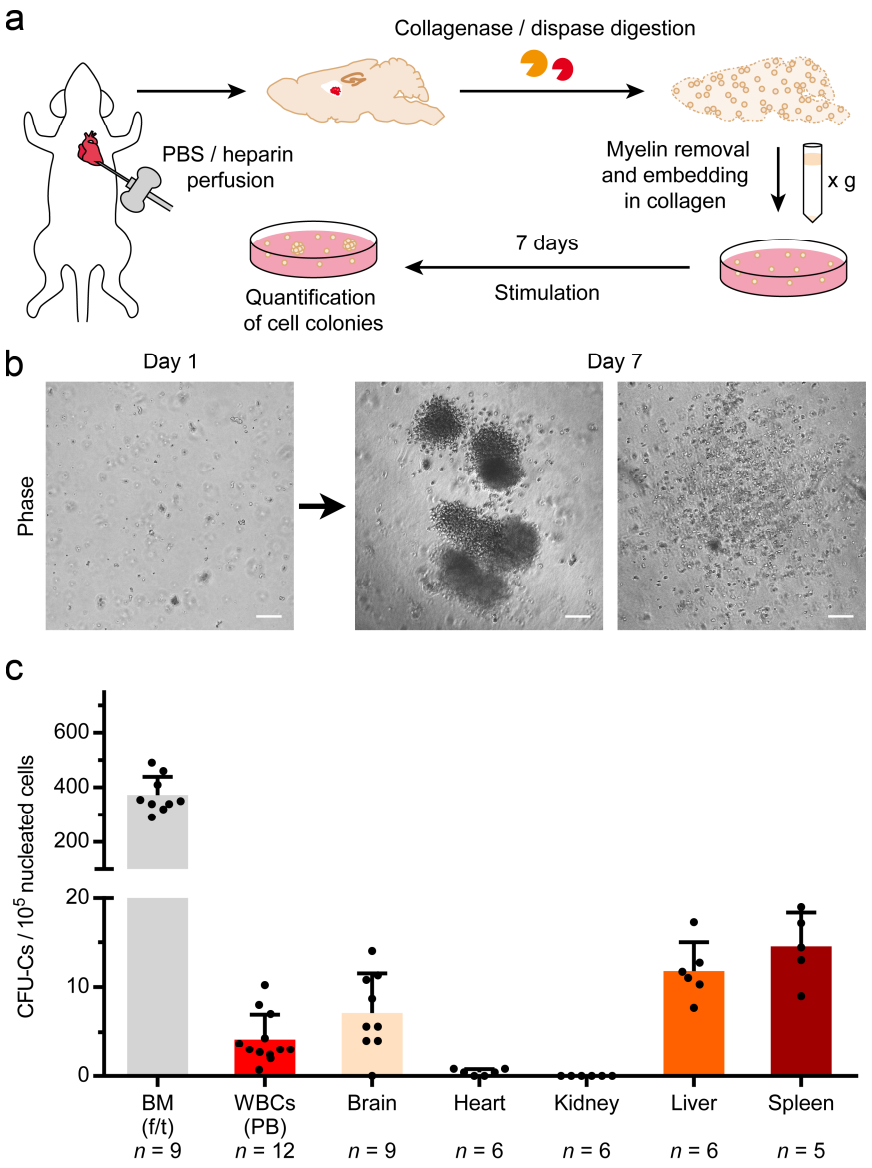

Figure 13 | Rare colony-forming units-culture (CFU-C) were detected in cell suspensions isolated from the brains of adult mice. (**a**) Schematic overview of the experimental procedure. Whole brains were harvested from transcardially perfused mice, minced and digested with collagenase/dispase to obtain single cell suspensions. Following myelin removal, cells were seeded in a collagen matrix and cultured in the presence of hematopoietic growth factors for 7 days in order to detect and quantify colony-forming cells. (**b**) Cell colonies of different morphologies developed in collagen-based CFU assays with adult brain cell isolates. Scale bars: 100 µm. (**c**) CFU-Cs were detected in different hematopoietic and non-hematopoietic tissues including the brain. Results represent the means of at least two independent experiments including a total of n = 5 - 12 mice per tissue. Error bars indicate SDs. BM: bone marrow; f/t: femur/tibia; WBCs: white blood cells; PB: peripheral blood.

3.2.2 CFU-Cs were enriched at the brain surface

To localize the rare CFU-Cs within the brain, the latter was dissected into multiple fractions from which single cells were isolated and analyzed in collagen-based CFU assays. The brain was split into a pooled fraction of hippocampus and olfactory bulbs, which harbor NSCs[189,190], the choroid plexus, which is an important entry route for PB cells[191,192], and a superficial layer including the meninges, which was peeled off the remaining cerebral tissue (Fig. 14*a*). Cells from hippocampus and olfactory bulbs rarely gave rise to colonies in CFU assays (0.2 ± 0.3 per 10^5 cells) and no CFU-Cs were detected in the choroid plexus (Fig. 14*b*). However, CFU-Cs were enriched within the meningeal fraction (3.4 ± 2.8 per 10^5 cells), while only 0.3 ± 0.3 CFU-Cs per 10^5 cells were observed in the remaining cerebrum. Within the cerebellum, from which the meninges had not been peeled off, 0.8 ± 0.8 CFU-Cs per 10^5 cells were detected.

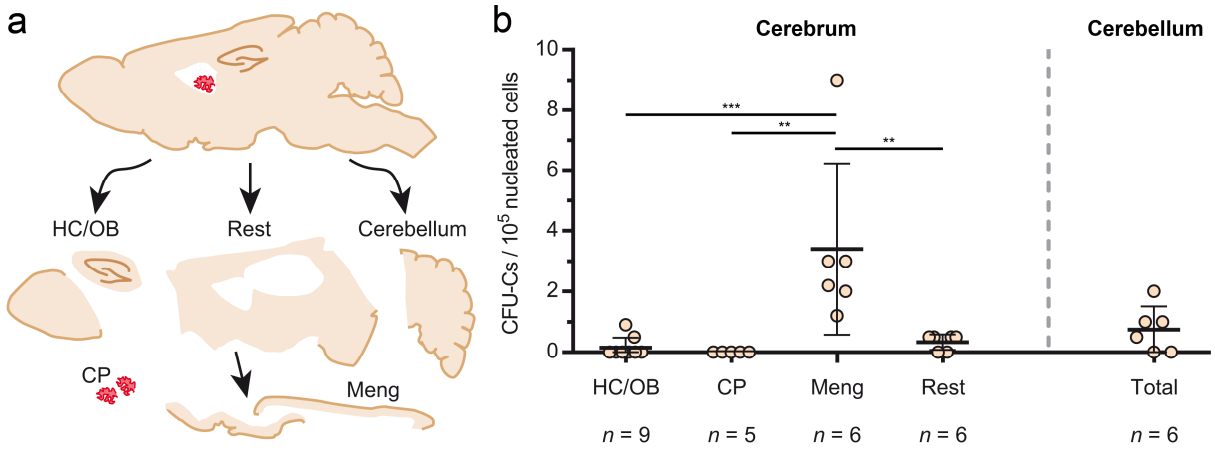

Figure 14 | CFU-Cs were enriched at the brain surface. (**a**) Schematic overview of brain dissection. The cerebrum of adult mice was split into the following fractions: hippocampus (HC) + olfactory bulbs (OB), choroid plexus (CP), meninges (Meng), and remaining cerebral tissue (Rest). The cerebellum was left intact. (**b**) Single cell suspensions were prepared from the different brain fractions as shown in **a** and analyzed in parallel in collagen-based CFU assays. Results represent the means of at least two independent experiments including a total of n = 5 - 9 mice. Error bars indicate SDs. Statistical analysis was performed using ordinary one-way ANOVA with Tukey's multiple comparisons test. $^{**}P < 0.01$, $^{***}P < 0.001$.

3.2.3 CFU-Cs resided behind the BBB and did not express markers of CNS macrophages

Next, it was examined whether brain-derived colonies in CFU assays actually indicated tissue-resident progenitors, or if they could be explained otherwise. The following alternative sources for clonogenic activity were suspected:

1. ***Spillover of BM cells from the skull***

During dissection of the brain, the skull was opened with scissors exposing its marrow (Fig. 15*a*), which naturally harbors a high frequency of CFU-Cs (Fig. 15*b*). A spill of ~10^4 BM cells would therefore suffice to generate the entire clonogenic activity found in the brain. This scenario would also explain the superficial localization of brain-derived CFU-Cs.

2. ***Circulating HSPCs being trapped inside the tissue intravascularly***

Although transcardial perfusion removes most of the circulating blood, it does not reliably eliminate all intravascular cells from tissues[193], which was also indicated by some visible red staining of erythrocytes within cell preparations. As HSPCs are constantly trafficking in the circulation, these might explain the CFU-Cs found in brain cell isolates.

3. ***Proliferation of mature CNS macrophages (or a subpopulation thereof)***

The capacity for self-renewal[75,125] and extensive proliferation[142,145,154] has been attributed to brain macrophages, including those in the subdural meninges[98]. Importantly, the collagen-based CFU assay included several growth factors, which have been shown to stimulate macrophage proliferation[194–197]. Hence division of mature phagocytes might have been the reason for colony formation.

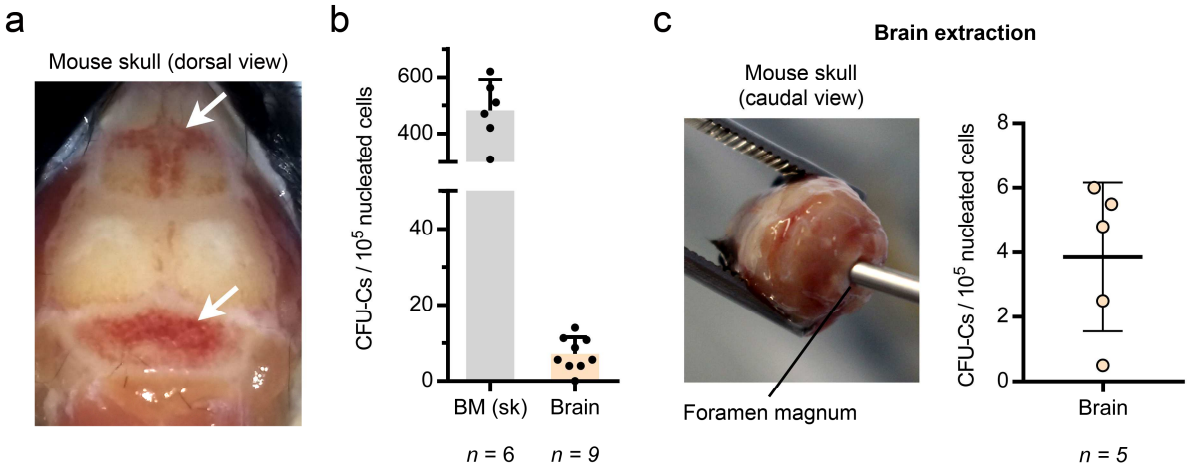

Figure 15 | CFU-Cs were detected within brain cell isolates even when leaving the skull intact during dissection. (**a**) Dorsal view of a mouse skull after transcardial perfusion. BM is indicated by remaining erythroid cells (arrows). (**b**) Mouse skull harbors high CFU-C activity. BM cells were isolated from the dorsal skull of adult mice and analyzed in collagen-based CFU assays. The result represents the mean of two independent experiments including $n = 6$ mice. The error bar indicates SD. Brain-derived CFU-C data from Fig. 13*c* was included as a reference. BM (sk): skull bone marrow. (**c**) Left: Photographic display of the procedure to isolate the brain without damaging the skull. Instead of opening the skull with scissors and risking a potential spill of skull BM onto the brain, the tissue was sheared inside the cranium and removed with a syringe through the foramen magnum. The isolate was analyzed in collagen-based CFU assays (right side). The result represents the mean of two independent experiments including a total of $n = 5$ mice. The error bar indicates SD.

In an initial experiment, a possible contamination by BM cells from the skull was addressed. This time, the skull was not cut with scissors to remove the brain. Instead, the brain was sheared inside the cranium with a small spatula and tissue fragments were flushed/sucked out with PBS, using a large needle inserted through the foramen magnum (Fig. 15*c*). Within the resulting single cell suspension, 4 ± 2 CFU-Cs per 10^5 cells were detected. This value was less than the frequency observed after normal brain dissection, which was possibly due to the harsher procedure or the incomplete retrieval of the meninges. Still, it demonstrated that BM contamination alone could not account for the observed clonogenic activity within brain cell isolates.

Next, a cell sorting approach was set up to simultaneously examine the contribution of circulating and BM-resident HSPCs as well as mature CNS macrophages to the clonogenic activity within brain cell suspensions. In this experiment, the B6.Iba1-GFP reporter strain was used, which tags mature CNS macrophages via endogenous GFP expression[198]. To label intravascular and BM-resident cells, mice were intravenously (i.v.) injected with anti-CD45 APC antibody (Fig. 16*a*)[193,199]. Within a circulation time of 5 min, 5 µg of antibody stained nearly all $CD45^+$ leukocytes in PB, which includes circulating HSPCs (Fig. 16*b*). A significant fraction of skull BM cells (29 ± 5 %) was also labeled by this approach, resulting from leakage of antibody through the fenestrated BM sinusoids[199]. Importantly, increasing the antibody amount (10 µg) and circulation time (60 min) led to efficient labeling of skull BM (85 ± 7 %). To assure that HSPCs were stained via this method, skull BM was prepared from anti-CD45 APC injected mice and sorted based on APC fluorescence. In subsequent CFU assays, clonogenic activity was distributed over the APC^- as well as the APC^+ fraction (Fig. S2), demonstrating the functionality of the approach.

Following i.v. injection, mice were sacrificed and transcardially perfused to remove excess antibody. Single cells were prepared from the brain and fractionized via cell sorting (for upstream gating see Fig. S3). Cells that had been stained by the injected antibody (IV-$CD45^+$) were removed from the suspension. The remaining fraction was split into GFP^+ CNS macrophages and a GFP^- "non-macrophage" population. Subsequent to cell sorting, viable cells were counted and analyzed in collagen-based CFU assays.

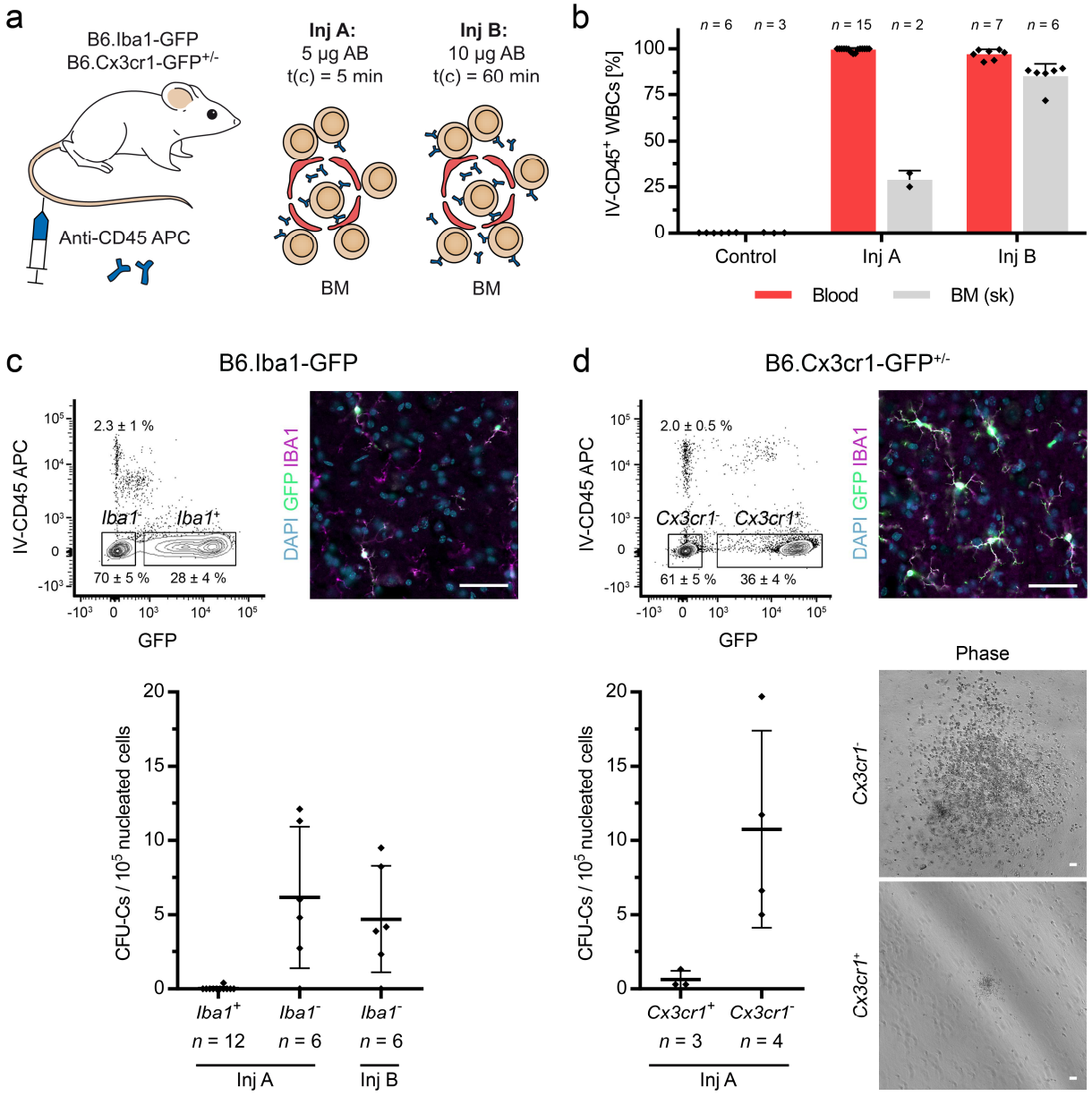

Figure 16 | CFU-Cs resided behind the BBB and did not express markers of resident CNS macrophages. (**a**) Overview of the experimental procedure. B6.Iba1-GFP and B6.Cx3cr1-GFP$^{+/-}$ mice were intravenously (i.v.) injected with anti-CD45 APC antibody, following injection (Inj) scheme A or B. AB: antibody; t(c): circulation time; BM: bone marrow. (**b**) I.v. injected anti-CD45 antibody efficiently labeled BM-resident cells and/or circulating white blood cells depending on the injection scheme applied, as demonstrated by flow cytometry. WBCs: white blood cells; BM (sk): skull bone marrow. Results represent the means of at least two independent experiments including a total of n = 2 - 15 mice per group. Error bars indicate SDs. (**c**) Brain-derived CFU-Cs were contained within the *Iba1*$^{-}$ ("non-macrophage") fraction and were not affected by the removal of IV-CD45^{+} cells from brain isolates. B6.Iba1-GFP mice

Figure 16 (continued) were injected i.v. with anti-CD45 antibody, following scheme A (labeling intravascular cells) or B (labeling intravascular and BM cells) as shown in **a** and **b**. Labeling of CNS macrophages in the reporter strain was demonstrated by IBA1 IHC-fr of parenchymal brain sections. Scale bar: 50 µm. Whole brain cell suspensions were prepared from injected mice and sorted according to the depicted gating scheme, removing IV-CD45$^+$ cells and splitting the remaining population into *Iba1*$^+$ (GFP$^+$) and *Iba1*$^-$ (GFP$^-$). The CFU-C content in different fractions was analyzed in collagen-based CFU assays at day 7. Results represent the means of at least two independent experiments, including a total of n = 6 - 12 mice per group. Error bars indicate SDs. (**d**) Brain CFU-Cs mainly resided in the *Cx3cr1*$^-$ fraction. Cx3cr1-GFP$^{+/-}$ mice were treated as described in **c**. Results represent the means of one experiment including n = 3 - 4 mice. Error bars indicate SDs. CFU-Cs within the *Cx3cr1*$^+$ fraction only gave rise to small colonies as shown in representative phase contrast images taken at day 7 of culture. Scale bars: 50 µm. All plots are contour plots with 5 % contour levels including outliers.

In contrast to the "non-macrophage" population, *Iba1*$^+$ (GFP$^+$) cells displayed virtually no clonogenic activity at day 7 of culture (Fig. 16*c*), which was not due to a lacking co-stimulation by other brain cells (Fig. S4). More importantly, removing IV-CD45$^+$ cells did not reduce CFU-C frequency in the *Iba1*$^-$ (GFP$^-$) fraction, regardless of which injection scheme was applied. This demonstrated that neither intravascular HSPCs nor skull BM accounted for CFU-Cs in brain cell isolates. Accordingly, it suggested that CFU-C resided behind the continuous endothelium of the BBB, as they were not reached by the injected anti-CD45 antibody.

Finally, because most research on CNS macrophage self-renewal is based on *Cx3cr1* lineage tracing[98,142,145,200], the possibility of an immature *Iba1*$^-$ *Cx3cr1*$^+$ clonogenic subpopulation of CNS macrophages was excluded. To this end, the sorting experiment was repeated with B6.Cx3cr1-GFP$^{+/-}$ reporter mice (Fig. 16*d*). Consistent with previous results, clonogenic activity was mainly contained in the *Cx3cr1*$^-$ (GFP$^-$) fraction. Although some *Cx3cr1*$^+$ (GFP$^+$) cells gave rise to colonies, the latter were about 20-times less frequent and also considerably smaller than the ones deriving from the inverse population.

3.2.4 Brain-derived CFU-Cs displayed complete erythro-myeloid potential *in vitro*

CFU assays can reveal the quantity, but also the quality of progenitors. This is based on the cell types developing within a single colony, which can be deduced from the morphology of the cluster. Diverse colony shapes in the collagen-based CFU assay already implied that multiple cell types were generated from brain-resident CFU-Cs. However, while the collagen-based assay has several advantages, such as easier scalability as well as the possibility of staining and fixing colonies for long-term storage, it is not suited for colony grading. Methylcellulose-based assays allow a better resolution of colony types because of their superior optical clarity. The latter was therefore chosen to assess the differentiation potential of brain-resident CFU-Cs.

Within cultures of brain-derived cells, colonies of all erythro-myeloid cell types, including mixed colonies, were identified (Fig. 17). These comprised (but were not limited to) burst-forming units-erythroid (BFU-E), colony-forming units-megakaryocyte (CFU-Mk), colony-forming units-granulocyte (CFU-G), colony-forming units-macrophage (CFU-M), and colony-forming units-granulocyte/macrophage (CFU-GM). Colony types were verified via Pappenheim staining of cytospins prepared from individual colonies. Consistently, macrophages positive for the markers IBA1, F4/80, CD11B, and PU.1 as well as $Ly6G^+$ neutrophils and $GP1B\alpha^+$ megakaryocytes could be differentiated from brain cells in suspension culture (Fig. S5).

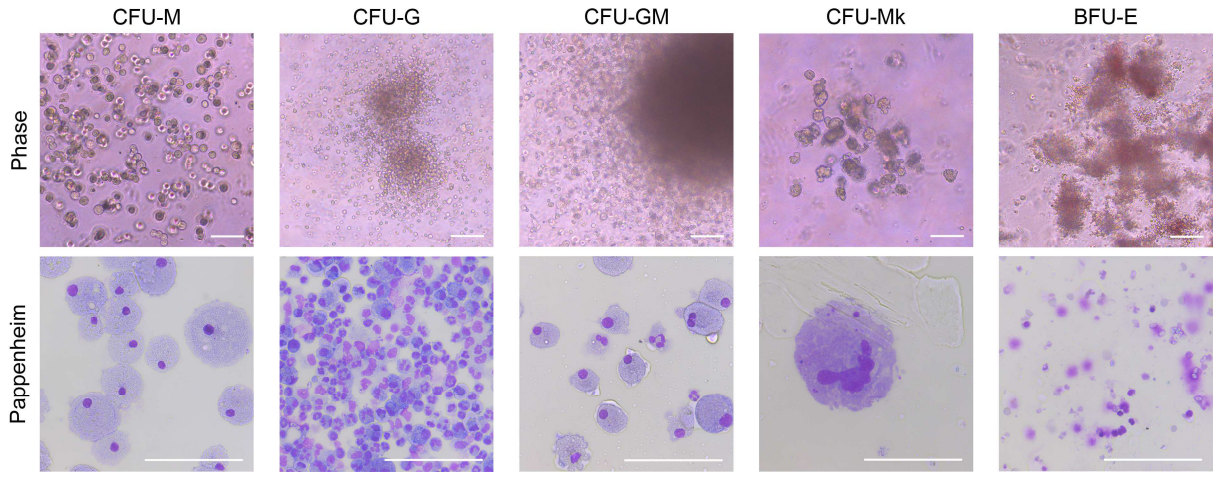

Figure 17 | Brain-derived CFU-Cs displayed complete erythro-myeloid potential *in vitro*. Single cell suspensions were prepared from brains of adult mice and analyzed in methylcellulose-based CFU assays. Arising colony types were microscopically assessed at day 7 - 10 of culture and verified via Pappenheim staining of cytospins prepared from individual colonies. Representative phase contrast images and corresponding Pappenheim stainings are shown. Scale bars: 100 µm. CFU-M: colony-forming unit-macrophage; CFU-G: colony-forming unit-granulocyte; CFU-GM: colony-forming unit-granulocyte/ macrophage; CFU-Mk: colony-forming unit-megakaryocyte; BFU-E: burst-forming unit-erythroid.

3.2.5 Adult brain produced a unique pattern of colony types compared to BM and PB

In a next step, the ratios of most abundant colony types that developed in methylcellulose-based CFU assays (BFU-E, CFU-G, CFU-M, CFU-GM) were compared between brain, PB, and BM (Fig. 18). It was found that the CFU patterns significantly differed between these tissues. In detail, brain resembled PB as both tissues harbored a relatively high frequency of BFU-E (PB: 45 ± 12 %, brain: 34 ± 11 %) compared to BM (12 ± 3 %). Conversely, brain most strikingly differed from PB by its high abundance of CFU-GM (PB: 4 ± 4 %, brain: 15 ± 9 %), which in turn was similar to BM (14 ± 6 %). Importantly, the colony pattern of BM was independent of the anatomical site and did not significantly differ between femur/tibia and skull.

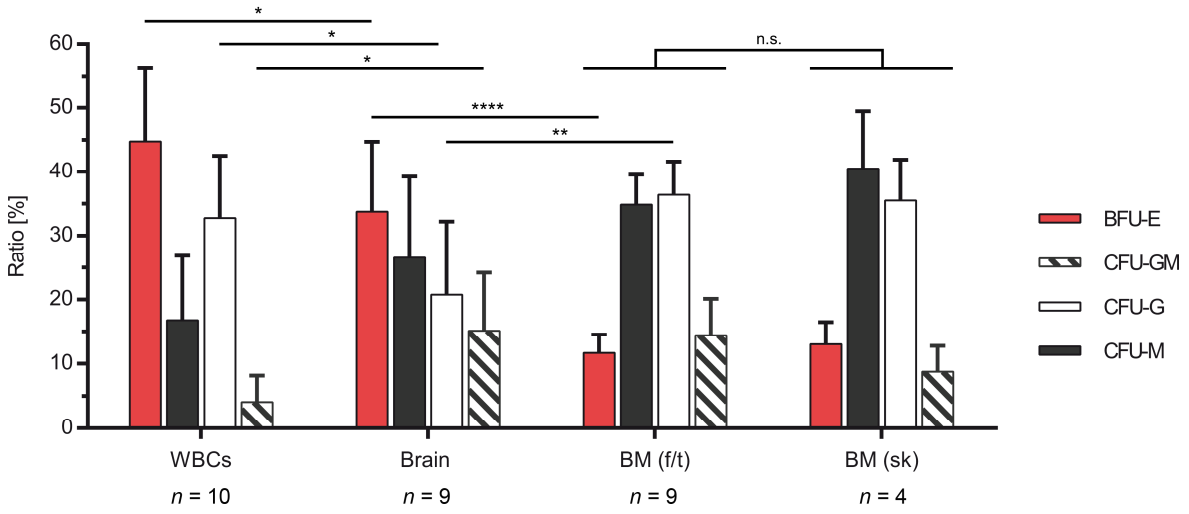

Figure 18 | Adult brain produced a unique pattern of colony types compared to BM and PB. Cell isolates from brain, mixed PB, and BM (skull or femur/tibia) were analyzed in methylcellulose-based CFU assays. At day 7 - 10 of culture, colonies were microscopically graded into different types (BFU-E, CFU-M, CFU-G, CFU-GM, see Figure 17). As the cumulative frequency of other colony types, such as CFU-Mk, was < 5 % in all tissues, the latter were not included into the analysis. Results represent the means of at least two independent experiments including a total of n = 4 - 10 mice. Error bars indicate SDs. For each mouse, every tissue was analyzed in parallel. Statistical analysis was performed using ordinary two-way ANOVA with Tukey's multiple comparisons test. *P < 0.05, **P < 0.01, **** P < 0.0001, n.s.: non-significant. WBCs: white blood cells; BM: bone marrow; f/t: femur/tibia; sk: skull.

3.2.6 Brain-derived CFU-Cs constituted a heterogeneous population displaying the immunophenotype of BM-resident myeloid progenitors

After having determined the myeloid differentiation potential of brain-resident CFU-Cs, their immunophenotype was examined. To this end, brain-derived cells were split into various fractions via cell sorting, which were individually tested in subsequent collagen-based CFU assays. Sequential experiments demonstrated that brain-resident progenitors were exclusively contained within the $CD45^+$ LIN^- (CD5, TER-119, CD11B, 7-4, CD45R, GR-1) $SCA\text{-}1^-$ $c\text{-}KIT^+$ population (Fig. 19*a*), which also defines MyPs in the adult BM[16].

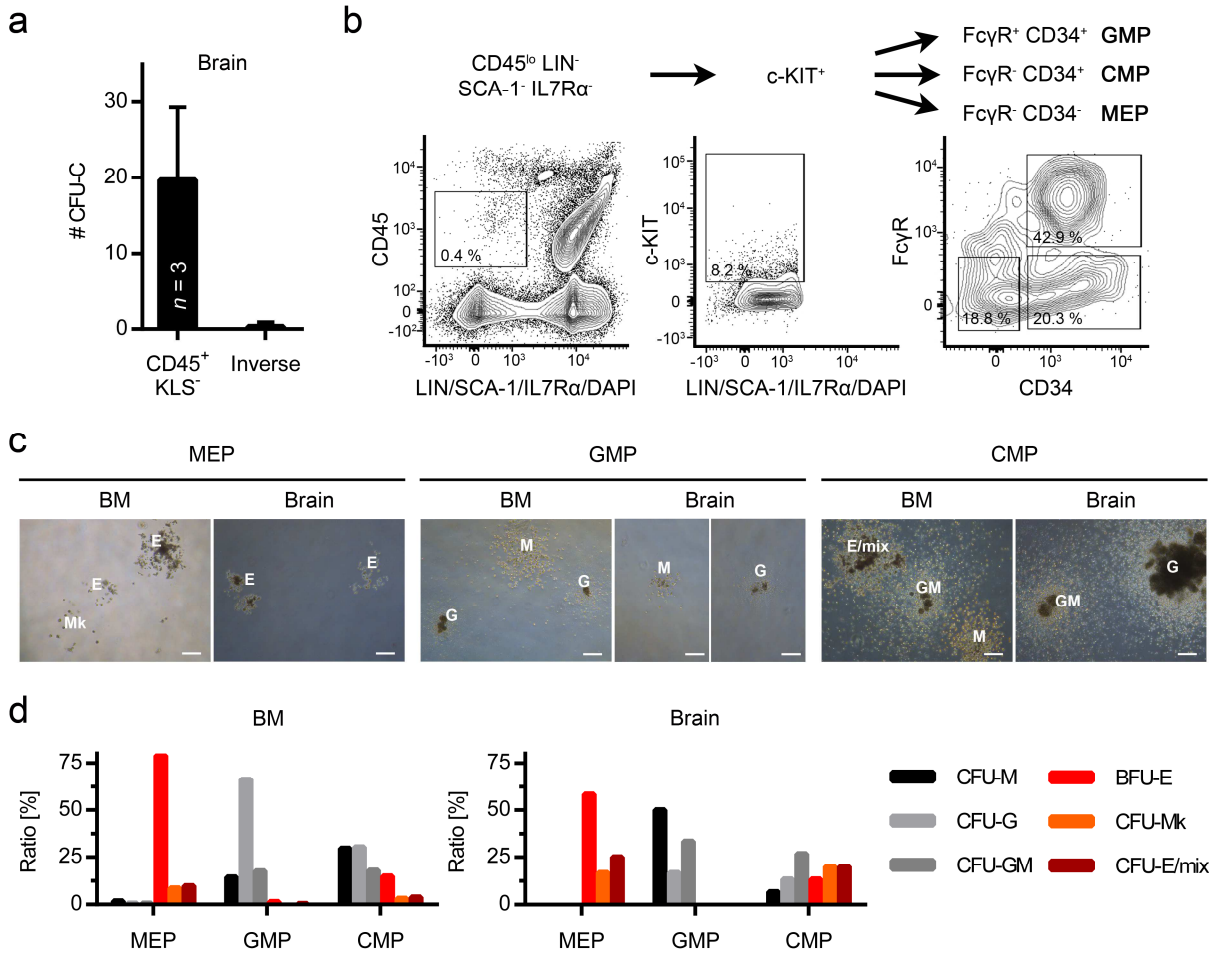

Figure 19 | Brain-derived CFU-Cs constituted a heterogeneous population and displayed the same immunophenotype as BM-resident myeloid progenitors. (**a**) Brain-derived CFU-Cs were exclusively contained within the CD45$^+$ LIN$^-$ SCA-1$^-$ c-KIT$^+$ (CD45$^+$ KLS$^-$) population. Brain homogenates from adult mice were successively sorted into various cell fractions and their CFU-C content was analyzed in collagen-based CFU assays at day 7 - 14 of culture. Shown are the absolute number of colonies that developed within the CD45$^+$ KLS$^-$ fraction (or parts of the complete phenotype) versus the cumulative number of colonies found in inverse populations. Results represent the means of three independent experiments. Error bars indicate SDs. (**b**) Gating strategy to sort CD45$^{+/lo}$ LIN$^-$ SCA-1$^-$ IL7Rα$^-$ c-KIT$^+$ MyPs from brain or BM isolates (representative plots of brain cells are depicted), which were further divided into FcγR$^+$ CD34$^+$ granulocyte/macrophage progenitors (GMP), FcγR$^-$ CD34$^+$ common myeloid progenitors (CMP) and FcγR$^-$ CD34$^-$ megakaryocyte/erythrocyte progenitors (MEP). Depicted plots are contour plots with 5 % contour levels including outliers. Full gating included upstream steps to exclude debris and to select single cells based on FSC/SSC characteristics. If applicable, gating was guided by isotype and FMO controls. (**c, d**) Sorted MyP fractions from brain and BM showed comparable *in vitro*

Figure 19 (continued) potential. Brain and BM cells were sorted into the GMP, CMP, and MEP phenotypes as described in **b** and corresponding CFU types were analyzed in methylcellulose-based CFU assays at day 7. (**c**) Representative phase contrast images of CFU assays conducted with the different MyP fractions from brain and BM. E: erythroid; Mk: megakaryocyte; G: granulocyte; M: macrophage; E/mix: mixed erythroid (including at least an erythroid component plus megakaryocytes, macrophages, or granulocytes); GM: granulocyte/macrophage. Scale bars: 250 µm. (**d**) Ratio of CFU types within the different MyP fractions sorted from BM and brain. Sorting into GMPs, CMPs, and MEPs was performed once.

In a next step, brain-resident CFU-Cs were identified via the MyP surface phenotype ($CD45^{+/lo}$ LIN^- $IL7R\alpha^-$ $SCA\text{-}1^-$ $c\text{-}KIT^+$) and further split into the phenotypes of CMPs, MEPs, and GMPs based on the differential expression of Fcγ receptor (FcγR) and $CD34^{16}$ (Fig. 19*b*). Sorted cells were analyzed in methylcellulose-based CFU assays. The resulting colony-patterns were compared to a positive control from BM. As expected, BM-derived MEPs gave rise to erythroid colonies including BFU-E, CFU-Mk, and CFU-E/mix, while GMPs produced CFU-M, CFU-G, and CFU-GM (Fig. 19*c* and *d*). CMPs exhibited clonogenic potential that comprised both myeloid branches. Also, average colony size was larger than in the other two progenitor fractions, in accordance with the less committed phenotype of CMPs (Fig. S6). Importantly, brain-derived progenitors behaved similarly when split into CMP, MEP, and GMP fractions. They therefore constituted a heterogeneous cell population that resembled BM-resident MyPs in immuno-phenotype and associated potential.

3.2.7 Brain-derived hematopoietic colonies had a history of *Flt3* expression

During the embryonal period, YS-derived EMPs and their progeny invade the developing brain to establish the microglia pool[26,101,102]. Some of these progenitors might quiescently persist into early adulthood and give rise to colonies in CFU assays. To elaborate the origin of brain-resident progenitors, the *Flt3*^{Cre} x *Rosa26*$^{mT/mG}$ model was used, which stably labels fetal and adult HSC-derived MPPs and their progeny via a switch from tomato to GFP expression[27,201,202] (Fig. 20*a*). To this end, single cell suspensions were prepared from PB, skull BM, and brains of adult *Flt3*^{Cre} x *Rosa26*$^{mT/mG}$ mice.

Flow cytometric analysis demonstrated the functionality of the model, as about 90 % of CD45^{+} cells in PB and skull BM were *Flt3*^{Cre} GFP^{+} (Fig. 20*b*). In brain, HSC-derived lymphocytes (CD45^{hi}, CD11B^{-} cells) thus could be clearly distinguished from YS-derived microglia (CD45^{lo} CD11B^{+} cells), which remained tomato^{+}. Cells from skull BM and brain were analyzed in collagen-based CFU assays and colonies were assessed for tomato and GFP fluorescence (Fig. 20*c*).

In accordance with the flow cytometry data, 86 ± 10 % of BM-derived colonies were GFP^{+}. The proportion of GFP^{+} colonies was slightly decreased when analyzing brain cells, but the majority was still *Flt3*^{Cre} GFP^{+} (68 ± 8 %). Thus, even if it cannot be excluded that some *Flt3*-independent progenitors persisted in the brains of adult mice, most brain-derived cell colonies showed a history of *Flt3* expression, pointing to descendance from fetal or adult HSCs.

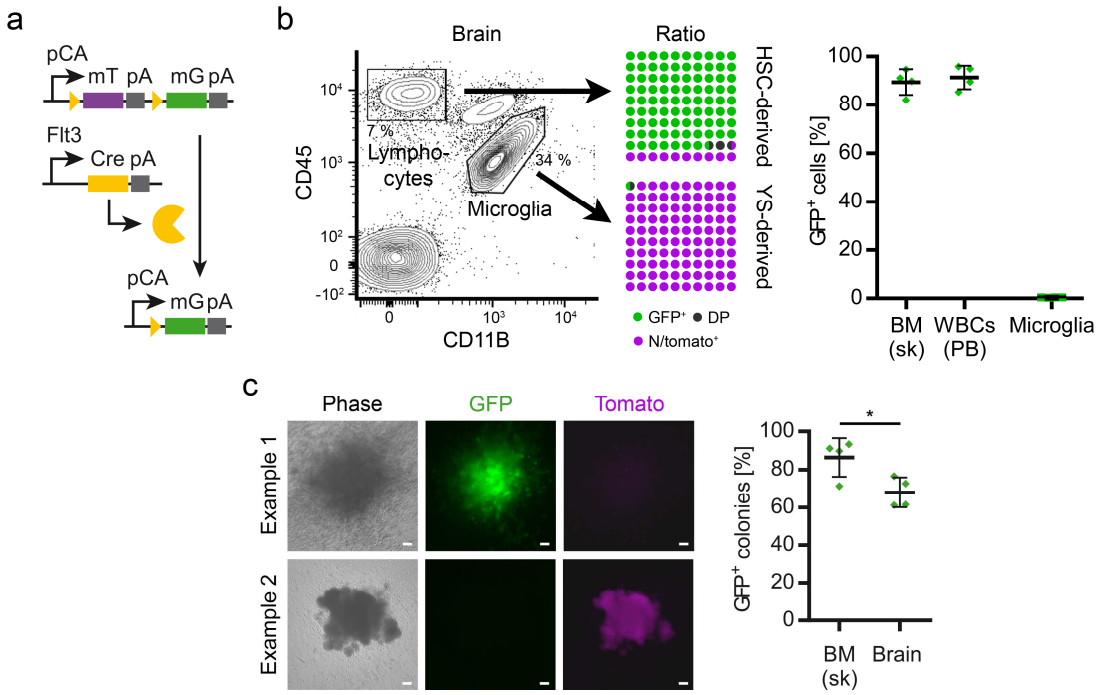

Figure 20 | Brain-derived hematopoietic colonies had a history of *Flt3* expression. (**a**) Principle of tracing *Flt3*$^{+}$ cell progeny in *Flt3*^{Cre} x *Rosa26*$^{mT/mG}$ mice. Every cell is labeled by ubiquitously expressed tomato. As cells activate the *Flt3* promoter, the tomato gene gets excised by Cre recombinase, enabling stable expression of a downstream GFP gene[202]. pCA: chicken β-actin promoter; mT: membrane-targeted tomato; mG: membrane-targeted GFP; pA: polyadenylation sequence. (**b**) The *Flt3*^{Cre} model distinguishes between different cell ontogenies. Single cell suspensions were prepared from BM, PB, and brains of adult *Flt3*^{Cre} x *Rosa26*$^{mT/mG}$ mice and analyzed by flow cytometry. BM and PB cells were pre-gated on CD45^{+} hematopoietic cells. HSC-derived cells in PB, BM and brain were predominantly *Flt3*^{Cre} GFP^{+}, while CD45^{lo} CD11B^{+} microglia that descend from the YS remained tomato^{+}. The depicted FACS plot is a contour plot with 5 % contour levels including outliers. Each colored dot of the ratio dot plot represents 1 % of cells. DP: double positive; N/tomato: negative or tomato-positive; BM (sk): skull bone marrow; WBCs: white blood cells; PB: peripheral blood. Results represent the means of two independent experiments including a total of $n = 4$ mice. Error bars indicate SDs. (**c**) Hematopoietic colonies that derived from the BM and brain of *Flt3*^{Cre} x *Rosa26*$^{mT/mG}$ mice were mostly GFP^{+}. Single cell suspensions were prepared from skull BM and brains of *Flt3*^{Cre} x *Rosa26*$^{mT/mG}$ mice and analyzed in collagen-based CFU assays. Tissues from each mouse were always analyzed in parallel. Tomato and GFP fluorescence of colonies was examined at day 7 of culture. Results represent the means of two independent experiments including a total of $n = 4$ mice. Error bars indicate SDs. Statistical analysis was performed using a paired Student's *t* test. *$P < 0.05$. Scale bars: 250 µm.

3.3 No evidence for progenitor contribution during forced CNS macrophage repopulation *in vivo*

3.3.1 CNS macrophages rapidly repopulated the brain after transient PLX5622 treatment

In order to test the contribution of brain-resident MyPs to the CNS macrophage pool, forced repopulation of microglia/macrophages was studied *in vivo*. To this end, macrophages were depleted from the brains of living mice using the CSF-1R inhibitor PLX5622, as described earlier. It has been shown that CNS macrophages rapidly repopulate the brain upon inhibitor withdrawal[154,203,204]. To determine the kinetics of this process, female C57BL/6 mice at the age of 6 weeks were fed with 1200 mg PLX5622 (kg chow)$^{-1}$ for 7 days to deplete CNS macrophages, before switching to standard chow to induce their repopulation. Mice were sacrificed after depletion or during the recovery period at days 1, 2, 3, 7, and 14 after drug withdrawal. Eventually, the density of IBA1$^+$ microglia/macrophages was analyzed in the neocortical region of sagittal brain slices (Fig. 21*a*).

In accordance with previous results, PLX5622-treatment reduced IBA1$^+$ cells in the brain by ~90 % (Fig. 21*b* and Fig. S7*a*). One day after inhibitor withdrawal, the density of CNS macrophages remained unchanged. Yet the surviving cells started displaying an activated morphology with thickened cell processes and elevated IBA1-immunoreactivity (Fig. 21*a*). Activation of repopulating cells was also evident from CD45 upregulation and increased cell size (Fig. S7*b* and *c*). Expansion of IBA1$^+$ cell numbers was already noticeable at day 2 of recovery. One day later, microglia/ macrophage density had almost reached its original value. At day 7 of recovery, IBA1$^+$ cells were about twice as abundant as in control samples, before they returned to normal levels at day 14.

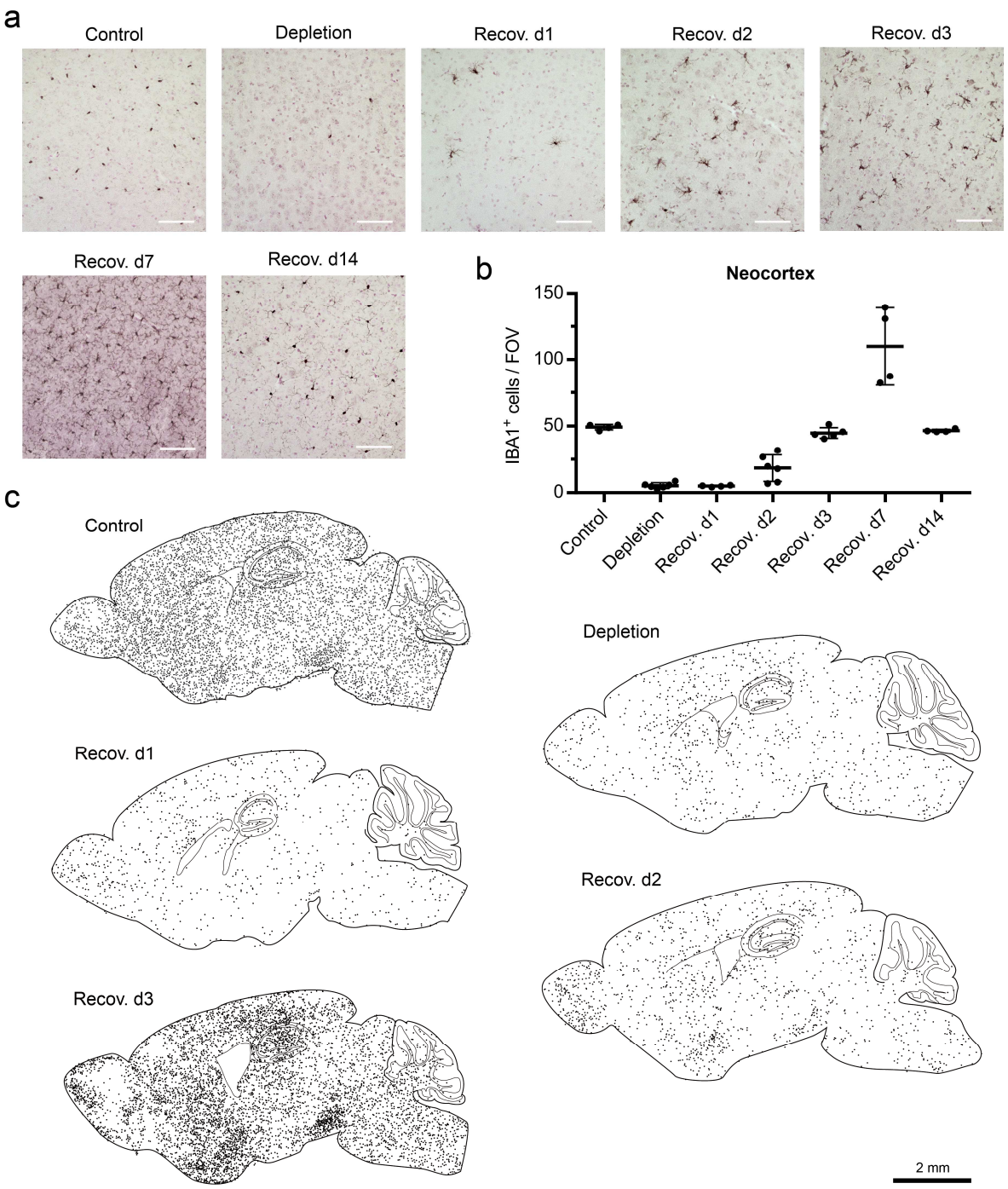

Figure 21 | CNS macrophages rapidly repopulated the brain after transient PLX5622 treatment. (**a**) Representative fields of view (FOV) within the neocortical region, taken from IBA1-immunostained sagittal brain sections of mice that had been fed with 1200 mg PLX5622 (kg chow)$^{-1}$ for 7 days (depletion) or had been allowed to recover (recov.) for 1 - 14 days following withdrawal of the drug. Scale bars: 100 µm. (**b**) IBA1^{+} cell densities in the neocortex during the experiment described in **a**. For each mouse, 2 x 3 FOVs were analyzed within the neocortical region of two 10 µm sagittal brain slices with a spacing

Figure 21 (continued) of 30 µm. Results represent the means of one experiment including n = 4 - 6 mice per group/time point. Error bars indicate SDs. (**c**) The spatial pattern of early CNS macrophage repopulation appeared heterogeneous, but seemed to correlate with varying regional microglia/ macrophage densities under homeostatic conditions. Whole sagittal brain sections are shown, which derived from the same experiment described in **a**. IBA1$^+$ cells were manually selected in ImageJ using the multi-point tool. Eventually, dots were extracted from the image and projected onto a drawing of the respective section. Images are representative of n = 5 - 10 mice per group/time point and two independent experiments.

When studying whole sagittal brain sections during the early repopulation period (days 1 - 3 after drug withdrawal), CNS macrophage recovery did not appear to originate from concise proliferative niches such as the meninges (Fig. 21*c*). Still, the spatial distribution of repopulating cells at day 2 and 3 seemed heterogeneous and apparently reproduced regional differences in homeostatic brain macrophage density. Interestingly, clusters of multiple IBA1$^+$ repopulating cells (with merging cell borders) were not encountered during the observation period. Instead, CNS macrophages were loosely scattered, although in varying regional concentrations.

In a second, independent experiment, mRNA levels of *Cx3cr1* and *Transmembrane protein 119* (*Tmem119*) were quantified in the brain during the repopulation period (Fig. 22*a*). *Cx3cr1* is strongly expressed in all CNS macrophages[98,205], while *Tmem119* has been shown to specifically mark mature microglia[206]. The experiment largely confirmed the kinetics determined by IHC-P, as global *Cx3cr1* mRNA levels showed a strong reduction following PLX5622-treatment, rapid rebound after drug withdrawal, overshoot, and eventually returned to original expression at day 14 of recovery. However, repopulation seemed to proceed more slowly in this experiment, as *Cx3cr1* mRNA expression only reached about 50 % of control levels on day 3 of recovery. This was not due to a lack of correlation between global *Cx3cr1* mRNA expression and CNS macrophage density or regional differences in repopulation, as correspondingly lower numbers of IBA1$^+$ cells were confirmed via IHC-P (Fig. S8).

Compared to *Cx3cr1, Tmem119* mRNA expression recovered more slowly in the brain and did not return to control levels even 14 days after PLX5622 withdrawal. This might be due to the downregulation of *Tmem119* upon cell activation[206], which would be consistent with CNS macrophages still showing a slightly more activated morphology including increased IBA1-immunoreactivitiy at the day 14 time point (Fig. 21*a*). Nevertheless, the slowly recovering *Tmem119* mRNA levels were in support of recently published studies demonstrating that forced microglia repopulation occurs independently of infiltrating monocytes[145,159], as the latter have been shown to not acquire microglia signature genes such as *Tmem119* upon CNS engraftment[139–142]. Likewise, *Ccr2* mRNA levels were not elevated in the brain during repopulation (Fig. 22*b*) and the fraction of Ly6C$^+$ myeloid cells in the CNS remained unchanged (Fig. S7*d*). This further argued against an invasion of CCR2$^+$ Ly6C$^+$ inflammatory monocytes, even though peripheral monocytes recovered more quickly after PLX5622 withdrawal and were up to 4 times more abundant in PB during the early recovery period (Fig. S9).

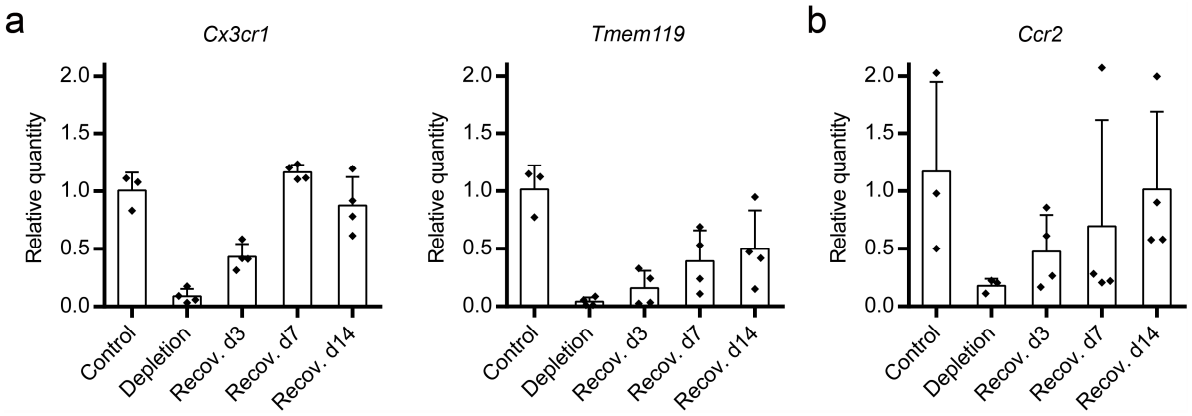

Figure 22 | Characterization of forced CNS macrophage repopulation via RT-qPCR. (**a**) *Cx3cr1* mRNA expression dropped to 10 % of control levels in the brain following treatment with PLX5622, but returned to homeostatic levels within 14 days after drug withdrawal. The microglia signature gene *Tmem119* showed a slower course of recovery. Mice were sacrificed directly after treatment with

Figure 22 (continued) 1200 mg PLX5622 (kg chow)$^{-1}$ for 7 days (depletion) or during the recovery (recov.) period at days 3, 7, and 14 following withdrawal of the drug. Gene expression was measured by quantitative RT-PCR in lysates of one brain hemisphere, relative to the housekeeping gene *Gapdh*. (**b**) *Ccr2* mRNA did not increase in the brain during forced CNS macrophage repopulation, arguing against an invasion of CCR2^{+} inflammatory monocytes. Mice were treated and analyzed as described in **a**. Results represent the means of one experiment including n = 3 - 4 mice per group/time point. Error bars indicate SDs.

3.3.2 The frequency of CFU-Cs in the brain was unaltered during PLX5622-mediated CNS macrophage depletion and early recovery

In an approach to examine the contribution of brain-resident MyPs to CNS macrophages, clonogenic activity in the brain was analyzed during forced repopulation. It was hypothesized that the elimination of brain macrophages should constitute an activating stimulus that might induce transient expansion of a contributing progenitor pool in order to fuel the rapid recovery to homeostatic cell numbers. To this end, female C57BL/6 mice at the age of 10 - 13 weeks were fed with 1200 mg PLX5622 (kg chow)$^{-1}$ for 7 days to deplete CNS macrophages, before changing the food to normal chow to induce their repopulation (Fig. 23*a*). Mice were sacrificed after PLX5622 treatment or during the early recovery period (days 1 - 3), as progenitor expansion was assumed to take place before significant increase of mature microglia/macrophages, which were shown to return to normal numbers already at day 3 after drug withdrawal. Clonogenic activity in brain cell isolates was quantified via collagen-based CFU assays.

Right after PLX5622 treatment as well as at day 1 of recovery, CFU-C frequencies were within range of control values (control: 5.1 ± 3.4 per 10^5 cells; depletion: 3.9 ± 3.4 per 10^5 cells; d1 of recovery: 5.5 ± 0.5 per 10^5 cells) (Fig. 23*b*). At day 2, the CFU-C frequency appeared to increase (9.4 ± 7.9 per 10^5 cells), before returning to control levels at day 3 (4.3 ± 2.1 per 10^5 cells). However, the increase at day 2 was mainly owed to a single outlier value. Its removal

would have lowered the mean CFU-C frequency to 6.8 ± 4.2 per 10^5 cells. In general, no statistically significant difference was detected between the recovery time points and the control group. Same was true for CFU-Cs in PB, which were assessed simultaneously as a control.

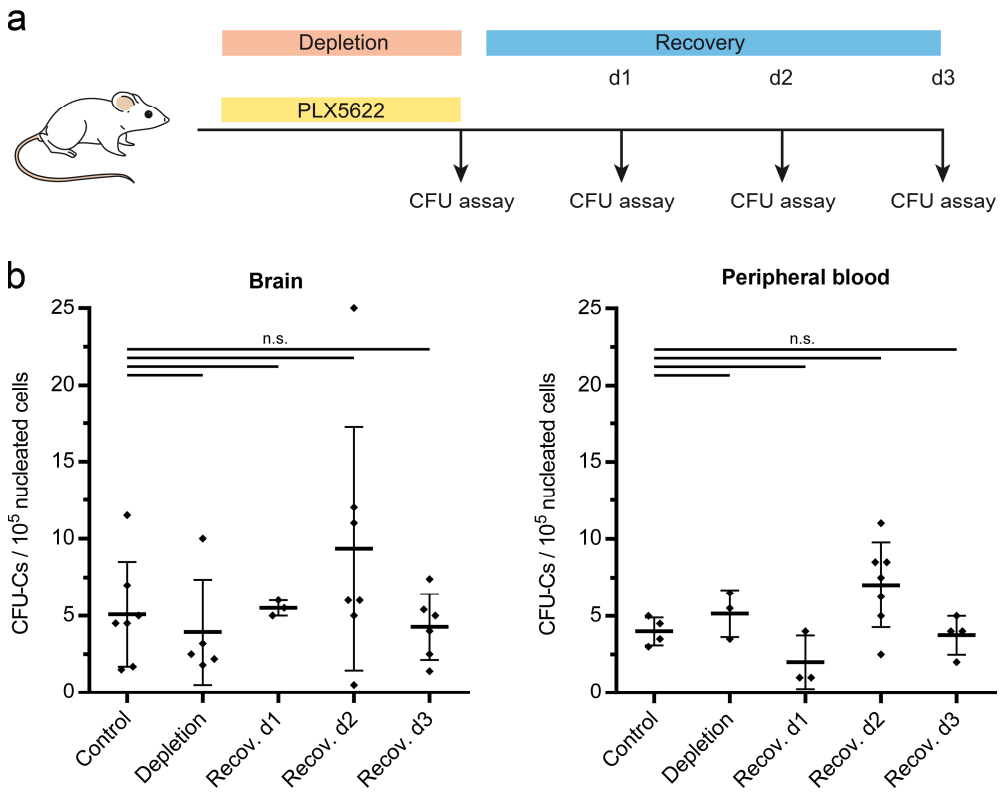

Figure 23 | CFU-C frequency in the brain and PB was unaltered during PLX5622-mediated CNS macrophage depletion and early recovery. (**a**) Overview of the experimental setting. Mice were fed with 1200 mg PLX5622 (kg chow)$^{-1}$ for 7 days (depletion) and analyzed 1, 2, and 3 days following withdrawal of the drug (recovery). Mixed PB and brain were examined in collagen-based CFU assays. (**b**) CFU-C frequencies in brain and mixed PB during the experiment described in **a**. Results represent the means of up to three independent experiments including a total of n = 3 - 7 mice per group/time point. Error bars indicate SDs. Statistical analysis was performed using ordinary one-way ANOVA with Dunnett's multiple comparisons test. n.s.: non-significant.

4 Discussion

4.1 No evidence for special macrophage progenitors in the circle of Willis

4.1.1 What information does phenotypic analysis of the vessel wall provide?

In this study, the presence of AMPCs within the CNS was examined by marker analysis *in situ* as well as in an *ex vivo* culture assay, focusing on the CW as an exemplary CNS-associated vascular structure. In paraffin sections, no $CD45^+$ $SCA\text{-}1^+$ cells, which have been described as the most robust minimal phenotype of AMPCs[59,175], were detected within the CW's adventitia. One could argue that this may result from insufficient sensitivity of the analysis, as IHC-P suffers from diminished antigenicity due to fixation and paraffin embedding as well as a relatively low number of analyzable cells per section. In their own studies, Psaltis et al. described AMPCs mainly by flow cytometry, which does not have these disadvantages, but lacks histological information[59,175]. However, adventitial $CD45^+$ $SCA\text{-}1^+$ cells were also demonstrated in histologic sections of the aorta[59], which could be reproduced in own experiments via the same IHC-P protocol. Flow cytometric analysis of the CW was not pursued, as enzymatic digestion of the small vascular structure resulted in an insufficient quantity of cells, even after pooling the CWs of up to 10 mice.

Generally, one would expect to encounter committed AMPCs in some histological sections, if they were a biologically relevant component of the vessel wall. However, it has to be taken into account that the progenitors might deviate from the suggested $CD45^+$ $SCA\text{-}1^+$ phenotype, which has not been confirmed in independent studies yet.

In conjunction with the lack of AMPC-like cells, histological analysis clearly demonstrated a difference between the outer vascular layer of the aorta and the fine adventitia of the CW,

which showed no or much lower expression of SCA-1. Yet it stained positive for other markers associated with the adventitial "vasculogenic zone" such as FLK-1 and CD34[207].

4.1.2 What can we learn from *ex vivo* vessel culture?

Immunological markers can be acknowledged as a first indication for the presence or absence of progenitors. However, only the functional capacity for extensive proliferation and differentiation unequivocally defines a precursor population. Therefore, the *ex vivo* culture of CW vessel fragments was established to study possible AMPC activity. The CWFA has several strengths and weaknesses, which are summarized in Tab. 1. One disadvantage is the presence of around 100 mature macrophages per explanted fragment. The latter bear the capacity for cell division and can therefore account for the expansion of $CD11B^+$ macrophage-like cells, which was observed in response to stimulation with myeloid growth factors (CSF-1, IL-34, GM-CSF) under hypoxic conditions. Hence, macrophage-depleted vessels were analyzed in the CWFA to separate possible progenitor activity from macrophage proliferation.

Two different depletion regimens were used. Pre-treatment of mice with the CSF-1R inhibitor PLX5622 strongly reduced the macrophage content in dissected vessels to about 10 - 20 %, while macrophages were completely eliminated after incubation with mannosylated clodronate liposomes. Under the assumption that progenitors are responsible for the majority of macrophage expansion in culture, the number of macrophages at day 7 should strongly depend on the number of progenitors per vessel fragment, which is supposedly constant, but should be more or less independent of the number of mature macrophages at day 0. However, macrophage output at day 7 was proportional to mature cell input at the start of the culture. Under the additional assumption that the depletion regimens affected only differentiated cells, but not possible progenitors, the observed expansion of $CD11B^+$ macrophage-like cells should be the sole result

of mature cell division. This was underscored by the complete abolishment of macrophage expansion following clodronate liposome treatment. As the depleting effect of clodronate liposomes relies on efficient phagocytosis, a functional property that is predominantly assigned to differentiated cells, it is unlikely that the treatment would have also affected putative AMPCs. Likewise, AMPCs should at least be independent of CSF-1 signaling, because they were not reduced in *op*/*op* mice[175]. However, as the CSF-1R also mediates IL-34 signaling[208], a possible effect of PLX5622 on AMPCs cannot be completely excluded.

Table 1 | The strengths and weaknesses of the CWFA.

Strengths	Weaknesses
Vascular niche remains intact	Artificial *ex vivo* condition
All vascular cells are screened for progenitor activity in parallel	Alternative sources of macrophage expansion such as mature cells have to be excluded
Progenitor activity is tested independently of candidate markers	It is difficult to separate vessels from meninges via manual dissection
Almost no loss of cells. Therefore low cell quantities can be analyzed	Low yield of fragments (5 - 6) per mouse plus 50 % failure rate in culture

But could mature cells actually be the only source of the extensive cellular expansion, which was observed in the CWFA? Macrophage quantity increased about 20-fold within 7 days of culture, which would require that every single cell underwent 4 - 5 divisions. The average duration of one cell cycle would therefore be around 36 h. This falls within the range of cell cycle lengths, which have been estimated for macrophages (20-40 h depending on maturation stage)[209], as well as homeostatic (32 h)[107] or reactive microglia (40 h)[114].

Psaltis and co-workers tested aortic disaggregates in CFU assays and found around 15 CFU-M per 10^5 cells, which they attributed to AMPCs. They calculated that the aorta of a 12 weeks old mouse should harbor around 200 - 300 of these cells[175], which would correspond to

8 - 12 progenitors per mm vessel lengths (of a 25 mm aorta). However, the adventitial surface decreases substantially in conjunction with a decline of the vessel diameter. If AMPC abundance dropped accordingly, few cells would be expected to reside in 2 - 3 mm CW fragments. In fact, the prevalence of AMPCs was found to display spatial heterogeneity, being higher in aorta than in the femoral or carotid arteries[59]. It is therefore conceivable that the CW, which is even more distant from the aorta, contains only few to no AMPCs. This would conform to the thin SCA-1$^-$ adventitia of the CW, which might not comprise a functional niche for progenitors anymore.

Of course, the experimental setup cannot fully exclude the presence of AMPCs in the CW. In the described CWFA protocol, several growth factors were included, which are known to stimulate myeloid progenitors[210] and are involved in microglia/macrophage homeostasis (mainly GM-CSF, CSF-1, and IL-34)[211–214]. Additionally, vessels were subjected to hypoxic conditions, which have been suggested to induce the differentiation of pericytes into microglia-like cells[150,151]. Yet AMPC activity might require different stimuli. The adventitial precursors were further classified as "late outgrowth progenitors" by Psaltis et al., as corresponding colonies appeared only after 10 - 14 days of culture in CFU assays[59]. A similar lag in colony-formation has been described for macrophage-restricted progenitors in thymus and lymph nodes[215]. However, vessel culture was stopped already after 7 days, as the prominent expansion of macrophages in control samples often led to degradation of the collagen matrix shortly after this time point. It is important to note that in the phenotyping experiments described under 3.2.6, brain-derived CD45$^+$ SCA-1$^+$ "AMPC-like" cells were cultured in collagen-based CFU assays, which include additional growth factors (e.g. SCF, IL-3, TPO), for up to 14 days, but still failed to form colonies. Nevertheless, it might be interesting to repeat the CWFA with macrophage-depleted vessels under the conditions of a CFU assay and with prolonged culture periods. The latter would further reduce the probability that AMPCs were just overlooked.

4.1.3 Could brain-derived CFU-Cs represent AMPCs?

Several lines of evidence contradict the idea that CFU-Cs, which were detected in whole brain homogenates, represent in fact AMPCs. First, brain-resident progenitors were exclusively contained within the SCA-1$^-$ fraction, while AMPCs were defined as SCA-1-positive[59,175]. Second, AMPCs were described as "late outgrowth" progenitors[60], whereas brain-derived CFU-Cs produced large colonies already within 7 days of culture. Lastly, AMPCs were found to be committed macrophage precursors, as they were almost exclusively classified as CFU-M in CFU assays[59,175]. However, only about 25 % of colonies that arose from brain CFU-Cs were of pure macrophage identity, while the rest adopted other, including mixed, myeloid fates. Brain-resident CFU-Cs therefore resembled normal MyPs, which was corroborated by the presence of CMP, GMP, and MEP subfractions. MyPs were also described in the aorta by Psaltis et al., but were clearly separated from AMPCs[59].

4.2 Myeloid progenitors within the adult mouse brain

4.2.1 Do myeloid progenitors actually reside inside the brain?

In this study, rare CFU-Cs were detected in brain homogenates from adult mice, confirming previous reports about hematopoietic potential in cerebral cell isolations[183–185]. Due to the crude character of cell preparation, it is important to determine whether the cells actually reside inside the CNS tissue, or constitute a contamination by other sources, such as the circulating blood. In earlier studies, this issue has mostly been neglected or only addressed with the statement that CFUs were less frequent in PB than in the brain[184]. However, the frequency of circulating HSPCs follows a circadian rhythm[44] and the cellular composition of the blood varies depending on the sampling location[216,217]. Therefore, this comparison is error-prone, especially as the occurrence of CFU-Cs was relatively similar in PB and brain. More importantly, skull BM has never been taken into account as a possible contaminating source. Yet one can easily imagine that BM cells might leak onto the brain during surgical opening of the cranium. Due to the high progenitor content, a spill of ~10^4 BM cells would suffice to explain the CFU-C frequencies within brain cell suspensions. The enrichment of CFU-Cs at the brain surface could even be interpreted as a sign for such contamination.

However, extraction of CNS tissue through the foramen magnum did not reduce CFU-C incidence in brain homogenates, indicating that the latter did not depend on extensive damage to the skull. Moreover, progenitors in the brain showed a differentiation bias towards the erythroid lineage *in vitro*, while skull BM rarely gave rise to erythroid colonies under the same conditions. The erythroid tendency, though, was reminiscent of circulating HSPCs, while the overall colony pattern significantly differed in both tissues. Taking into account the average frequency of circulating HSPCs in PB (4 ± 3 CFU-Cs per 10^5 nucleated cells) as well as the mean residual

leukocyte count in brain tissue following perfusion (2.3 ± 1 % IV-CD45$^+$ cells among ~1 x 10^6 total cells), intravascular CFU-Cs should only account for around 0.1 colonies per 10^5 brain-derived cells, assuming that HSPCs are not enriched in CNS-perfusing blood. Moreover, intravascular cells naturally are most accessible to intravenously injected anti-CD45 antibody, but the removal of IV-CD45$^+$ cells did not impact CFU-C frequency among brain cells. By adapting the injection protocol, the IgG efficiently penetrated through the fenestrated sinusoidal blood vessels of skull BM, where it stained resident HSPCs. Also in these experiments, IV-CD45$^-$ cells from the brain contained similar frequencies of colony-forming cells. Importantly, phenotyping analysis clearly demonstrated that brain-derived CFU-Cs in principal were recognized by the same anti-CD45 antibody. Hence, the IgG's inability to reach and stain brain CFU-Cs after intravenous injection illustrated their residence behind the tight junctions of the continuous CNS blood vessel endothelium. Taken together, these data provide the strongest evidence yet that brain-derived CFU-Cs are actually located inside brain tissue.

4.2.2 How well can we determine the abundancy of brain-resident progenitors?

The incidence of brain-derived CFU-Cs was found to be 7 ± 4 per 10^5 cells, leading to an estimated total number of 40-70 progenitors per cell preparation. This frequency is comparable to previous studies (Tab. 2), while being the lowest of published progenitor occurrences. It should be noted that in this study, the number of colonies was counted already 7 days after plating, which predominantly detected primitive progenitors with large burst size. Therefore the data do not account for the presence of late outgrowth progenitors (colony-formation > day 10)[215], which might further increase the frequency of cerebral CFU-Cs. Interestingly, Alliot et al. estimated a much higher absolute number of brain-resident progenitors (~10,000 per mouse), as the investigators stated to recover around 80-times more total cells per brain[185]. It is important to note

that this study used relatively young mice (> 4 weeks), which is known to increase cellular yield from the CNS, but probably does not reflect the true adult situation.

Generally, the frequency of brain-resident CFU-Cs is expected to vary based on the protocol of cell isolation, method for progenitor detection, as well as age and genetic background of the animal. Taking this into account, it is rather surprising that multiple studies, which differed significantly in these aspects, reported a relatively narrow range of progenitor incidences (Tab. 2). It can be speculated that the method of tissue dissociation might have a major impact on progenitor yield, as Perry F. Bartlett and Alliot et al. reported higher frequencies after digestion with trypsin/EDTA[184,185], while Asakura et al. described an incidence comparable to own findings based on a similar digestion with collagenase/dispase[183]. In the presented study, the latter was still preferred, as trypsin would have also degraded injected antibodies[218]. In order to also ensure disintegration of collagen-rich vessels, a relatively harsh digestion was performed (60 min incubation with intermittent trituration). However, it is known that HSPCs are easily affected by such manipulations. Intensive digestions, long processing times, and stress during cell sorting are likely to evoke that the progenitor frequency is underestimated. It will therefore be important to further optimize cell isolation and processing in order to determine the actual frequency of brain-resident MyPs and to obtain higher cell quantities for more detailed analyses.

Table 2 | Studies describing hematopoietic progenitors in the adult mouse brain.

Progenitors per 10^5 cells (mean)	Assay	Mouse strain	Age [weeks]	Digestion	Reference
14	Spleen CFU assay (d9)	CBA/CaHWehi	8 - 10	Trypsin/EDTA	Bartlett[184]
12*	*In vitro* limiting dilution assay	C57BL/6	> 4	Trypsin/EDTA	Alliot et al.[185]
9	Culture CFU assay (d14)	Balb/c	4 - 8	Collagenase /dispase	Asakura et al.[183]
7	Culture CFU assay (d7)	C57BL/6	10 - 14	Collagenase /dispase	Own results

* Mean frequency within the whole brain was calculated from regional data.

4.2.3 Where are progenitors located inside the brain?

Although clonogenic cells have been observed in the adult mouse brain before, little is known about their exact location. Alliot et al. found a relatively high frequency of progenitors in forebrain and brainstem (~13-14 per 10^5 cells), while they were less abundant in the cerebellum (~3 per 10^5 cells)[185], which in principle conforms with own results. However, the investigators stated to have carefully removed the meninges before dissociation of the tissue[185]. Conversely, own fractionation experiments demonstrated that CFU-Cs were enriched at the surface of the brain, pointing to a leptomeningeal localization. The dura mater is unlikely to harbor the observed clonogenic cells, as i.v. injected antibodies are expected to also penetrate through the fenestrated endothelium of dural blood vessels[219] and stain resident $CD45^+$ cells, which would thus have been removed in sorting experiments. The data do not confirm resident progenitors inside the choroid plexus, which have been reported in rats[186]. Also, CFU-Cs were almost undetectable in neurogenic zones, arguing against transdifferentiation of neural stem cells, which might occur under experimental conditions[180,182]. It is still conceivable that the detected

progenitors reside at meningeal vessels. As antibody diffusion is blocked at the tight junctions of continuous endothelium, also progenitors within the vessel wall would not have been eliminated by the IV-CD45-based sorting strategy.

With regard to recent high-dimensional mass and fluorescence cytometry studies that demonstrated a much broader spectrum of immune cells in the healthy CNS than previously thought[220,221], it can be speculated that brain-resident MyPs might be intermingled with these immune populations, which were also most prominent in the meninges[221]. Intriguingly, in the context of these exhaustive analyses, Korin et al. even detected a cohort of $CD45^{lo}$ "undefined cells" in the brain, which lacked myeloid differentiation markers, but partly expressed CXCR4[221], an important chemokine receptor on HSPCs[39].

4.2.4 What is the origin of brain-resident progenitors?

When Alliot et al. observed rapidly proliferating cells in brain cell cultures almost 30 years ago, they termed them "microglia progenitors", as their experimental approach specifically examined cells that differentiated into a macrophage-like phenotype in response to CSF-1 stimulation[185]. They also suggested the progenitors to originally derive from the YS and to persist into adulthood[102]. Since then, knowledge on microglia development and maintenance has expanded considerably. While the YS origin of microglia has been confirmed, terminally differentiated microglia as well as other macrophage populations inside the CNS have been shown to self-renew independently of infiltrating or resident progenitors[75,145].

Still, the persistence of YS-derived precursors inside the brain, from which microglia descent during embryonal development[26,27], was not excluded, especially as the erythroid-tended colony pattern of brain CFU-Cs was reminiscent of EMPs[29,222]. Microglia progenitors have been observed to enter the brain rudiment mainly via the lateral ventricles as well as the meningeal

surface[95]. It is therefore imaginable that some of these precursors seed meningeal niches during this process where they are maintained into adulthood. However, this would require either dormancy or the potential for self-renewal. Interestingly, it has been shown that the E9 YS already contains HSC-like cells that cannot engraft into adult BM niches yet, but show long-term multilineage reconstitution upon transfer into myeloablated newborns[223,224]. These immature HSCs would be available for engraftment of the developing brain concomitant to microglia invasion around E9.5-10[20,101,102]. It is equally conceivable that the rare brain-resident CFU-Cs might just be remnants of brain-colonizing YS progenitors, which persist in a quiescent state *in vivo* and are gradually lost during adulthood.

CFU-Cs in the adult brain displayed the MyP phenotype $CD45^{lo}$ LIN^- c-KIT^+ SCA-1^-, which overlaps with embryonal EMPs[16,29]. However, EMPs have been shown to homogenously express FcγR (also known as CD16/32), while still producing all erythro-myeloid cell types[29]. On the contrary, MyPs in the adult brain constituted a heterogeneous population of CMPs ($Fc\gamma R^-$, $CD34^+$), MEPs ($Fc\gamma R^-$, $CD34^-$), and GMPs ($Fc\gamma R^+$, $CD34^+$) that - like their HSC-derived counterparts in the adult BM - showed restricted potential in CFU assays. To exclude that persisting EMPs merely had changed their surface marker expression, brain CFU-Cs were analyzed in the *Flt3*^{Cre} x *Rosa26*$^{mT/mG}$ strain, which stably labels HSC-derived MPPs and their progeny[27,201]. YS-derived EMPs as well as EMP-derived cells do not express *Flt3* and are therefore not tagged in this model[27,29]. Yet the majority of colonies that developed from brain cell suspensions of *Flt3*^{Cre} x *Rosa26*$^{mT/mG}$ mice had a history of *Flt3* expression. It can therefore be concluded that these cells descent from fetal or adult HSCs, but not from YS EMPs.

The similarity between progenitors in the brain and MyPs in the BM raises the question whether there is constant cellular exchange between these locations, as it has been shown for other organs[41]. Although brain-derived MyPs were not intravascular at the time of cell isolation,

their erythroid-tended *in vitro* potential (reminiscent of circulating HSPCs) may suggest a supply by trafficking progenitors. However, in contrast to other organs such as the liver, no marked progenitor exchange between PB and brain has been observed within 14 days of parabiosis[41], indicating at least a slow turnover of brain-resident progenitors. This matches own findings about the overall different progenitor composition in brain and PB, which contradicts an instantaneous and complete harmonization of both compartments.

Experiments with anemic white spotting W^f/W^f mice further have shown that hematopoietic deficiency in the BM was not reflected in the brain, which was interpreted as lack of interconnection between these tissues via trafficking HSPCs[184]. W^f/W^f mice bear a mutation in the receptor tyrosine kinase c-KIT[225], which was also detected on brain-resident MyPs. The c-KIT receptor mediates SCF signaling, an important niche factor for HSPCs in the BM[4]. It has to be taken into account that travelling HSPCs might not depend as much on c-KIT signaling as resident progenitors in the BM or that extramedullary niches such as the brain might contain other factors that could compensate for c-KIT deficiency. Therefore, a missing effect on brain-resident MyPs in *c-Kit*-mutants does not necessarily falsify exchange between BM and brain.

Still it is tempting to speculate about the presence of self-renewing HSCs inside the CNS, as it has already been done by Perry F. Bartlett[184]. The spleen colony-forming assays he performed with brain homogenates actually had the potential to provide first evidence for such cells[184]. In this assay, single cell suspensions are injected intravenously into irradiated mice, where some of them give rise to macroscopically discriminable nodules in the spleen[226]. It has been shown that spleen colonies that are present at day 7 - 8 after transplantation (CFU-$S_{d7\text{-}8}$) derive mostly from committed progenitors[178,227], while CFU-$S_{d10\text{-}12}$ indicate ST-HSCs[17,227]. Unfortunately, the author analyzed brain-derived splenic colonies at day 9 after transplantation, which leaves progenitor identity ambiguous[184].

Yet it is not unthinkable that HSCs might be seeded in the CNS behind the BBB, may it be transiently or permanently. For instance, HSCs have been demonstrated to independently emerge from hemogenic endothelium within the embryonic head at around E10.5 in addition to the AGM regions[228]. They also seem to be preferentially recruited to the brain upon BM transplantation as compared to late hematopoietic progenitors[136]. Whether significant amounts of LT-HSCs are actually present in the adult brain under steady-state conditions will have to be analyzed in serial transplantation experiments.

4.2.5 What might be the relevance of myeloid progenitors inside the brain?

Brain-resident progenitors were capable of producing all erythro-myeloid cell types *in vitro*, while their colony-pattern significantly differed from BM and PB, suggesting a tissue-specific composition of cells. It remains unknown whether there is also lymphoid potential inside the CNS, as the latter goes undetected in the employed CFU assays. Compared to BM-resident progenitors, brain-derived MyPs displayed a strong tendency towards the erythroid lineage, which is consistent with previous reports[184]. While this finding is useful to discriminate progenitor populations, it is important to note that *in vitro* potential does not necessarily correlate with actual differentiation in the living animal[37], as required factors, which are abundant in the artificial environment, might not be encountered in the *in vivo* situation. In order to elucidate actual differentiation pathways *in vivo*, specific lineage tracing models would have to be employed.

It is questionable whether brain-resident MyPs would ever produce erythrocytes within the CNS. However, they might locally supply e.g. granulocytes, macrophages, and dendritic cells in the steady-state and/or during injury/inflammation, without the need for BBB passage. Intriguingly, HSPCs have been shown to be active players in immunologic processes. They sense

pathogens via Toll-like receptors[41,67] and react with proliferation, differentiation[41,67] and extensive cytokine production[72,229]. It is therefore conceivable that MyPs exert a surveillance function in the brain, as it has been postulated for other organs[41]. Due to high proliferative capacity, even a small progenitor pool would be able to significantly shape local immune reactions especially during the initiation phase, when peripheral immune cells have not yet infiltrated the CNS in high numbers. In this process, the direct contact of MyPs to local cues might actually result in the generation of innate immune cells that are specifically adapted to the prevailing brain environment, as recent studies have shown that "trained immunity" is already formed on the level of the HSPC compartment[7,230]. A meningeal localization would be optimally suited for such tasks, because interstitial and cerebrospinal fluid washes macromolecules from all over the CNS into the subarachnoid space prior to drainage into meningeal lymphatics[231,232].

Hence, brain-resident MyPs might have broad implications for the field of neuro-immunology. In addition, they have practical meaning for researchers studying the adult mouse brain, as co-isolation of resident hematopoietic progenitors might explain the reported transdifferentiation of primary brain pericytes into microglia/macrophages *in vitro*[150–152] as well as the putative hematopoietic potential of NSCs[180,181].

4.3 CNS macrophages self-renew independently of brain-resident progenitors

In order to test the contribution of local progenitors to brain macrophage maintenance, the experimental model of forced brain macrophage repopulation via CSF-1R inhibition was revisited. In this system, first evidence for microglial progenitors was observed by Elmore et al. in 2014[154]. It is important to note that the inhibitor PLX3397 was used in the latter study, which also affects the kinases FLT3, PDGFR, and c-KIT[233,234]. In the presented work however, the molecule PLX5622 was employed, as PLX3397 is no longer available for preclinical investigations. PLX5622 is a more selective CSF-1R inhibitor (Plexxikon Inc., personal communication) and also leads to rapid CNS macrophage depletion. Elimination of brain macrophages was less efficient than described by Elmore et al. (~99 %, PLX3397)[154], but was comparable to recently published studies using PLX5622[204,235,236]. The treatment exerted a systemic effect on tissue macrophages and also reduced circulating monocytes, which has not been reported consistently in previous studies[237,238]. Yet the effect on blood monocytes was comparable to what has been observed in adult *Csf-1r*$^{-/-}$ and *op*/*op* mice[239].

Upon inhibitor withdrawal, CNS macrophages repopulated the brain within 14 days, following a kinetic that matched observations by other investigators[145,159,235,236]. Importantly, it is now well-established that circulating cells do not contribute to microglia/macrophage recovery following PLX5622 treatment[145,159], which was confirmed in own experiments, making it an ideal model to study the activity of local progenitors.

In this work, it was demonstrated that the adult mouse brain harbored progenitors with broad erythro-myeloid potential. This includes differentiation towards monocytes/macrophages and thus possibly microglia. In previous studies, it was found that a subset of repopulating microglia co-expressed the typical progenitor markers CD34 and c-KIT[154], which were also

present on brain-derived MyPs. This might point towards a contribution of MyPs to microglia recovery. However, the debate about NESTIN and microglial progenitors has vividly shown that marker expression is insufficient to justify precursor activity[142,145,154,159].

Brain-resident MyPs were found to constitute a rare population inside the adult brain (around 1 progenitor per 5,000 mature brain macrophages). If these cells significantly contributed to CNS macrophage recovery via rapid proliferation and differentiation, one would expect to find foci of repopulating cells. Yet prominent clusters of multiple IBA1$^+$ cells were not observed during the recovery period, contrasting reports by other investigators[142,154]. Repopulation also did not appear to originate from the brain surface, where brain-resident MyPs were found to be concentrated. Instead, the spatial distribution of repopulating cells seemed to correlate with homeostatic CNS macrophage densities and turnover rates, which have been shown to differ among brain regions[107,112,114,240]. It is conceivable that the same mechanisms (e.g. availability of growth factors) that mediate a faster turnover of microglia/macrophages in the steady-state also lead to a faster repopulation in regions such as the hippocampus or olfactory bulb. Conversely, brain-resident MyPs were hardly detectable in especially these anatomical sites.

In addition, it was hypothesized that brain-resident MyPs that were activated by a strong repopulating stimulus should transiently expand in an “emergency reaction” to be able to rapidly restore CNS macrophage numbers, which would be noticeable by an increased number of CFU-Cs during the recovery period. In order to test this hypothesis, clonogenic activity was analyzed in brain homogenates during early repopulation (up to day 3 after drug withdrawal). Although the kinetics of brain macrophage recovery showed some degree of inter-experimental variance, first expansion of IBA1$^+$ cells was robustly observed within this time-window. More importantly, Elmore et al. described a sudden emergence of proliferating *Cx3cr1*$^-$ cells already at day 2 of recovery[154], which could point towards MyP activity. Yet there was no major change of

brain-derived CFU-C frequency during early CNS macrophage repopulation, falsifying concomitant expansion of the progenitor pool.

The most valid arguments against a contribution of brain-resident MyPs to microglia/macrophage repopulation stem from recent fate mapping studies. Based on the *Cx3cr1*^{CreER} mouse model, it was demonstrated that CNS macrophages repopulate from a *Cx3cr1*$^{+}$ population following genetic or pharmacological (PLX5622) depletion[142,145,159]. However, the vast majority of brain-resident progenitors were shown to be *Cx3cr1*$^{-}$ in the steady-state. *Cx3cr1*$^{+}$ clonogenic cells only constituted a minor subpopulation and displayed reduced proliferative capacity in CFU assays, noticeable by small colony size. These cells might represent MDPs or dendritic cell progenitors within the MyP population, which already express the differentiation marker *Cx3cr1*[15,241]. The lifespan of such late progenitors is usually limited, which notably is the basis of the *Cx3cr1*^{CreER}-mediated, specific targeting of CNS macrophages[143,144]. Hence also the brain-resident *Cx3cr1*$^{+}$ progenitor subset was probably not tagged anymore at the time when brain macrophage repopulation was induced in the lineage tracing studies. In conclusion, it is highly unlikely that MyPs in the brain are involved in acute CNS macrophage recovery.

Moreover, brain-resident progenitors do not contribute to normal microglia maintenance, as they produced GFP^{+} progeny in *Flt3*^{Cre} x *Rosa26*$^{mT/mG}$ mice. Microglia, on the other hand, have been shown to lack recombination in *Flt3*^{Cre} mice at least until 1 year of age[27,98]. Other CNS macrophages, such as subdural meningeal and perivascular macrophages, are also largely independent of *Flt3*$^{+}$ progenitors[98].

5 Conclusion and Outlook

Based on the herein described findings, there was no evidence for AMPCs, as characterized in peripheral arteries, in the adult mouse CNS. Yet a heterogeneous population of MyPs was recovered from the brain, in accordance with previously observed cerebral hematopoietic activity. In the context of their detailed characterization, they were found to likely occupy a meningeal location behind the BBB. It is still conceivable that the meningeal vasculature provides a niche for these cells. To clarify this issue in further studies, an adapted form of the *ex vivo* vessel culture, which was established in this thesis, could be employed.

Even though brain-resident MyPs do not seem to contribute to microglia maintenance, they might be important participants in neuroinflammation. Extramedullary HSPCs have received increasing attention over the last years, as it becomes clear that these cells are an integral part of immunity, apart from merely producing functional blood cell types. It is tempting to speculate that, among the already described tissue-associated HSPCs, a population of hematopoietic progenitors behind the BBB would be of exceptional significance.

In order to elucidate the relevance of brain-resident MyPs in CNS disease, some remaining questions have to be addressed: Are progenitors in the brain replaced by trafficking HSPCs? And if so, what is the kinetics of their turnover? Parabionts and refined BM chimeras can provide answers to these questions. Care should be taken in selecting appropriate models, as classical preconditioning for BM transfer (irradiation or chemotherapy) also eliminates extramedullary progenitors. However, new approaches have become available that are based on genetics[242,243] or use antibody-directed toxins for preconditioning[244], which do not cross the BBB. If MyPs in the brain were actually not or only slowly replenished from the BM, which has already been implicated in previous studies[41], this could be exploited to differentially target the brain-resident and peripheral progenitor compartments. The arising system could eventually be combined with various disease models in order to define the significance of local MyPs in neuroinflammation.

6 Materials

6.1. Reagents and supplies

6.1.1 Media

Table 3 | Cell culture media

Product name	Manufacturer	Cat. #
Dulbecco's modified Eagle's medium (DMEM)	Thermo Fisher Sci.	41966-029
Iscove's modified Dulbecco's medium (IMDM)	Thermo Fisher Sci.	12440053
Mouse methylcellulose complete media	R&D Systems	HSC007
Opti-MEM™, GlutaMAX™	Thermo Fisher Sci.	51985026
Roswell Park Memorial Institute (RPMI) 1640 medium without phenol red	Thermo Fisher Sci.	11835-063
StemSpan™ serum-free expansion medium (SFEM)	STEMCELL technologies	09650

6.1.2 Buffers and solutions

Table 4 | Ready-to-use buffers and solutions

Product name	Manufacturer	Cat. #
Dulbecco's phosphate buffered saline (DPBS) - Ca^{2+}/Mg^{2+}	Sigma-Aldrich	D8537
10x Hank's balanced salt solution (HBSS) - Ca^{2+}/Mg^{2+}	Thermo Fisher Sci.	14185-045
6x Loading dye	Thermo Fisher Sci.	R0611
Phosphate buffered saline (PBS) salt	AppliChem	A0964
2x RNA gel loading dye	Thermo Fisher Sci.	R0641

Table 5 | Self-prepared buffers and solutions

Name	Ingredients	Concentration
Ammonium-chloride (AMC) buffer (10x) pH = 7.3	NH_4Cl	1.5 M
	$NaHCO_3$	100 mM
	$Na_2EDTA \bullet 2\ H_2O$	10 mM
DAB staining solution	Phosphate buffer	
	Nickel sulfate	0.25 mg mL^{-1}
	Glucose	0.2 % (w/v)
	NH_4Cl	0.38 mg mL^{-1}
	DAB	0.48 mg mL^{-1}
	Glucose oxidase	4 µg mL^{-1}
Digestion medium (2x)	Medium A	
	Collagenase Type 2	2 mg mL^{-1}
	Dispase II	1 mg mL^{-1}
	Benzonase	50 U mL^{-1}
	Penicillin G / streptomycin	0.2 U mL^{-1}
Eosin staining solution	Eosin Y	0.1 % (w/v)
Hematoxylin staining solution	Hematoxylin	0.1 % (w/v)
	$NaJO_3$	0.02 % (w/v)
	$KAl(SO_4)_2$	5 % (w/v)
	Chloral hydrate	5 % (w/v)
	Citric acid	0.1 % (w/v)
Lysis buffer for genotyping	Sodium hydroxide	25 mM
	EDTA	200 µM
Medium A, pH = 7.4	RPMI 1640 without phenol red	
	HEPES	10 mM
Medium B, pH = 7.4	HBSS - Ca^{2+}/Mg^{2+}	
	HEPES	10 mM
	EDTA	1 mM
Mowiol mounting solution	Tris-HCl (pH = 8.5)	0.1 M
	Glycerol	25 % (w/v)
	Mowiol-488	10 % (w/v)
	DABCO	25 mg mL^{-1}
Myelin removal medium, pH = 7.4	Medium B	
	Albumin fraction V	20 % (w/v)
Nuclear fast red staining solution	Nuclear fast red	0.1 % (w/v)
	Aluminium sulfate-18-hydrate	5 % (v/v)
Phosphate buffer, pH = 7.4	KH_2PO_4	18 mM
	Na_2HPO_4	82 mM
Sorensen's phosphate buffer, pH = 6.95	0.1 M KH_2PO_4 in dH_2O	4 parts
	0.1 M Na_2HPO_4 in dH_2O	6 parts
Sorting medium, pH = 7.4	HBSS - Ca^{2+}/Mg^{2+}	
	HEPES	25 mM
	EDTA	1 mM
	Fetal bovine serum	2 % (v/v)
	Penicillin G / streptomycin	0.1 U mL^{-1}
Tris-acetate-EDTA (TAE) (50x) pH = 8.3	Tris free base	2 M
	Acetic acid	5.71 % (v/v)
	$Na_2EDTA \bullet 2\ H_2O$	50 mM

6.1.3 Chemicals

Table 6 | Chemicals

Product name	Manufacturer	Cat. #
Acetic acid	ROTH	3738.4
Agarose	Biozym	840004
Albumin fraction V (pH 7.0)	AppliChem	A1391
Aluminium sulfate-18-hydrate	Sigma-Aldrich	450308
Ammonium chloride (NH_4Cl)	ROTH	P726.2
Chloroform	AppliChem	A1585
Citric acid	AppliChem	A1350
Chloral hydrate	AppliChem	A4431
DABCO	ROTH	0718.2
DePeX	Serva	18243.02
Di-sodium ethylene diamine tetraacetate di-hydrate ($Na_2EDTA \bullet 2\ H_2O$)	Merck	8418.0250
Di-sodium hydrogen phosphate	AppliChem	131679.1211
D(+)-Glucose	AppliChem	A1422
D(+)-Saccharose (sucrose)	ROTH	4621.1
Ethanol	ROTH	9065.4
Glycerol	AppliChem	A3552
Heparin sodium (5,000 U mL^{-1})	Ratiopharm	
Hydrochloric acid	Sigma-Aldrich	30721
Hydrogen peroxide	ROTH	9683.1
2-[4-(2-hydroxyethyl)piperazin-1-yl] ethanesulfonic acid (HEPES) sodium salt	AppliChem	A1070,0100
$KAl(SO_4)_2$	AppliChem	A2811
2-methylbutane (isopentane)	ROTH	3927.1
Mowiol 4-88	ROTH	0713.1
$NaJO_3$	Merck	7412159
Nickel(II) sulfate hexa-hydrate	Merck	1.06727.0100
Paraffin wax	Merck	1.11609.2504
Paraformaldehyde	ROTH	0335.4
Penicillin G sodium salt	AppliChem	A7000
PLX5622, formulated in AIN-76A standard rodent chow	Plexxicon Inc.	
Potassium di-hydrogen phosphate	AppliChem	A3620
2-Propanol (isopropanol)	ROTH	6752.4
Sodium citrate di-hydrate	ROTH	4088.1
Sodium hydroxide	AppliChem	A3910
Streptomycin sulfate salt	Sigma-Aldrich	S6501
Tris free base	ROTH	4855.2
TriZol	Ambion	15596018
O.C.T^{TM} compound	Sakura	4583
Triton X-100	Sigma-Aldrich	T-9284
Xylole, 99.9 %, redistilled	University of Würzburg	

6.1.4 Biochemicals / enzymes

Table 7 | Biochemicals / enzymes

Product name	Manufacturer	Cat. #
Benzonase® nuclease, purity > 90 %	Merk Millipore	70746
Collagenase type 2	Worthington biochemical	LS004177
Rat collagen I (5 mg mL^{-1})	Cultrex	3440-100-01
Dispase II	Thermo Fisher Sci.	17105-041
Fetal bovine serum	Thermo Fisher Sci.	10270-106
Glucoseoxidase type VII	Sigma-Aldrich	G2133
Normal goat serum	Sigma-Aldrich	G9023
PureCol® bovine collagen (3 mg mL^{-1})	Advanced Biomatrix	5005

6.1.5 Kits

Table 8 | Kits and ready-to-use reagents

Product name	Manufacturer	Cat. #
GeneRuler™ 1 kb	Thermo Fisher Sci.	SM0311
GeneRuler™ 100 bp	Thermo Fisher Sci.	SM0321
Mannosylated macrophage depletion kit	Encapsula NanoSciences LLC	8914
QuantiTect® reverse transcription kit	QIAGEN	205311
Red mastermix (2x)	Genaxxon bioscience	M3029.0000
SsoAdvanced™ universal SYBR® green supermix	BIO-RAD	1725270
VECTASTAIN® ABC HRP kit	Vector Laboratories	PK-4000

6.1.6 Antibodies

Table 9 | Unconjugated primary antibodies for immunofluorescence microscopy

Antigen	Clone	Origin	Dilution	Manufacturer	Cat. #
CD11B	M1/70	Rat	1:1000	eBiosciences	14-0112 - 82
CD34	MEC 14.7	Rat	1:100	Abcam	ab8158
CD45.2	30-F11	Rat	1:500	eBioscience	14-0451
F4/80	BM-8	Rat	1:200	eBioscience	14-4801-85
FLK-1	Polyclonal	Goat	1:100	Santa Cruz Biotechnology	sc-48161
GP1Bα		Rat	1:500	B. Nieswandt (University of Würzburg)	-
IBA1	Polyclonal	Rabbit	1:500	Wako	019-19741
Ly6G	RB6-8C5	Rat	1:500	eBioscience	14-5931-81
SCA-1	Polyclonal	Goat	1:100	R&D Systems	AF1226

Table 10 | Antibodies and antibody cocktails for flow cytometry

Antigen	Clone	Fluorochrome	Dilution	Manufacturer	Cat. #
CD45.2	30-F11	APC	1:500	BioLegend	103112
SCA-1	D7	FITC	1:200	BD Biosciences	557405
SCA-1	D7	biotinylated	1:40	Miltenyi	130-101-995
CD117 / c-KIT	REA791	PE	1:50	Miltenyi	130-111-693
CD117 / c-KIT	REA791	VioBright™ 515	1:50	Miltenyi	130-111-696
CD11B	M1/70	PE	1:500	BD Biosciences	557397
CD127 / IL7Rα	REA680	biotinylated	1:20	Miltenyi	130-110-373
FcγR (CD16/32)	93	Brilliant Violet™ 711	1:50	BioLegend	101337
CD34	MEC14.7	PE	1:100	BioLegend	119307
„LIN-cocktail“ (CD5, TER-119, CD11B, 7-4, CD45R, GR-1)		biotinylated	1:20	Miltenyi	130-092-613
Ly6C	HK1.4	PE-Cy7	1:500	BioLegend	128017

Table 11 | Isotype controls for flow cytometry

Origin	Subclass/clone	Fluorochrome	Manufacturer	Cat. #
Rat	IgG2a, κ	PE	BioLegend	400507
Rat	IgG2b, κ	PE	BD Biosciences	553989
Rat	IgG2c, κ	PE-Cy7	BioLegend	400721
Human	REA293	VioBright™ 515	Miltenyi	130-113-457
Human	REA293	PE	Miltenyi	130-104-613

6.1.7 Secondary reagents and dyes

Table 12 | Secondary reagents and dyes

Product name	Manufacturer	Cat. #
7-AAD	BD Pharmingen™	51-68981E
Brillialt Violet 421™ streptavidin	BioLegend	405226
Brilliant Violet 510 ™ streptavidin	BioLegend	405233
Biotinylated goat anti-rabbit IgG (H+L)	Vector Laboratories	BA-1000
Biotinylated goat anti-rat IgG (H+L)	Vector Laboratories	BA-9400
Cy™3-conjugated AffiniPure donkey anti-goat IgG (H+L)	Jackson ImmunoResearch Laboratories Inc.	705-165-003
Cy™3-conjugated AffiniPure goat anti-rat IgG (H+L)	Jackson ImmunoResearch Laboratories Inc.	112-165-003
Cy™5-conjugated AffiniPure goat anti-rabbit IgG (H+L)	Jackson ImmunoResearch Laboratories Inc.	111-175-144
Cy™5-conjugated AffiniPure goat anti-rat IgG (H+L)	Jackson ImmunoResearch Laboratories Inc.	112-175-143
4′,6-diamidin-2-phenylindol (DAPI)	Roche	10236276001
3,3′-diaminobenzidin (DAB)	Sigma-Aldrich	D5637
Eosin Y	AppliChem	A0822
Fixable viability stain (FVS) 450	BD Biosciences	562247
Giemsa-stain, modified solution	Sigma-Aldrich	48900-1L-F
Hematoxylin	Chroma	50837

Table 12 (continued)

Product name	Manufacturer	Cat. #
May-Grünwald-Solution	Sigma-Aldrich	63590-1L
Midori Green	Nippon Genetics Europe	MG04
NeutrAvidin Protein, DyLight® 550	Thermo Fisher Sci.	84606
Nuclear fast red	Merck	5189
Rabbit-peroxidase-anti-peroxidase (PAP)	Jackson ImmunoResearch Laboratories Inc.	323-005-024
Trypan blue	ROTH	CN76.2

6.1.8 Cytokines and growth factors

Table 13 | Cytokines and growth factors

Product name	Manufacturer	Cat. #
Mouse interleukin-34 (mIL-34) protein, His tag	Sino Biologicals	50055-M08H
Recombinant human erythropoietin (hEPO)	PeproTech	100-64
Recombinant murine colony-stimulating factor-1 (mCSF-1)	PeproTech	315-02
Recombinant murine granulocyte-macrophage colony-stimulating factor (mGM-CSF)	PeproTech	315-03
Recombinant murine interleukin-3 (mIL-3)	PeproTech	213-13
Recombinant murine stem cell factor (mSCF)	PeproTech	205-03
Recombinant murine thrompopoietin (mTPO)	PeproTech	315-14
Recombinant murine vascular endothelial growth factor$_{165}$ (mVEGF$_{165}$)	PeproTech	450-32

6.1.9 Primers

Table 14 | Primers for genotyping

Target gene	Forward primer (5‘-3‘)	Reverse primer (5‘-3‘)
Iba1-eGFP transgene	CTGCCAGCCTAAGACAACCA	ACTTGTGGCCGTTTACGTCG

Table 15 | Primers for RT-PCR

Target mRNA	Forward primer (5‘-3‘)	Reverse primer (5‘-3‘)
Mouse *Ccr2*	AACAGTGCCCAGTTTTCTATAGG	CGAGACCTCTTGCTCCCCA
Mouse *Cx3cr1*	ACCGGTACCTTGCCATCGT	ACACCGTGCTGCACTGTCC
Mouse *Gapdh*	AGGTCGGTGTGAACGGATTTG	TGTAGACCATGTAGTTGAGGTCA
Mouse *Tmem119*	GTGTCTAACAGGCCCCAGAA	AGCCACGTGGTATCAAGGAG

6.1.10 Supplies

Table 16 | Supplies

Product name	Manufacturer	Cat. #
1.5 mL reaction tubes	Ratiolab	5615000
2 mL reaction tubes	Ratiolab	5615101
12-well cell culture plate	Greiner Bio-one	665180
14 G needle (Sterican®)	B.Braun	4665473
15 mL conical tube	Sarstedt	62.554.502
20 G needle (Neoject®)	Dispomed	10030
21 G Venofix® A	B.Braun	4056337
24 G needle (Neoject®)	Dispomed	10017
24-well cell culture plate	Greiner Bio-one	662160
27 G needle (Neoject)	Dispomed	10020
30 G needle	Becton Dickinson	324826
40 µm cell strainer	SPL	93040
50 mL conical tube	Sarstedt	62.547.254
6-well cell culture plate	Greiner Bio-one	657160
70 µm cell strainer	SPL	93070
96-well cell culture plate	Greiner Bio-one	655180
Coated cytospin glass slides	Tharmac	JC311
Single Cellfunnel®	Tharmac	JC320
MicroAmp™ fast 96-well reaction plate	Applied biosystems	4346907
MicroAmp™ optical adhesive film	Applied biosystems	4311971
Petri dish	Greiner Bio-one	633180
Sterile FACS tubes	Sarstedt	55.476.013
SuperFrost™ plus microscope slides	R. Langenbrinck	03-0060
Syringe for Perfusor® (50 mL)	B.Braun	8728810F

6.2 Animals

Mice were bred and/or maintained at the facilities of the Centre for Experimental Molecular Medicine (Zinklesweg 10, 97078 Würzburg), the Department for Functional Materials in Medicine and Dentistry (Röntgenring 11, 97070 Würzburg), the Institute of Physiology (Röntgenring 9, 97070 Würzburg), or purchased from Charles River Laboratories. Animals were kept in a specific pathogen-free environment under standard housing and barrier conditions (12 h light-dark cycle, 19-22 °C room temperature, 40-60 % humidity). B6.Iba1-GFP mice were obtained from Shinichi Kohsaka (National Institute of Neuroscience, Kodaira, Tokyo, Japan[198]). The colony was maintained by crossing heterozygous mice with wildtype animals of the same genetic background. Genotyping was performed by PCR on lysed ear-punches collected after

weaning. To avoid imprinting of the transgene, only transgenic males were used for breeding[198]. Heterozygous B6.Cx3cr1-GFP mice were kindly provided by Andreas Beilhack, (Medizinische Klinik und Poliklinik II & Universitäts-Kinderklinik, Julius-Maximilians-Universität, Würzburg) and B6.*Flt3*^{Cre} x *Rosa26*$^{mT/mG}$ mice by Christian Schulz (Medizinische Klinik und Poliklinik I, Ludwig-Maximilians-Universität, Munich). As the cre recombinase is located on the Y-chromosome, only male B6.*Flt3*^{Cre} x *Rosa26*$^{mT/mG}$ mice were analyzed. Mice were used in experiments at 6 - 8 weeks (PLX5622 treatments) or 10 - 14 weeks of age (CFU assays). Animals of either gender were included if not stated otherwise. All procedures were performed in accordance with the *German Law on the Protection of Animals* and the *Guide for Care and Use of Laboratory Animals*[245], and were approved by the government of lower Franconia, Germany (approval number: 55.2 DMS-2532-2-109).

6.3 Instruments

Table 17 | Instruments

Instrument name	Manufacturer
Perfusor® VI	B.Braun
Tissue embedding system, TP1020	Leica Biosystems
Paraffin pouring station, 2080/K	BAVIMED
Microtome SM2010 R	Leica Biosystems
Cryostat CM3050S	Leica Biosystems
Inverted fluorescence microscope	Leica Biosystems
BZ-9000 fluorescence microscope - Plan Apo 4x/0.2 - Plan Apo 10x/0.45 - Plan Apo 20x/0.75 - Plan Apo 40x/0.95	KEYENCE (Nikon objectives)
Axioscope 2 mot *plus* - Plan-NEOFLUAR 5x/0.15 - Plan-NEOFLUAR 10x/0.30 - Plan-APOCHROMAT 20x/0.8	Zeiss (Zeiss objectives)
A1R+ confocal microscope	Nikon
FACSCanto™ II	BD Biosystems
FACSAria™ III	BD Biosystems
Veriti™ 96-well thermal cycler	Applied Biosystems
Nanodrop 2000c spectrophotometer	Thermo Scientific
StepOnePlus™ real-time PCR system	Applied Biosystems
Cellspin® II cytocentrifuge	Tharmac

6.4 Software

Statistics were performed using GraphPad Prism version 6.01 for Windows, GraphPad Software, La Jolla California USA, www.graphpad.com. Flow cytometry data was analyzed using FlowJo X 10.0.7r2. Images were edited and analyzed using ImageJ version 1.49m, Wayne Rasband, National Institutes of Health, USA.

7 Methods

7.1 Cell and tissue processing for cytological and histological stainings

7.1.1 Perfusion fixation

Mice were euthanized via CO_2-asphyxiation and immediately dissected for perfusion. The abdomen and thoracic cavity were opened and the heart exposed. A section was made in the right atrium and the perfusion needle was carefully introduced into the tip of the left ventricle, while solution was already flowing. The needle was secured with a hemostat. Perfusion was performed with the pressure of ~1 m liquid column above the animal and at a rate of 10 mL min^{-1}. First, blood was flushed out with PBS at 20 - 25 °C until the liver had lost its reddish color, usually for 1 - 2 mins. Then, the solution was changed to 4 % (w/v) paraformaldehyde in PBS (pH = 7.4) at 20 - 25 °C and perfusion was continued for 15 min. Before the brain was removed, perfused mice were chilled on ice for 2 h to allow formaldehyde crosslinking and therefore preserve tissue integrity during dissection.

7.1.2 Paraffin embedding

Fresh or perfusion-fixed tissue was immersed in 4 % (w/v) paraformaldehyde in PBS (pH = 7.4) and incubated overnight at 4 °C with mild movement. Following 4 consecutive washes in PBS for 30 minutes at 20 - 25 °C, tissue was processed directly for paraffin embedding or stored up to

several days in PBS at 4 °C. Samples were washed twice in 70 % (v/v) ethanol at 20 - 25 °C with mild movement, before they were further dehydrated via consecutive incubations in ethanol/xylene (20 - 25 °C) and eventually embedded in molten paraffin wax using the TP1020 embedding carousel from Leica Biosystems (Tab. 18).

Table 18 | Procedure to dehydrate and paraffinize tissues.

Solution	Incubation [min]
70 % (v/v) ethanol	30
70 % (v/v) ethanol	60
80 % (v/v) ethanol	150
80 % (v/v) ethanol	150
96 % (v/v) ethanol	150
100 % (v/v) ethanol	60
100 % (v/v) ethanol	120
100 % (v/v) ethanol	120
100 % (v/v) xylene	60
100 % (v/v) xylene	120
100 % (v/v) xylene	120
Paraffin wax	210
Paraffin wax	210

7.1.3 Embedding for cryosectioning

Fresh or perfusion-fixed tissue was immersed in 4 % (w/v) paraformaldehyde in PBS (pH = 7.4) and incubated overnight at 4 °C with mild movement. Following 4 consecutive washes in PBS for 30 minutes at 20 - 25 °C, the tissue was transferred into 10 % (w/v) sucrose in PBS and incubated for several hours at 20 - 25 °C with mild movement, until the tissue had sunk to the bottom of the tube. The solution was changed to 20 % (w/v) sucrose in PBS and incubation was continued overnight at 4 °C with mild movement. The tissue was embedded in O.C.T. compound in a mold build from copper foil and rapidly frozen in an isopentane bath, cooled by liquid nitrogen. Frozen tissues were stored at -80 °C.

7.1.4 Cytospin preparations

Cytological samples on microscope glass slides were prepared via cytospin. Cells that e.g. had been obtained via picking of individual colonies in CFU assays were resuspended in ~200 µL PBS - Ca^{2+}/Mg^{2+} and loaded into a cytofunnel assembled on a cytoslide. Cells were spun onto the slide at 30 x g and 20 - 25 °C for 10 min. For subsequent immunocytochemistry, slides were immediately immersed in ice-cold 2 % (w/v) paraformaldehyde in PBS (pH = 7.4) and incubated for 10 min at 2 - 8 °C, followed by 1 - 2 washes with PBS. For Pappenheim staining, slides were air dried overnight at 20 - 25 °C.

7.2 Immunostaining of cells and tissues

7.2.1 Immunofluorescence staining of paraffin sections

Paraffin sections were deparaffinized in xylene and gradually rehydrated via consecutive incubations in varying dilutions of ethanol in dH_2O (Tab. 19).

Table 19 | Procedure to deparaffinize and rehydrate paraffin sections for IHC-P.

Solution	Incubation [min]
100 % (v/v) xylene	10
100 % (v/v) xylene	10
100 % (v/v) ethanol	5
100 % (v/v) ethanol	5
96 % (v/v) ethanol	5
80 % (v/v) ethanol	5
70 % (v/v) ethanol	5
dH_2O	5

Buffer for demasking (10 mM sodium-citrate, pH = 6.0 or 10 mM Tris plus 1 mM EDTA, pH = 9.0) was preheated in a microwave in temperature-stable glassware. Samples were immersed in boiling buffer and incubated for 30 min at 95 °C. The setup was cooled down at 20 - 25 °C for 30 min. Samples were put beneath the tap and buffer was diluted by a constant flow of dH_2O for 5 min. Further washing was performed with 0.25 % (v/v) Triton X-100 in PBS,

three times for 5 min each. Sections were surrounded with a lipid marker and covered with PBS plus 5 % (v/v) normal goat serum to block unspecific binding for 2 h. Blocking solution was discarded by blotting the edge of the glass slide on absorbent paper and replaced with primary antibody, diluted in 1 % (v/v) normal goat serum in PBS. After incubation overnight at 4 °C, excess antibody was removed via three consecutive 5 min washes in PBS. Sections were covered with secondary antibody, diluted in PBS plus 1 % (v/v) normal goat serum, and incubated for 1 h, protected from light. This was followed by three consecutive 5 min washes in PBS in the dark. When necessary, the last two steps were repeated, while incubation was done with streptavidin- or neutravidin-conjugated fluorochromes. To counterstain nuclei, DAPI was included in the last incubation step at 1 µg mL^{-1}. Eventually, sections were mounted with coverslips and mowiol mounting solution and let solidify at 2 - 8 °C before microscopic analysis.

All washes and incubations were performed at 20 - 25 °C, if not stated otherwise. To reduce evaporation, all incubation steps were conducted in a humidified chamber. For washing steps, slides were transferred into a cuvette and placed on a shaker.

7.2.2 DAB-staining of paraffin sections

Paraffin sections were deparaffinized in xylene and gradually rehydrated via consecutive incubations in varying dilutions of ethanol in dH_2O (Tab. 20).

Table 20 | Procedure to deparaffinize and rehydrate paraffin sections for IHC-P.

Solution	Incubation [min]
100 % (v/v) xylene	10
100 % (v/v) xylene	10
100 % (v/v) ethanol	5
100 % (v/v) ethanol	5
96 % (v/v) ethanol	5
80 % (v/v) ethanol	5
70 % (v/v) ethanol	5
dH_2O	5

To block endogenous peroxidase activity, sections were incubated in 3 % (v/v) H_2O_2 in dH_2O for 10 min in the dark, followed by two consecutive 5 min washes in dH_2O. Buffer for demasking (10 mM sodium-citrate, pH = 6.0 or 10 mM Tris plus 1 mM EDTA, pH = 9.0) was preheated in a microwave in temperature-stable glassware. Samples were immersed in boiling buffer and incubated for 30 min at 95 °C. The setup was cooled down at 20 - 25 °C for 30 min. Samples were put beneath the tap and buffer was diluted by a constant flow of dH_2O for 5 min. Further washing was performed with 0.25 % (v/v) Triton X-100 in PBS, three times for 5 min each. Sections were surrounded with a lipid marker and covered with PBS plus 5 % (v/v) normal goat serum to block unspecific binding for 2 h. Blocking solution was discarded by blotting the edge of the glass slide on absorbent paper and replaced with primary antibody, diluted in PBS plus 1 % (v/v) normal goat serum. After incubation overnight at 4 °C, excess antibody was removed via three consecutive 5 min washes in PBS. Sections were covered with biotinylated secondary antibody, diluted in PBS plus 1 % (v/v) normal goat serum, and incubated for 1 h. Following three 5 min washing steps with PBS, samples were incubated with peroxidase anti-peroxidase, diluted in PBS plus 1 % (v/v) normal goat serum, for 30 min. Excess reagent was removed via three 5 min washes in PBS, before incubating sections with AB-complex for 30 min. Samples were washed twice with PBS and another two times with 0.1 M phosphate buffer for 5 min each. To develop the staining, sections were incubated in DAB staining solution for 5 - 30 min in the dark. Staining was regularly checked at a microscope and eventually stopped by transferring the samples in PBS. Following three consecutive 3 min washes in PBS and one wash in dH_2O for 1 min, sections were incubated in nuclear fast red staining solution for 2 min. Excess dye was removed by washing in dH_2O for 1 min. Samples were gradually dehydrated via consecutive incubations in ethanol/xylene (Tab. 21) and mounted with DePex and a coverslip.

Table 21 | Procedure to dehydrate sections after IHC-P.

Solution	Incubation [min]
70 % (v/v) ethanol	1
80 % (v/v) ethanol	1
96 % (v/v) ethanol	1
100 % (v/v) ethanol	3
100 % (v/v) ethanol	3
100 % (v/v) xylene	5
100 % (v/v) xylene	5

All washes and incubations were performed at 20 - 25 °C, if not stated otherwise. To reduce evaporation, all incubation steps were conducted in a humidified chamber. For washing steps, slides were transferred into a cuvette and placed on a shaker.

7.2.3 Immunofluorescence staining of frozen sections

Frozen sections were air-dried for 60 min at 20 - 25 °C and washed/permeabilized with 0.25 % (v/v) Triton X-100 in PBS for 10 min at 20 - 25 °C. Sections were surrounded with a lipid marker and covered with PBS plus 5 % (v/v) normal goat serum to block unspecific binding for 1 h at 20 - 25 °C in a humidified chamber. Blocking solution was discarded by blotting the edge of the glass slide on absorbent paper and replaced with primary antibody, diluted in PBS plus 1 % (v/v) normal goat serum. Following incubation overnight at 4 °C in a humidified chamber, excess antibody was removed via three consecutive 5 min washes in PBS at 20 - 25 °C. For washing, slides were transferred into a cuvette on a shaker. Sections were then covered with secondary antibody, diluted in PBS plus 1 % (v/v) normal goat serum, and incubated for 1 h at 20 - 25 °C in a humidified chamber, protected from light. To counterstain nuclei, DAPI was included in the antibody dilution at 1 µg mL^{-1}. This was followed by three consecutive 5 min washes in PBS at 20 - 25 °C in the dark. Eventually, sections were mounted with coverslips and mowiol mounting solution and let solidify at 2 - 8 °C before microscopic analysis.

7.2.4 Immunocytochemistry

Cells seeded on cover slips in 24-well plates were briefly washed with PBS and fixed in 0.5 mL of 2 % (w/v) paraformaldehyde in PBS (pH = 7.4) for 10 min on ice (Cytological preparations that were obtained via cytospin were handled comparably). The fixative was discarded and the cells were washed again with PBS before they were permeabilized in 0.5 mL of 0.25 % (v/v) Triton X-100 in PBS for 10 min at 20 - 25 °C. The solution was discarded and replaced by 250 µL of PBS plus 1 % (w/v) BSA per well to block unspecific binding for 30 min at 20 - 25 °C. Primary antibody was diluted in PBS plus 0.2 % (w/v) BSA and 250 µL of the dilution per well were incubated overnight at 4 °C. Excess antibody was removed via 3 consecutive 5 min washes with 0.5 mL PBS at 20 - 25 °C. This was followed by incubation with secondary antibody (250 µL per well), which had been diluted in PBS plus 0.2 % (w/v) BSA and 1 µg mL^{-1} DAPI, for 1 hour at 20 - 25 °C in the dark. Again, 3 consecutive 5 min washes were performed with 0.5 mL PBS at 20 - 25 °C, while protecting the samples from light. Eventually, the coverslip was removed from the well and mounted onto a clean glass slide with mowiol mounting solution.

7.2.5 Whole-mount immunofluorescence staining of CWFAs

CWFAs in 96-well plates were briefly washed with 200 µL PBS per well before they were fixed with 200 µL of 4 % (w/v) paraformaldehyde in PBS (pH = 7.4) for 1 h at 20 - 25 °C. The fixative was discarded and the wells washed with 200 µL PBS. Samples were stored in fresh PBS at 2 - 8 °C for up to 2 weeks. On the day of staining, the supernatant was removed and the wells were washed twice with 200 µL of 0.25 % (v/v) Triton X-100 in PBS for 15 min at 20 - 25 °C. This was followed by an incubation with 100 µL PBS plus 5 % (v/v) normal goat serum to block unspecific binding for 2 h at 20 - 25 °C. Primary antibody (anti-CD11B, 1:1000) was diluted in PBS plus 1 % (v/v) normal goat serum and 50 µL per well were incubated overnight at 4 °C. Excess antibody was removed via 3 consecutive 15 min washes with 200 µL of 0.1 % (v/v) Triton X-100 in PBS per well at 20 - 25 °C, before 50 µL of biotinylated secondary antibody (1:1000) in PBS plus 1 % (v/v) normal goat serum were added and incubated for 2 h at 20 - 25 °C. Again, 3 consecutive washes were performed with 200 µL of 0.1 % (v/v) Triton X-100 in PBS per well for 15 min at 20 - 25 °C. 50 µL of neutravidin DyLight® 550 (1:1000) and DAPI (1 µg mL^{-1}) in PBS were added per well and incubated for 2 h at 20 - 25 °C in the dark. This was followed by 3 consecutive washes with 200 µL of 0.1 % (v/v) Triton X-100 in PBS per well for 15 min at 20 - 25 °C, while protecting the samples from light. Eventually, the collagen gel at the bottom of the well was carefully detached with a needle and transferred into a drop of mowiol mounting solution on a clean glass slide. The gel was gently spread with forceps under a dissecting microscope before carefully putting on a cover slip. The samples were let solidify at 2 - 8 °C before microscopic analysis.

7.2.6 Extracellular staining for flow cytometry

For flow cytometry staining, 2 - 5 x 10^5 cells were resuspended in 50 µL of antibody-mixture, diluted in PBS - Ca^{2+}/Mg^{2+} plus 1 % (v/v) FBS, and incubated for 10 min at 2 - 8 °C in the dark. Cells were washed once with four volumes of buffer and centrifuged at 500 x g and 4 °C for 5 min. The cells were resuspended in 100-200 µL of PBS - Ca^{2+}/Mg^{2+} plus 1 % (v/v) FBS and 1 µM DAPI or 7-AAD (1:100). Cells were incubated for at least 5-10 min on ice in the dark, before analysis at a flow cytometer. In contrast to DAPI or 7-AAD, viability staining with FV450 was performed before antibody incubation. To this end, cells were washed once with protein-free PBS - Ca^{2+}/Mg^{2+}, before they were resuspended in 50 µL of FVS450 (1:1000), diluted in protein-free buffer, and incubated for 30 min on ice in the dark. After an additional washing step with four volumes of PBS - Ca^{2+}/Mg^{2+} plus 1 % (v/v) FBS, antibody staining was conducted as described.

7.3 Automated quantification of $IBA1^+$ cells in brain slices

To quantify $IBA1^+$ cells in sagittal brain slices after PLX5622 treatment (Fig. 11*b*), 10 µm paraffin sections were stained with fluorescent antibodies and acquired in total with a confocal microscope at 20x magnification. Several Z-planes were recorded for all individual images to balance unevenness of the sample, which were fused to a maximal projection. Images were stitched to create an overview image using NIS elements (Nikon). “Macro A” was used in ImageJ to automatically count $IBA1^+$ cells. Accuracy was verified by comparing the output with manually counted control samples. To determine the analyzed area in mm^2 and calculate $IBA1^+$ cell density, “non-tissue” area was measured via “Macro B” and subtracted from the total image area, measured by “Macro C”. Macros are listed on the following page.

Macro A

```
originalImage = getTitle();
selectWindow(originalImage);
run("Gamma...", "value=0.40");
run("Duplicate...", "title=new");
selectWindow("new");
run("Gaussian Blur...", "sigma=7");
setAutoThreshold("Default");
//run("Threshold...");
setThreshold(0, 45);
run("Make Binary", "thresholded remaining black");
run("Dilate");
run("Dilate");
run("Dilate");
run("Dilate");
run("Dilate");
run("Invert");
selectWindow(originalImage);
run("Subtract Background...", "rolling=500");
run("Duplicate...", "title=[bg]");
selectWindow("bg");
run("Gaussian Blur...", "sigma=10");
imageCalculator("Subtract create",
originalImage,"bg");
rename("one");
close("bg");
imageCalculator("Substract create", "one","new");
close("new");
close(originalImage);
setThreshold(50, 255);
//setThreshold(50, 255);
setOption("BlackBackground", false);
run("Convert to Mask");
rename(originalImage+"_analyzed");
run("Analyze Particles...", "size=13-70 clear
summarize");
```

Macro B

```
originalImage = getTitle();
selectWindow(originalImage);
run("Gamma...", "value=0.40");
run("Gaussian Blur...", "sigma=7");
setAutoThreshold("Default");
//run("Threshold...");
setThreshold(0, 45);
run("Make Binary", "thresholded remaining black");
run("Set Scale...", "distance=806.5 known=1
unit=mm");
run("Analyze Particles...", "size=0.0001-Infinity clear
summarize");
```

Macro C

```
originalImage = getTitle();
selectWindow(originalImage);
setAutoThreshold("Default");
//run("Threshold...");
setThreshold(0, 255);
run("Set Scale...", "distance=806.5 known=1
unit=mm");
run("Analyze Particles...", "size=0-Infinity clear
summarize");
```

7.4 Histochemical staining techniques

7.4.1 Hematoxylin and eosin staining

Sections were deparaffinized in xylene and gradually rehydrated via consecutive incubations in varying dilutions of ethanol in dH_2O (Tab. 22).

Table 22 | Procedure to deparaffinize and rehydrate paraffin sections for hematoxylin and eosin staining.

Solution	Incubation [min]
100 % (v/v) xylene	10
100 % (v/v) xylene	10
100 % (v/v) ethanol	2
100 % (v/v) ethanol	2
96 % (v/v) ethanol	2
80 % (v/v) ethanol	2
70 % (v/v) ethanol	2
dH_2O	2

Rehydrated samples were incubated in hematoxylin staining solution for 10 min at 20 - 25 °C, shortly rinsed with dH_2O and washed under running tap water for 10 min. After a brief rinse with dH_2O, sections were incubated in eosin staining solution for 10 min at 20 - 25 °C. Following a short wash in dH_2O, samples were gradually dehydrated via consecutive incubations in ethanol/xylene (Tab. 23) and mounted with DePeX and a coverslip.

Table 23 | Procedure to dehydrate sections after hematoxylin and eosin staining.

Solution	Incubation [min]
96 % (v/v) ethanol	2
100 % (v/v) ethanol	5
100 % (v/v) ethanol	5
100 % (v/v) xylene	5
100 % (v/v) xylene	5

7.4.2 Pappenheim staining of cytospin preparations

Cytological samples were air dried overnight at 20 - 25 °C on a glass slide. Samples were fixed in 100 % methanol for 10 min at 20 - 25 °C, before staining with filtered May-Grünwald solution, diluted 1:2 in Sorensen's phosphate buffer (pH = 6.95), for 7 min at 20 - 25 °C in a humidified chamber. The staining solution was drained from the slide and replaced with filtered Giemsa solution, diluted 1:7 in Sorensen's phosphate buffer (pH = 6.95). After a 10 min incubation at 20 - 25 °C in a humidified chamber, the solution was drained from the slide. Three consecutive washes were performed in Sorensen's phosphate buffer (pH = 6.95) for 10 seconds, 4 min, and 3 min. Excess solution was removed with tissue paper and the slide was dried overnight at 20 - 25 °C. Samples were mounted with DePeX and a coverslip following a brief equilibration in 100 % xylene.

7.5 Circle of Willis fragment assay (CWFA)

C57BL/6J mice at the age of 8 - 12 weeks were sacrificed via CO_2-asphyxiation. Animals were thoroughly sprayed with 70 % (v/v) ethanol before the abdomen and thoracic cavity were opened and the mice were transcardially perfused with sterile, ice-cold PBS - Ca^{2+}/Mg^{2+} at a flow rate of 10 mL min^{-1} using a perfusion pump. Perfusion was performed until the liver was completely devoid of blood, usually for 2 min. The brain was dissected and stored in sterile PBS - Ca^{2+}/Mg^{2+} on ice. Subsequently, the circle of Willis was isolated by peeling the meninges from the ventral side of the brain. They were transferred into a 30 mm dish filled with sterile, ice-cold PBS - Ca^{2+}/Mg^{2+}, where vessels were separated from the surrounding meningeal tissue using sterile scissors and forceps under a dissecting microscope. A mm^2 grid was placed beneath the dish to cut vessels into 2 - 3 mm fragments. The latter were transferred into a new dish filled with sterile Opti-MEM™ plus 0.1 U mL^{-1} penicillin G / streptomycin, on ice. Groups of 5-15

fragments were transferred under a laminar flow into 6-wells, filled with 2 mL of sterile serum-free Opti-MEM™ plus 0.1 U mL^{-1} penicillin G / streptomycin, using sterile forceps. The plate was incubated at 37 °C, 5 % CO_2, 2 % O_2 (hypoxia) for 24 - 36 h to starve the vessels of growth factors. Care was taken that every vessel was immersed in medium and did not float on the surface due to attached air bubbles. For embedding of vessel fragments, a 1 mg mL^{-1} collagen type I solution was prepared on ice by diluting the collagen stock solution in DMEM. To neutralize the acidic pH, 1 µL of 1 M NaOH was added per mL of the mixture. 50 µL of the prepared solution were pipetted into a well of a sterile 96-well flat bottom plate, while avoiding the introduction of air bubbles. The solution was distributed to only 3 - 5 wells at a time to avoid premature polymerization of the collagen. Vessels were grabbed with sterile forceps, briefly dipped in extra collagen solution, and fully immersed in the pre-distributed matrix. Correct placement of the vessel in the center of the well was assessed at an inverted microscope. Polymerization of the collagen was completed by incubation at 37 °C, 5 % CO_2 for 45 - 60 min. Eventually, 150 µL of Opti-MEM™, supplemented with 5 % (v/v) FBS, 0.1 U mL^{-1} penicillin G / streptomycin, 20 ng mL^{-1} CSF-1, 20 ng mL^{-1} IL-34, 20 ng mL^{-1} GM-CSF, and 30 ng mL^{-1} VEGF-A, was added dropwise onto the center of the well, taking care not to destroy the still fragile collagen matrix. Vessels were cultured at 37 °C, 5 % CO_2, 2 % O_2 (hypoxia). Medium was first changed on the fourth day of culture, then every second day.

7.6 Clodronate liposome treatment in the CWFA

Treatment with clodronate-loaded liposomes was implemented into the CWFA protocol. As perivascular macrophages in the CNS express the mannose-receptor (CD206)[246], mannosylated liposomes were used to further improve targeting of vessel-resident phagocytes. Incubation with liposomes was conducted during growth factor starvation in serum-free Opti-MEM™, plus

0.1 U mL^{-1} penicillin G / streptomycin. Liposomes were added to the medium at 0.5 mg clodronate mL^{-1} (1:10 dilution of the liposome stock) and the vessels were incubated for 36 h at 37 °C, 5 % CO_2, 2 % O_2 (hypoxia). To avoid sedimentation of the particles, the plate was rocked slowly during incubation. Excess liposomes were removed after treatment by transferring the fragments into 2 mL of fresh medium. Eventually, vessels were embedded in a collagen matrix and cultured as described in the CWFA protocol.

7.7 Treatment of mice with CSF-1R inhibitor

Female C57BL/6 mice at the age of 6 - 8 weeks were treated with the CSF-1R inhibitor PLX5622 (Plexxicon, Inc.) for 7 - 21 days. The inhibitor was formulated in AIN-76A standard rodent chow at concentrations of 300 - 1200 mg kg^{-1} and administered *ad libitum*.

7.8 Cell preparation from adult mouse tissues

7.8.1 Isolation of peripheral blood leukocytes

PB was collected during transcardial perfusion of CO_2-asphyxiated animals with PBS - Ca^{2+}/Mg^{2+} plus 5 U mL^{-1} heparin using a 10 mL syringe equipped with a 20 gauge needle. 1 - 2 mL of blood was drawn from the thoracic cavity while being flushed out through the opened right atrium of the heart and transferred into a 50 mL conical tube filled with 10 mL of PBS - Ca^{2+}/Mg^{2+} on ice. The cells were centrifuged at 300 x g and 4 °C for 10 min. The supernatant was discarded and the cells were resuspended in 1 mL of PBS - Ca^{2+}/Mg^{2+}, before adding 9 mL of 1x AMC buffer and mixing the sample by briefly inverting the tube. Following incubation for 5 min at 20 - 25 °C, the tube was filled up with ice-cold PBS - Ca^{2+}/Mg^{2+} and the cells were spun down at 300 x g and 4 °C for 10 min. The supernatant was discarded and the cells were resuspended in PBS - Ca^{2+}/Mg^{2+} or medium for further processing.

7.8.2 Isolation of BM cells

Mice were euthanized via CO_2-asphyxiation. Animals were thoroughly sprayed with 70 % (v/v) ethanol and the hind limbs were collected. Skin and muscle were removed under a laminar flow and femora and tibiae were cut open at the epiphysis. A 24 gauge needle fitted on a syringe was inserted into the bone cavity and the marrow was flushed out with ice-cold PBS - Ca^{2+}/Mg^{2+} onto a 70 µm cell strainer placed on top of a 50 mL conical tube. To isolate BM from the skull, bone was cut into small pieces with scissors and crushed in 10 mL of ice-cold PBS - Ca^{2+}/Mg^{2+} using mortar and pestle until it had lost its reddish color. The suspension was filtered through a 70 µm cell strainer into a 50 mL conical tube. BM cells were centrifuged at 300 x g and 4 °C for 10 min. The supernatant was discarded and the cells were resuspended in 1 mL of PBS - Ca^{2+}/Mg^{2+}, before adding 9 mL of 1x AMC buffer and mixing the sample by briefly inverting the tube. Following incubation for 5 min at 20 - 25 °C, the tube was filled up with ice-cold PBS - Ca^{2+}/Mg^{2+} and the cells were spun down at 300 x g and 4 °C for 10 min. The supernatant was discarded and the cells were resuspended in PBS - Ca^{2+}/Mg^{2+} or medium for further processing.

7.8.3 Isolation of single cells from adult brain

C57BL/6J mice at the age of 10 - 14 weeks were sacrificed via CO_2-asphyxiation. Animals were thoroughly sprayed with 70 % (v/v) ethanol and the abdomen and thoracic cavity were opened carefully. Transcardial perfusion was performed with sterile, ice-cold PBS - Ca^{2+}/Mg^{2+} plus 5 U mL^{-1} heparin at a flow rate of 10 mL min^{-1} using a perfusion pump. To this end, the right atrium was cut open and the needle was carefully inserted ~5 mm through the tip of the left ventricle, while flow was already started. Perfusion was continued until the liver was completely devoid of blood, but at least for 2 min. The brain was dissected under a laminar flow using sterile

scissors and forceps and transferred onto a 100 mm petri dish on ice, which had been filled with 2.5 mL of Medium A. The tissue was minced with two scalpels into 1 - 2 mm-thick pieces and transferred into a 15 mL conical tube using a 5 mL serological pipette. The preparation was mixed with 3 mL of 2x digestion medium and incubated for 60 min at 37 °C in a water bath. Every 15 min, the digest was thoroughly triturated 5 times using a 5 mL serological pipette. Following incubation, samples were immediately transferred on ice and filled up to 15 mL with ice-cold Medium B. Enzymes were removed via centrifugation at 300 x g and 4 °C for 10 min. To lyse residual red blood cells, the homogenate was resuspended in 1 mL of PBS - Ca^{2+}/Mg^{2+} and 3 mL of freshly diluted 1x AMC buffer were added. The suspension was mixed by inverting the tube and incubated for 5 min at 20 - 25 °C. Samples were subsequently filled up with ice-cold PBS - Ca^{2+}/Mg^{2+} and centrifuged at 300 x g and 4 °C for 10 min. The pellet was then resuspended in 10 mL of ice-cold myelin removal medium via drawing into a 10 mL serological pipette for at least ten times. Samples were spun at 700 x g and 4 °C for 10 min. The supernatant, including a dense layer of myelin and cell debris, was carefully removed. Cells were resuspended in 5 mL ice-cold Medium B and filtered through a 40 µm cell strainer, which had been equilibrated with an equal volume of buffer, into a fresh 15 mL conical tube. Following centrifugation at 300 x g and 4 °C for 10 min, the supernatant was removed completely. Cells were resuspended in 0.2 mL ice-cold Medium B or IMDM plus 2 % (v/v) FBS and stored on ice until further processing.

Animals were perfused in a clean laboratory environment. Further dissection, tissue processing, and handling of single cell suspensions were performed under a laminar flow using sterile cell culture grade plastic ware. All buffers and media were at least sterilized via filtration through a 0.22 µm filter. Centrifugation steps were carried out in a swing-rotor centrifuge. When isolating

cells from brain fractions (hippocampus / olfactory bulbs, meninges, and choroid plexus), digestion and cell processing were performed in 1.5 mL tubes and volumes were reduced accordingly (e.g. digestion: 500 µL, myelin-removal: 1 mL, filtration was omitted). Trituration in 1.5 mL tubes was conducted using 1000 µL pipette tips that had been cut ~0.5 cm beneath the top and autoclaved.

7.9 CFU assays

7.9.1 Collagen-based CFU assay

Following isolation, single cells were counted using a Neubauer hemocytometer and 0.1 % (w/v) trypan-blue in PBS and 1.1-times the final cell number per 12-well (final cell numbers: BM: 5×10^3; spleen: 1×10^5, PB, brain, liver, kidney: 2×10^5) was transferred into a 1.5 mL tube. The suspension was centrifuged at 300 x g and 4 °C for 10 min. The supernatant was removed carefully. Cells were resuspended in 530 µL of StemSpan™ SFEM, supplemented with 12.5 % (v/v) FBS, 0.125 U mL^{-1} penicillin G / streptomycin, 37.5 ng mL^{-1} mSCF, 12.5 ng mL^{-1} mTPO, 12.5 ng mL^{-1} mIL-3, 12.5 ng mL^{-1} hEPO, 12.5 ng mL^{-1} mGM-CSF, and 12.5 ng mL^{-1} mIL-34, and stored on ice. 130 µl of ice-cold rat collagen I (5 mg mL^{-1}) were drawn into a cut, sterile 200 µL pipette tip. The pipette holding the collagen was shortly laid aside. Care was taken to continue the procedure without any delay in order to avoid premature polymerization of the collagen. 3 µL of 1M NaOH were added to 530 µL of cell suspension, immediately followed by adding the prepared collagen aliquot and vigorous mixing by pipetting. As soon as the collagen smear had dissolved completely, 600 µL of the mixture were distributed onto a 12-well plate and incubated at 37 °C and 5 % CO_2 for 7 days. To reduce evaporation, plates were placed within a small chamber accompanied by an uncovered dish filled with sterile water. Eventually, plates

were placed onto a grid printed on transparent film and counted using an inverted microscope. Colonies were defined as cell clusters composed of a minimum of 30 cells.

7.9.2 Methylcellulose-based CFU assay

Complete methylcellulose media was divided into single-use aliquots of 2.4 mL in sterile 5 mL tubes using a 14 gauge needle fitted onto a 3 mL luer lock syringe and stored at -20 °C. Immediately before use, aliquots were thawed at 20 - 25 °C for about 30 min. Following their isolation, cells were resuspended in IMDM plus 2 % (v/v) FBS and counted using a Neubauer hemocytometer and 0.1 % (v/v) trypan-blue in PBS. Cell concentration (in cells mL^{-1}) was adjusted with IMDM plus 2 % (v/v) FBS so that it represented 11-times the final cell number per 6-well (final cell numbers: BM: 1 x 10^4; PB, brain: 3 x 10^5). 240 µL of the cell suspension were thoroughly mixed with an aliquot of complete methylcellulose media plus 0.1 U mL^{-1} penicillin G / streptomycin using a 14 gauge needle fitted onto a 2 mL syringe, before immediately distributing the mixture onto non-treated 6-well plates using 1 mL per well. Plates were placed within a small chamber accompanied by an uncovered dish filled with sterile water and incubated at 37 °C and 5 % CO_2 for 7-10 days. Cultures were not moved during the incubation time to not disturb forming colonies. Eventually, plates were placed onto a grid printed on transparent film and counted / graded using an inverted microscope. Colonies were defined as cell clusters composed of a minimum of 30 cells. Grading was performed based on the characteristics described in Tab. 24 and was trained in advance with BM-derived colonies, the identity of which was verified via Pappenheim staining of cytospin preparations. Verification was also done in the experimental setup whenever colony identity was unclear. Colonies from brain, PB, and BM were always graded on the same day and in an alternating fashion to ensure reliable outcomes.

Table 24 | Grading of colonies in methylcellulose-based CFU assays.

Colony type	Characteristics
Burst-forming unit-erythroid (BFU-E)	- very small, irregularly shaped cells - cell borders not discernable/appear fused - colony is composed of many clusters - red color (hemoglobin)
Colony-forming unit-granulocyte (CFU-G)	- small or medium sized, round cells - densely packed colonies with dark cores, where individual cells are not discernable
Colony-forming unit-macrophage (CFU-M)	- large, smooth, round cells - often loosely packed colonies
Colony-forming unit-granulocyte/macrophage (CFU-MG)	- mix of CFU-G and CFU-M - often larger colony sizes
Colony-forming unit-megakaryocyte (CFU-Mk)	- very large, irregularly shaped cells with protrusions - loosely packed colonies
Colony-forming unit-erythroid/megakaryocyte (CFU-E/Mk)	- mix of BFU-E and CFU-Mk
Colony-forming unit-erythroid/mix (CFU-E/mix)	- mix of ~BFU-E and Mk/M/G (not clearly distinguishable)

7.10 Staining of intravascular leukocytes and BM cells via antibody injection.

Mice were immobilized in a restrainer and the tail was carefully heated for about 1 min under an infra-red light source to induce dilation of the vasculature. Using a 30 gauge needle, 5 µg or 10 µg of anti-CD45 APC antibody (BioLegend #103112) in 100 µl of sterile PBS - Ca^{2+}/Mg^{2+} were slowly injected into the tail vein, together with 2500 U heparin kg^{-1} body weight. Correct placement of the needle was checked via mild aspiration. Following a circulation time of 5 or 60 minutes, mice were euthanized via CO_2-asphyxiation. Each injected mouse was checked for sufficient staining of blood leukocytes (> 90 % positive cells) or skull BM cells (> 60 % positive cells). Insufficiently labeled animals were excluded from the experiment.

7.11 Cell sorting

To obtain enough cells for cell sorting, brain cells of 5-6 mice were pooled per experiment. Cells were mixed with antibodies diluted in sorting medium and stained at a cell concentration of 10^7 cells mL^{-1} for 10 min at 2 - 8 °C in the dark. If anti-CD16/32 was used, the cells were pre-incubated with this antibody alone for 5 min to stain / block Fc receptors. Cells were washed once with four volumes of buffer and centrifuged at 300 x g and 4 °C for 10 min. If necessary, additional incubation with streptavidin BV421 was performed for 5 min at 2 - 8 °C in the dark, followed by an extra washing step. Cells were resuspended in sorting medium plus 1 µM DAPI at about 2 - 4 x 10^6 cells mL^{-1} and transferred into sterile FACS tubes that had been incubated with 50 % (v/v) FBS in PBS overnight at 4 °C to minimize cell adherence to the plastic surface. Sorting was performed at a BD FACSAria™ III cell sorter, equipped with a 70 µm nozzle. Cells were divided into up to 4 fractions and sorted into sterile 15 mL or 2 mL tubes filled with sorting medium (5 mL or 1 mL, respectively) that had been supplemented with an extra 10 % (v/v) of FBS. After the sort, cell suspensions were filled up with sterile PBS - Ca^{2+}/Mg^{2+} and centrifuged at 300 x g and 4 °C for 10 min. Cells were resuspended in 0.1 - 0.2 mL IMDM plus 2 % (v/v) FBS. Eventually, living cells were counted in each fraction based on trypan blue exclusion using a Neubauer hemocytometer.

7.12 Molecular biology

7.12.1 RNA isolation & quality control

For RNA isolation, ~250 mg of brain tissue was snap-frozen in liquid N_2 and stored at -80 °C until further processing. The tissue was rapidly thawed and mixed with 1 mL of TRIzol reagent in a 10 mL round bottom tube before homogenizing it with a blender. The homogenate was incubated for 5 min at 20 - 25 °C. After addition of 200 µL chloroform, the tube was shaken vigorously for about 15 seconds. The mixture was incubated for 2 - 3 min at 20 - 25 °C followed by centrifugation at 12,000 x g and 4 °C for 15 min. The aqueous top layer was carefully removed and transferred into a fresh plastic tube, where 0.5 mL of isopropanol were added and the mixture was incubated for 10 min at 20 - 25 °C. After centrifugation at 12,000 x g and 4 °C for 10 min, the supernatant was discarded and the RNA pellet was resuspended in 1 mL of 75 % (v/v) ethanol. The sample was centrifuged at 7,500 x g and 4 °C for 5 min. The supernatant was discarded and the pellet was air dried for 5 - 10 min at 20 - 25 °C. RNA was resuspended in RNase-free water and incubated for 10 min at 60 °C to fully dissolve. Purity was tested at a NanoDrop spectro-photometer by measuring the absorption at 230, 260, and 280 nm (260/230 ratio = 1.8 - 2.2; 260/280 ratio = 1.8 - 2.2). RNA integrity was assessed via gel electrophoresis (see below) and visualization of 28S and 18S rRNA bands. Samples were stored at -80 °C until further use, while avoiding repeated freeze-thaw cycles.

7.12.2 cDNA synthesis

Complimentary DNA was reverse transcribed from RNA samples using the QuantiTect® reverse transcription kit while following the manufacturer's instructions. In brief, 1 µg of RNA was mixed with 7x concentrated gDNA wipeout buffer and RNase-free water to obtain a sample of 14 µL. The mix was incubated for 2 min at 42 °C and immediately chilled on ice. Next, 5µL of

5x concentrated Quantiscript RT buffer were added, along with 1 µL of RT primer mix and 1 µL of Quantiscript reverse transcriptase. The 20 µL sample was incubated for 15 min at 42 °C, followed by inactivation of the RT enzyme for 3 min at 95 °C. Samples were chilled on ice and stored at -20 °C until further use.

7.12.3 Quantitative polymerase chain reaction (qPCR)

For qPCR, 5 µL of cDNA (12.5 ng from whole brain), diluted in dH_2O, were mixed with 10 µL of 2x SsoAdvanced™ universal SYBR® green supermix and 200 nM (final conc.) forward and reverse primers, respectively. The sample was brought to a final volume of 20 µL with dH_2O and run in a qPCR thermal cycler following the protocol described in Tab. 25. Before performing relative quantifications in an experimental setting, specificity of the primers (via melting curve and gel electrophoresis of PCR products), amplification of genomic DNA (via -RT controls), as well as primer efficiency (= 90 - 110 %) and dynamic range (via a serial dilution of cDNA) of the experiment were tested. Negative controls without cDNA template were included in every run and for all primer pairs. Melting curve analysis was performed as a standard quality control procedure.

Table 25 | Protocol for quantitative polymerase chain reaction (qPCR).

Step	Temperature	Duration	Repetitions
1. Activation	95 °C	600 s	1x
2. Denaturation	95 °C	10 s	40x
3. Annealing/elongation	58 °C	25 s	
4. Melting curve	58 °C - 95 °C	0.3 °C / 15 s	1x

7.12.4 Genomic DNA preparation from ear punches

Ear punches were immersed in 100 µL lysis buffer for genotyping and incubated for 50 min at 90 °C with shaking. 100 µL of 40 mM Tris-HCl were added and the sample was centrifuged at 250 x g and 20 - 25 °C for 5 minutes. Eventually, 0.5 - 2 µL of the cleared supernatant were used in a standard PCR.

7.12.5 Genomic DNA preparation from cell colonies

Individual colonies were cut from collagen-based CFU assays under a dissecting microscope and transferred into a 0.25 mL reaction tube, before adding 10 µL of lysis buffer for genotyping. Samples were briefly spun down and incubated in a thermal cycler at 90 °C for 30 min with heated lid (105 °C). Next, 10 µL of 40 mM Tris-HCl were added and the tube was centrifuged at 10,000 x g and 20 - 25 °C for 5 min. Eventually, 2 µL of the cleared supernatant were used in a standard PCR.

7.12.6 Polymerase chain reaction (PCR)

For PCR, 0.5 - 2 µL of genomic DNA isolated from ear punches, colony lysates, or cDNA (25 - 100 ng) were mixed with 12.5 µL of 2x red master mix, 1 mM (final conc.) $MgCl_2$, and 200 nM (final conc.) of forward and reverse primers, respectively. The sample was brought to a final volume of 25 µL with dH_2O and run in a thermal cycler following the protocol described in Tab. 26.

Table 26 | Protocol for standard polymerase chain reaction (PCR).

Step	Temperature	Duration	Repetitions
1. Denaturation	95 °C	30 s	35x
2. Annealing	59 °C	30 s	
3. Elongation	72 °C	30 s	

7.12.7 DNA/RNA gel electrophoresis

Especially for analysis of RNA, gels were prepared fresh by boiling 1 - 1.5 % (w/v) agarose in TAE buffer until the agarose had completely dissolved. After the solution had cooled to ~50 °C, 1 µL Midori Green was added per 50 mL of volume. The solution was transferred into a thoroughly cleaned running chamber and was allowed to gel completely at 20 - 25 °C. For electrophoresis, the gel was immersed in fresh TAE buffer. 1 µg RNA was mixed with 2x RNA Gel Loading Dye for integrity testing. PCR products that had been generated in red master mix were analyzed directly, while products from qPCR were mixed with 6x loading dye. Gel electrophoresis of DNA samples was performed for about 45 minutes at 20 - 25 °C and 10 V cm^{-1}. RNA samples were run at lower voltage (3.5 V cm^{-1}) for 2 h at 4 °C. Bands were visualized under UV light and compared to 100 bp or 1 kb marker sets.

7.13 Experimental design and statistics

Controls were always performed in parallel to all experimental approaches. In addition to treatment controls, these included positive controls (if applicable) and reagent controls for ICC/IHC, as well as unstained, isotype, FMO, and compensation controls for flow cytometry. Apart from preliminary or supplementary analyses, at least two independent runs were conducted per experiment. As the same investigator performed dissections, cultures, and analysis of CWFAs and CFU assays, blinding was not applicable. To quantify $IBA1^+$ cells in brain sections after PLX5622 treatment, automated counting with ImageJ was applied, making blinding unnecessary.

Following the GrapPad statistics guide (https://www.graphpad.com/guides/prism/6/statistics/index.htm) , experiments with low sample size per group ($n < 7$) were neither tested for Gaussian distribution nor analyzed via nonparametric tests, as both operations have insufficient power at low n size, rendering them unfeasible in these situations. Instead, in these cases, data was assumed to be normally distributed and analyzed with Student's *t*-tests or ANOVAs. When comparing groups with $n > 7$, the compliance to a Gaussian distribution was tested using the D'Agostino & Pearson omnibus normality test, before analyzing parametric data with Student's *t*-tests or ANOVAs and nonparametric data with Mann-Whitney or Kruskal-Wallis tests. P values below 0.05 were considered statistically significant. All results are given as mean ± standard deviation (SD).

8 Bibliography

1. Alberts, B. *et al. Molecular Biology of The Cell. Biochemistry and Molecular Biology* (Garland Science, 2015).

2. Dzierzak, E. & Bigas, A. Blood Development: Hematopoietic Stem Cell Dependence and Independence. *Cell Stem Cell* **22,** 639–651 (2018).

3. Asada, N., Takeishi, S. & Frenette, P. S. Complexity of bone marrow hematopoietic stem cell niche. *International Journal of Hematology* **106,** 45–54 (2017).

4. Crane, G. M., Jeffery, E. & Morrison, S. J. Adult haematopoietic stem cell niches. *Nat. Rev. Immunol.* **17,** 573–590 (2017).

5. Schofield, R. The relationship between the spleen colony-forming cell and the haemopoietic stem cell. *Blood Cells* **4,** 7–25 (1978).

6. Mitroulis, I. *et al.* Modulation of Myelopoiesis Progenitors Is an Integral Component of Trained Immunity. *Cell* **172,** 147–161.e12 (2018).

7. Kaufmann, E. *et al.* BCG Educates Hematopoietic Stem Cells to Generate Protective Innate Immunity against Tuberculosis. *Cell* **172,** 176–190.e19 (2018).

8. Weissman, I. L., Anderson, D. J. & Gage, F. Stem and Progenitor Cells: Origins, Phenotypes, Lineage Commitments, and Transdifferentiations. *Annu. Rev. Cell Dev. Biol.* **17,** 387–403 (2001).

9. Kondo, M., Weissman, I. L. & Akashi, K. Identification of clonogenic common lymphoid progenitor in mouse bone marrow. *Cell* **91,** 661–672 (1997).

10. Akashi, K., Traver, D., Miyamoto, T. & Weissman, I. L. A clonogenic common myeloid progenitor that gives rise to all myeloid lineages. *Nature* **404,** 193–197 (2000).

11. Busch, K. *et al.* Fundamental properties of unperturbed haematopoiesis from stem cells in vivo. *Nature* **518,** 542–546 (2015).

12. Graef, P. *et al.* Serial Transfer of Single-Cell-Derived Immunocompetence Reveals Stemness of CD8+Central Memory T Cells. *Immunity* **41,** 116–126 (2014).

13. Gattinoni, L. *et al.* A human memory T cell subset with stem cell-like properties. *Nat. Med.* **17,** 1290–1297 (2011).

14. Rieger, M. a, Hoppe, P. S., Smejkal, B. M., Eitelhuber, A. C. & Schroeder, T. Hematopoietic Cytokines Can Instruct Lineage Choice. *Science (80-.).* **325,** 217–218 (2009).

15. Fogg, D. *et al.* A Clonogenic Bone Marrow Progenitor Specific for Macrophages and Dendritic Cells. *Science (80-.).* **311,** 83–87 (2006).

16. Mayle, A., Luo, M., Jeong, M. & Goodell, M. A. Mouse Hematopoietic Stem Cell Identification And Analysis. *Cytometry* **83,** 27–37 (2013).

17. Yang, L. *et al.* Identification of Lin-Sca1+kit+CD34+Flt3- short-term hematopoietic stem cells capable of rapidly reconstituting and rescuing myeloablated transplant recipients. *Blood* **105,** 2717–2724 (2005).

18. Yamane, T. Mouse Yolk Sac Hematopoiesis. *Front. Cell Dev. Biol.* **6,** 1–8 (2018).

19. Tober, J. *et al.* The megakaryocyte lineage originates from hemangioblast precursors and is an integral component both of primitive and of definitive hematopoiesis. *Blood* **109,** 1433–1441 (2007).

20. Palis, J., Robertson, S., Kennedy, M., Wall, C. & Keller, G. Development of erythroid and myeloid progenitors in the yolk sac and embryo proper of the mouse. *Development* **126,** 5073–5084 (1999).

21. Takahashi, K., Yamamura, F. & Naito, M. Differentiation, maturation, and proliferation of macrophages in the mouse yolk sac: A light-microscopic, enzyme-cytochemical, immunohistochemical, and ultrastructural study. *J. Leukoc. Biol.* **45,** 87–96 (1989).

22. Ginhoux, F. & Guilliams, M. Tissue-Resident Macrophage Ontogeny and Homeostasis. *Immunity* **44,** 439–449 (2016).

23. Ferkowicz, M. J. *et al.* CD41 expression defines the onset of primitive and definitive hematopoiesis in the murine embryo. *Development* **130,** 4393–4403 (2003).

24. Yamane, T., Hosen, N., Yamazaki, H. & Weissman, I. L. Expression of AA4.1 marks lymphohematopoietic progenitors in early mouse development. *Proc. Natl. Acad. Sci.* **106,** 8953–8958 (2009).

25. Yoshimoto, M. *et al.* Embryonic day 9 yolk sac and intra-embryonic hemogenic endothelium independently generate a B-1 and marginal zone progenitor lacking B-2 potential. *Proc. Natl. Acad. Sci. U. S. A.* **108,** 1468–1473 (2011).

26. Kierdorf, K. *et al.* Microglia emerge from erythromyeloid precursors via Pu.1- and Irf8-dependent pathways. *Nat. Neurosci.* **16,** 273–80 (2013).

27. Perdiguero, E. G. *et al.* Tissue-resident macrophages originate from yolk-sac-derived erythro-myeloid progenitors. *Nature* **518,** 547–551 (2015).

28. Hoeffel, G. *et al.* C-myb(+) erythro-myeloid progenitor-derived fetal monocytes give rise to adult tissue-resident macrophages. *Immunity* **42,** 665–78 (2015).

29. McGrath, K. E. *et al.* Distinct Sources of Hematopoietic Progenitors Emerge before HSCs and Provide Functional Blood Cells in the Mammalian Embryo. *Cell Rep.* **11,** 1892–1904 (2015).

30. Jaffredo, T., Gautier, R., Eichmann, A. & Dieterlen-Lièvre, F. Intraaortic hemopoietic cells are derived from endothelial cells during ontogeny. *Development* **125,** 4575–4583 (1998).

31. Bruijn, M. F. T. R. De *et al.* Hematopoietic Stem Cells Localize to the Endothelial Cell Layer in the Midgestation Mouse Aorta. *Immunity* **16,** 673–683 (2002).

32. Zovein, A. C. *et al.* Fate Tracing Reveals the Endothelial Origin of Hematopoietic Stem Cells. *Cell Stem Cell* **3,** 625–636 (2008).

33. Müller, A. M., Medvinsky, A., Strouboulis, J., Grosveld, F. & Dzierzak, E. Development of hematopoietic stem cell activity in the mouse embryo. *Immunity* **1,** 291–301 (1994).

34. Medvinsky, A. & Dzierzak, E. Definitive hematopoiesis is autonomously initiated by the AGM region. *Cell* **86,** 897–906 (1996).

35. Lux, C. T. *et al.* All primitive and definitive hematopoietic progenitor cells emerging before E10 in the mouse embryo are products of the yolk sac. *Blood* **111,** 3435–3438 (2008).

36. Adamo, L. *et al.* Biomechanical forces promote embryonic haematopoiesis. *Nature* **459,** 1131–5 (2009).

37. Höfer, T., Busch, K., Klapproth, K. & Rodewald, H.-R. Fate Mapping and Quantitation of Hematopoiesis In Vivo. *Annu. Rev. Immunol.* **34,** 449–478 (2016).

38. Christensen, J. L., Wright, D. E., Wagers, A. J. & Weissman, I. L. Circulation and chemotaxis of fetal hematopoietic stem cells. *PLoS Biol.* **2,** 368–377 (2004).

39. Karpova, D. & Bonig, H. Concise review : CXCR4 / CXCL12 signaling in immature hematopoiesis — lessons from pharmacological and genetic models. *Stem Cells* **33,** 2391–2399 (2015).

40. Wright, D. E. Physiological Migration of Hematopoietic Stem and Progenitor Cells. *Science (80-.).* **294,** 1933–1936 (2001).

41. Massberg, S. *et al.* Immunosurveillance by Hematopoietic Progenitor Cells Trafficking through Blood, Lymph, and Peripheral Tissues. *Cell* **131,** 994–1008 (2007).

42. Wright, D. E., Wagers, A. J., Gulati, A. P., Johnson, F. L. & Weissmann, I. L. Physiological Migration of Hematopoietic Stem and Progenitor Cells. *Science (80-.).* **294,** 1933–1936 (2001).

43. Abkowitz, J. L., Robinson, A. E., Kale, S., Long, M. W. & Chen, J. Mobilization of hematopoietic stem cells during homeostasis and after cytokine exposure. *Blood* **102,** 1249–1253 (2003).

44. Méndez-Ferrer, S., Lucas, D., Battista, M. & Frenette, P. S. Haematopoietic stem cell release is regulated by circadian oscillations. *Nature* **452,** 442–447 (2008).

45. Kollet, O. *et al.* Physiologic corticosterone oscillations regulate murine hematopoietic stem/progenitor cell proliferation and CXCL12 expression by bone marrow stromal progenitors. *Leukemia* **27,** 2006–15 (2013).

46. Casanova-Acebes, M. *et al.* Rhythmic modulation of the hematopoietic niche through neutrophil clearance. *Cell* **153,** 1025–35 (2013).

47. Gong, S. *et al.* Dynamics and correlation of serum cortisol and corticosterone under

different physiological or stressful conditions in mice. *PLoS One* **10,** e0117503 (2015).

48. McKim, D. B. *et al.* Social Stress Mobilizes Hematopoietic Stem Cells to Establish Persistent Splenic Myelopoiesis. *Cell Rep.* **25,** 2552–2562.e3 (2018).

49. Mocco, J. *et al.* SDF1-A facilitates Lin-/Sca1+ cell homing following murine experimental cerebral ischemia. *PLoS One* **9,** e85615 (2014).

50. Dutta, P. *et al.* Myocardial infarction activates CCR2+hematopoietic stem and progenitor cells. *Cell Stem Cell* **16,** 477–87 (2015).

51. Kobayashi, H., Suda, T. & Takubo, K. How hematopoietic stem/progenitors and their niche sense and respond to infectious stress. *Exp. Hematol.* **44,** 92–100 (2016).

52. Spencer, R. P. & Pearson, H. A. The Speen as a Hematological Organ. *Semin. Nucl. Med.* **5,** 95–102 (1975).

53. Cardier, J. E. & Barberá-Guillem, E. Extramedullary hematopoiesis in the adult mouse liver is associated with specific hepatic sinusoidal endothelial cells. *Hepatology* **26,** 165–175 (1997).

54. McKinney-Freeman, S. L. *et al.* Muscle-derived hematopoietic stem cells are hematopoietic in origin. *Proc. Natl. Acad. Sci.* **99,** 1341–1346 (2002).

55. Massberg, S. *et al.* Immunosurveillance by Hematopoietic Progenitor Cells Trafficking through Blood, Lymph, and Peripheral Tissues. *Cell* **131,** 994–1008 (2007).

56. Fu, J. *et al.* Human Intestinal Allografts Contain Functional Hematopoietic Stem and Progenitor Cells that Are Maintained by a Circulating Pool. *Cell Stem Cell* **24,** 227–239.e8 (2019).

57. Zlotoff, D. A. & Bhandoola, A. Hematopoietic progenitor migration to the adult thymus. *Ann. N. Y. Acad. Sci.* **1217,** 122–138 (2011).

58. Montfort, M. J., Olivares, C. R., Mulcahy, J. M. & Fleming, W. H. Adult blood vessels restore host hematopoiesis following lethal irradiation. *Exp. Hematol.* **30,** 950–956 (2002).

59. Psaltis, P. J. *et al.* Identification of a monocyte-predisposed hierarchy of hematopoietic progenitor cells in the adventitia of postnatal murine aorta. *Circulation* **125,** 592–603 (2012).

60. Ratajczak, M. Z. *et al.* Novel insight into stem cell mobilization-Plasma sphingosine-1-phosphate is a major chemoattractant that directs the egress of hematopoietic stem progenitor cells from the bone marrow and its level in peripheral blood increases during mobilization due to . *Leukemia* **24,** 976–985 (2010).

61. Golan, K. *et al.* S1P promotes murine progenitor cell egress and mobilization via S1P 1-mediated ROS signaling and SDF-1 release. *Blood* **119,** 2478–88 (2012).

62. Juarez, J. G. *et al.* Sphingosine-1-phosphate facilitates trafficking of hematopoietic stem cells and their mobilization by CXCR4 antagonists in mice. *Blood* **119,** 707–716 (2012).

63. Badami, C. D. *et al.* Hematopoietic progenitor cells mobilize to the site of injury after trauma and hemorrhagic shock in rats. *J. Trauma* **63,** 596–602 (2007).

64. Dalakas, E., Newsome, P. N., Harrison, D. J. & Plevris, J. N. Hematopoietic stem cell trafficking in liver injury. *FASEB J.* **19,** 1225–1231 (2005).

65. Kollet, O. *et al.* HGF, SDF-1, and MMP-9 are involved in stress-induced human CD34 + stem cell recruitment to the liver. *J. Clin. Invest.* **112,** 160–169 (2003).

66. Si, Y., Tsou, C. L., Croft, K. & Charo, I. F. CCR2 mediates hematopoietic stem and progenitor cell trafficking to sites of inflammation in mice. *J. Clin. Invest.* **120,** 1192–1203 (2010).

67. Nagai, Y. *et al.* Toll-like Receptors on Hematopoietic Progenitor Cells Stimulate Innate Immune System Replenishment. *Immunity* **24,** 801–812 (2006).

68. Megías, J. *et al.* Direct toll-like receptor-mediated stimulation of hematopoietic stem and progenitor cells occurs in vivo and promotes differentiation toward macrophages. *Stem Cells* **30,** 1486–1495 (2012).

69. Megías, J. *et al.* TLR2, TLR4 and Dectin-1 signalling in hematopoietic stem and progenitor cells determines the antifungal phenotype of the macrophages they produce. *Microbes Infect.* **18,** 354–363 (2016).

70. Baldridge, M. T., King, K. Y. & Goodell, M. A. Inflammatory signals regulate hematopoietic stem cells. *Trends Immunol.* **32,** 57–65 (2011).

71. Takizawa, H., Regoes, R. R., Boddupalli, C. S., Bonhoeffer, S. & Manz, M. G. Dynamic variation in cycling of hematopoietic stem cells in steady state and inflammation. *J. Exp. Med.* **208,** 273–284 (2011).

72. Allakhverdi, Z. & Delespesse, G. Hematopoietic progenitor cells are innate Th2 cytokine-producing cells. *Allergy* **67,** 4–9 (2012).

73. Mazo, I. B., Massberg, S. & von Andrian, U. H. Hematopoietic stem and progenitor cell trafficking. *Trends Immunol.* **32,** 493–503 (2011).

74. Davies, L. C., Jenkins, S. J., Allen, J. E. & Taylor, P. R. Tissue-resident macrophages. *Nat. Immunol.* **14,** 986–995 (2013).

75. Prinz, M., Erny, D. & Hagemeyer, N. Ontogeny and homeostasis of CNS myeloid cells. *Nat. Immunol.* **18,** 385–392 (2017).

76. Lawson, L. J., Perry, V. H., Dri, P. & Gordon, S. Heterogeneity in the distribution and morphology of microglia in the normal adult mouse brain. *Neuroscience* **39,** 151–170 (1990).

77. Nimmerjahn, A., Kirchhoff, F. & Helmchen, F. Resting Microglial Cells Are Highly Dynamic Surveillants of Brain Parenchyma in Vivo. *Science (80-.).* **308,** 1314–1318 (2005).

78. Hefendehl, J. K. *et al.* Homeostatic and injury-induced microglia behavior in the aging brain. *Aging Cell* **13,** 60–69 (2014).

79. Lopez-Atalaya, J. P., Askew, K. E., Sierra, A. & Gomez-Nicola, D. Development and maintenance of the brain's immune toolkit: Microglia and non-parenchymal brain macrophages. *Dev. Neurobiol.* **78,** 561–579 (2018).

80. Goldmann, T. & Prinz, M. Role of Microglia in CNS Autoimmunity. *Clin. Dev. Immunol.* **2013,** (2013).

81. Cunningham, C. L., Martinez-Cerdeno, V. & Noctor, S. C. Microglia Regulate the Number of Neural Precursor Cells in the Developing Cerebral Cortex. *J. Neurosci.* **33,** 4216–4233 (2013).

82. Squarzoni, P. *et al.* Microglia Modulate Wiring of the Embryonic Forebrain. *Cell Rep.* **8,** 1271–9 (2014).

83. Paolicelli, R. C. *et al.* Synaptic pruning by microglia is necessary for normal brain development. *Science (80-.).* **333,** 1456–8 (2011).

84. Wake, H., Moorhouse, A. J., Jinno, S., Kohsaka, S. & Nabekura, J. Resting Microglia Directly Monitor the Functional State of Synapses In Vivo and Determine the Fate of Ischemic Terminals. *J. Neurosci.* **29,** 3974- (2009).

85. Sierra, A. *et al.* Microglia shape adult hippocampal neurogenesis through apoptosis-coupled phagocytosis. *Cell Stem Cell* **7,** 48 (2010).

86. O'Loughlin, E., Madore, C., Lassmann, H. & Butovsky, O. Microglial phenotypes and functions in multiple sclerosis. *Cold Spring Harb. Perspect. Med.* **8,** 1–22 (2018).

87. Hickman, S., Izzy, S., Sen, P., Morsett, L. & El Khoury, J. Microglia in neurodegeneration. *Nat. Neurosci.* **21,** 1359–1369 (2018).

88. Roesch, S., Rapp, C., Dettling, S. & Herold-Mende, C. When immune cells turn bad—tumor-associated microglia/macrophages in glioma. *International Journal of Molecular Sciences* **19,** pii: E436 (2018).

89. Ma, Y., Wang, J., Wang, Y. & Yang, G. Y. The biphasic function of microglia in ischemic stroke. *Progress in Neurobiology* **157,** 247–272 (2017).

90. Donat, C. K., Scott, G., Gentleman, S. M. & Sastre, M. Microglial activation in traumatic brain injury. *Frontiers in Aging Neuroscience* **9,** 208 (2017).

91. Hansen, D. V., Hanson, J. E. & Sheng, M. Microglia in Alzheimer's disease. *J. Cell Biol.* **217,** 459–472 (2018).

92. Aguzzi, A. & Zhu, C. Microglia in prion diseases. *J. Clin. Invest.* **127,** 3230–3239 (2017).

93. Inoue, K. & Tsuda, M. Microglia in neuropathic pain: Cellular and molecular mechanisms and therapeutic potential. *Nat. Rev. Neurosci.* **19,** 138–152 (2018).

94. Yirmiya, R., Rimmerman, N. & Reshef, R. Depression as a Microglial Disease. *Trends Neurosci.* **38,** 637–658 (2015).

95. Tay, T. L., Savage, J. C., Hui, C. W., Bisht, K. & Tremblay, M. È. Microglia across the lifespan: from origin to function in brain development, plasticity and cognition. *J. Physiol.* **595,** 1929–1945 (2017).

96. Schulz, C. *et al.* A Lineage of Myeloid Cells independent of Myb and HSCs. *Science (80-.).* **336,** 86–90 (2012).

97. Hashimoto, D. *et al.* Tissue-resident macrophages self-maintain locally throughout adult life with minimal contribution from circulating monocytes. *Immunity* **38,** 792–804 (2013).

98. Goldmann, T. *et al.* Origin , fate and dynamics of macrophages at central nervous system interfaces. *Nat. Immunol.* **17,** 797–805 (2016).

99. Sheng, J., Ruedl, C. & Karjalainen, K. Most Tissue-Resident Macrophages Except Microglia Are Derived from Fetal Hematopoietic Stem Cells. *Immunity* **43,** 382–393 (2015).

100. Thion, M. S. & Garel, S. On place and time: microglia in embryonic and perinatal brain development. *Curr. Opin. Neurobiol.* **47,** 121–130 (2017).

101. Ginhoux, F. *et al.* Fate mapping analysis reveals that adult microglia derive from primitive macrophages. *Science* **330,** 841–5 (2010).

102. Alliot, F., Godin, I. & Pessac, B. Microglia derive from progenitors, originating from the yolk sac, and which proliferate in the brain. *Dev. Brain Res.* **117,** 145–152 (1999).

103. Ruhrberg, C. & Bautch, V. L. Neurovascular development and links to disease. *Cell. Mol. Life Sci.* **70,** 1675–1684 (2013).

104. Swinnen, N. *et al.* Complex invasion pattern of the cerebral cortex by microglial cells during development of the mouse embryo. *Glia* **61,** 150–163 (2013).

105. Daneman, R., Zhou, L., Kebede, A. A. & Barres, B. A. Pericytes are required for blood brain barrier integrity during embryogenesis. *Nature* **468,** 562–566 (2010).

106. Nikodemova, M. *et al.* Microglial numbers attain adult levels after undergoing a rapid decrease in cell number in the third postnatal week. *J. Neuroimmunol.* **278,** 280–8 (2015).

107. Askew, K. *et al.* Coupled Proliferation and Apoptosis Maintain the Rapid Turnover of Microglia in the Adult Brain. *Cell Rep.* **18,** 391–405 (2017).

108. Xu, J. *et al.* Temporal-Spatial Resolution Fate Mapping Reveals Distinct Origins for Embryonic and Adult Microglia in Zebrafish. *Dev. Cell* **34,** 632–641 (2015).

109. Ferrero, G. *et al.* Embryonic Microglia Derive from Primitive Macrophages and Are Replaced by cmyb-Dependent Definitive Microglia in Zebrafish. *Cell Rep.* **24,** 130–141 (2018).

110. Chen, S. K. *et al.* Hematopoietic origin of pathological grooming in Hoxb8 mutant mice. *Cell* **141,** 775–785 (2010).

111. De, S. *et al.* Two distinct ontogenies confer heterogeneity to mouse brain microglia. *Development* **145,** dev152306 (2018).

112. Lawson, L. J., Perry, V. H. & Gordon, S. Turnover of resident microglia in the normal adult mouse brain. *Neuroscience* **48,** 405–415 (1992).

113. Réu, P. *et al.* The Lifespan and Turnover of Microglia in the Human Brain. *Cell Rep.* **20,** 779–784 (2017).

114. Tay, T. L. *et al.* A new fate mapping system reveals context-dependent random or clonal expansion of microglia. *Nat. Neurosci.* **20,** 793–803 (2017).

115. Füger, P. *et al.* Microglia turnover with aging and in an Alzheimer's model via long-term in vivo single-cell imaging. *Nat. Neurosci.* **20,** 1371–1376 (2017).

116. Li, T. & Zhang, S. Microgliosis in the Injured Brain: Infiltrating Cells and Reactive Microglia Both Play a Role. *Neurosci.* **22,** 165–70 (2016).

117. Furth, R. V. A. N. & Cohn, Z. A. The origin an kinetics of mononuclear phagocytes. *J. Exp. Med.* **128,** 415–435 (1968).

118. Kennedy, D. W. & Abkowitz, J. L. Mature monocytic cells enter tissues and engraft. *Proc Natl Acad Sci U S A* **95,** 14944–14949 (1998).

119. Hickey, W. F. & Kimura, H. Perivascular Microglial Cells of the CNS Are Bone Marrow-Derived and Present Antigen in Vivo. *Science (80-.).* **239,** 290–292 (1986).

120. Priller, J. *et al.* Targeting gene-modified hematopoietic cells to the central nervous system : Use of green fluorescent protein uncovers microglial engraftment. *Nat. Med.* **7,** 1356–1361 (2001).

121. Bechmann, I. *et al.* Immune surveillance of mouse brain perivascular spaces by blood-borne macrophages. *Eur. J. Neurosci.* **14,** 1651–1658 (2001).

122. Hess, D. C. *et al.* Hematopoietic origin of microglial and perivascular cells in brain. *Exp. Neurol.* **186,** 134–44 (2004).

123. Simard, A. R. & Rivest, S. Bone marrow stem cells have the ability to populate the entire central nervous system into fully differentiated parenchymal microglia. *FASEB J.* **18,** 998–1000 (2004).

124. Kennedy, B. D. W. & Abkowitz, J. L. Kinetics of Central Nervous System Microglial and Macrophage Engraftment: Analysis Using a Transgenic Bone Marrow Transplantation Model. *Blood* **90,** 986–993 (1997).

125. Ajami, B., Bennett, J. L., Krieger, C., Tetzlaff, W. & Rossi, F. M. V. Local self-renewal can sustain CNS microglia maintenance and function throughout adult life. *Nat. Neurosci.* **10,** 1538–43 (2007).

126. Ajami, B., Bennett, J. L., Krieger, C., McNagny, K. M. & Rossi, F. M. V. Infiltrating monocytes trigger EAE progression, but do not contribute to the resident microglia pool. *Nat. Neurosci.* **14,** 1142–9 (2011).

127. Mildner, A. *et al.* Microglia in the adult brain arise from Ly-6ChiCCR2+ monocytes only under defined host conditions. *Nat. Neurosci.* **10,** 1544–53 (2007).

128. Serbina, N. V. & Pamer, E. G. Monocyte emigration from bone marrow during bacterial infection requires signals mediated by chemokine receptor CCR2. *Nat. Immunol.* **7,** 311–317 (2006).

129. Yoshida, Y. *et al.* X-ray irradiation induces disruption of the blood–brain barrier with localized changes in claudin-5 and activation of microglia in the mouse brain. *Neurochem. Int.* **119,** 199–206 (2018).

130. Kierdorf, K., Katzmarski, N., Haas, C. a & Prinz, M. Bone marrow cell recruitment to the brain in the absence of irradiation or parabiosis bias. *PLoS One* **8,** e58544 (2013).

131. Li, Y. Q., Chen, P., Haimovitz-Friedman, A., Reilly, R. M. & Wong, C. S. Endothelial apoptosis initiates acute blood-brain barrier disruption after ionizing radiation. *Cancer Res.* **63,** 5950–6 (2003).

132. Kaya, M. *et al.* Effects of lipopolysaccharide on the radiation-induced changes in the blood-brain barrier and the astrocytes. *Brain Res.* **1019,** 105–112 (2004).

133. Li, Y.-Q., Chen, P., Jain, V., Reilly, R. M. & Wong, C. S. Early Radiation-Induced Endothelial Cell Loss and Blood–Spinal Cord Barrier Breakdown in the Rat Spinal Cord. *Radiat. Res.* **161,** 143–52 (2004).

134. Menzel, F. *et al.* Impact of X-irradiation on microglia. *Glia* **66,** 15–33 (2018).

135. Han, W. *et al.* Cranial irradiation induces transient microglia accumulation, followed by long-lasting inflammation and loss of microglia. *Oncotarget* **7,** 82305–82323 (2016).

136. Capotondo, A. *et al.* Intracerebroventricular delivery of hematopoietic progenitors results in rapid and robust engraftment of microglia-like cells. *Sci. Adv.* **3,** e1701211 (2017).

137. Capotondo, A. *et al.* Brain conditioning is instrumental for successful microglia reconstitution following hematopoietic stem cell transplantation. *Proc. Natl. Acad. Sci.* **109,** 15018–15023 (2012).

138. Varvel, N. H. *et al.* Microglial repopulation model reveals a robust homeostatic process for replacing CNS myeloid cells. *Proc. Natl. Acad. Sci.* **109,** 18150–18155 (2012).

139. Lund, H. *et al.* Competitive repopulation of an empty microglial niche yields functionally distinct subsets of microglia-like cells. *Nat. Commun.* **9,** 4845 (2018).

140. Bennett, F. C. *et al.* A Combination of Ontogeny and CNS Environment Establishes Microglial Identity. *Neuron* **98,** 1170–1183 (2018).

141. Buttgereit, A. *et al.* Sall1 is a transcriptional regulator defining microglia identity and

function. *Nat. Immunol.* **17,** 1397–1406 (2016).

142. Bruttger, J. *et al.* Genetic Cell Ablation Reveals Clusters of Local Self-Renewing Microglia in the Mammalian Central Nervous System. *Immunity* **43,** 92–106 (2015).

143. Goldmann, T. *et al.* A new type of microglia gene targeting shows TAK1 to be pivotal in CNS autoimmune inflammation. *Nat. Neurosci.* **16,** 1618–1626 (2013).

144. Parkhurst, C. N. *et al.* Microglia promote learning-dependent synapse formation through brain-derived neurotrophic factor. *Cell* **155,** 1596–1609 (2013).

145. Huang, Y. *et al.* Repopulated microglia are solely derived from the proliferation of residual microglia after acute depletion. *Nat. Neurosci.* **21,** 530–540 (2018).

146. Fehrenbach, M. K., Tjwa, M., Bechmann, I. & Krueger, M. Decreased microglial numbers in Vav1-Cre+:dicer knock-out mice suggest a second source of microglia beyond yolk sac macrophages. *Ann. Anat. - Anat. Anzeiger* **218,** 190–198 (2018).

147. Varol, D. *et al.* Dicer Deficiency Differentially Impacts Microglia of the Developing and Adult Brain. *Immunity* **46,** 1030–1044.e8 (2017).

148. Nakagomi, T. *et al.* Brain vascular pericytes following ischemia have multipotential stem cell activity to differentiate into neural and vascular lineage cells. *Stem Cells* **33,** 1962–1974 (2015).

149. Dore-Duffy, P., Katychev, A., Wang, X. & Van Buren, E. CNS microvascular pericytes exhibit multipotential stem cell activity. *J. Cereb. Blood Flow Metab.* **26,** 613–624 (2006).

150. Özen, I. *et al.* Brain pericytes acquire a microglial phenotype after stroke. *Acta Neuropathol.* **128,** 381–396 (2014).

151. Sakuma, R. *et al.* Brain pericytes serve as microglia-generating multipotent vascular stem cells following ischemic stroke. *J. Neuroinflammation* **13,** 57 (2016).

152. Hutter-Schmid, B. & Humpel, C. Primary mouse brain pericytes isolated from transgenic Alzheimer mice spontaneously differentiate into a CD11b+ microglial-like cell type in vitro. *Exp. Gerontol.* **112,** 30–37 (2018).

153. Guimarães-Camboa, N. *et al.* Pericytes of Multiple Organs Do Not Behave as Mesenchymal Stem Cells In Vivo. *Cell Stem Cell* **20,** 345–359.e5 (2017).

154. Elmore, M. R. P. *et al.* Colony-stimulating factor 1 receptor signaling is necessary for microglia viability, unmasking a microglia progenitor cell in the adult brain. *Neuron* **82,** 380–97 (2014).

155. Waisman, A., Ginhoux, F., Greter, M. & Bruttger, J. Homeostasis of Microglia in the Adult Brain: Review of Novel Microglia Depletion Systems. *Trends Immunol.* **36,** 625–636 (2015).

156. Walker, A. S. *et al.* Nestin reporter transgene labels multiple central nervous system precursor cells. *Neural Plast.* **2010,** 894374 (2010).

157. Lendahl, U., Zimmerman, L. B. & McKay, R. D. G. CNS stem cells express a new class of intermediate filament protein. *Cell* **60,** 585–595 (1990).

158. Neradil, J. & Veselska, R. Nestin as a marker of cancer stem cells. *Cancer Sci.* **106,** 803–811 (2015).

159. Zhan, L. *et al.* Proximal recolonization by self-renewing microglia re-establishes microglial homeostasis in the adult mouse brain. *PLOS Biol.* **17,** e3000134 (2019).

160. Sieweke, M. H. & Allen, J. E. Beyond stem cells: self-renewal of differentiated macrophages. *Science* **342,** 1242974 (2013).

161. Aziz, A., Soucie, E., Sarrazin, S. & Sieweke, M. H. MafB/c-Maf Deficiency Enables Self-Renewal of Differentiated Functional Macrophages. *Science (80-.).* **326,** 867–872 (2009).

162. Tay, T. L. *et al.* A new fate mapping system reveals context-dependent random or clonal expansion of microglia. *Nat. Neurosci.* **20,** 793–803 (2017).

163. Tucker;, W. D. & Mahajan, K. Anatomy, Blood Vessels. *Treasure Island (FL): StatPearls Publishing* Available at: https://www.ncbi.nlm.nih.gov/books/NBK470401/. (Accessed: 9th February 2019)

164. Bautch, V. L. Stem cells and the vasculature. *Nat. Med.* **17,** 1437–43 (2011).

165. Psaltis, P. J. & Simari, R. D. Vascular wall progenitor cells in health and disease. *Circ. Res.* **116,** 1392–1412 (2015).

166. Zengin, E. *et al.* Vascular wall resident progenitor cells: a source for postnatal vasculogenesis. *Development* **133,** 1543–51 (2006).

167. Kramann, R. *et al.* Perivascular Gli1+ progenitors are key contributors to injury-induced organ fibrosis. *Cell Stem Cell* **16,** 51–66 (2015).

168. Kramann, R. *et al.* Adventitial MSC-like Cells Are Progenitors of Vascular Smooth Muscle Cells and Drive Vascular Calcification in Chronic Kidney Disease. *Cell Stem Cell* **19,** 628–642 (2016).

169. Majesky, M. W. *et al.* Differentiated Smooth Muscle Cells Generate a Subpopulation of Resident Vascular Progenitor Cells in the Adventitia Regulated by Klf4. *Circ. Res.* **120,** 296–311 (2017).

170. Ingram, D. A. . *et al.* Vessel wall–derived endothelial cells rapidly proliferate because they contain a complete hierarchy of endothelial progenitor cells. *Blood* **105,** 2783–2786 (2005).

171. Hu, Y. *et al.* Abundant progenitor cells in the adventitia contribute to atherosclerosis of vein grafts in ApoE-deficient mice. *J. Clin. Invest.* **113,** 1258–1265 (2004).

172. Passman, J. N. *et al.* A sonic hedgehog signaling domain in the arterial adventitia supports resident Sca1+ smooth muscle progenitor cells. *Proc. Natl. Acad. Sci.* **105,** 9349–9354 (2008).

173. Pasquinelli, G. *et al.* Thoracic Aortas from Multiorgan Donors Are Suitable for Obtaining Resident Angiogenic Mesenchymal Stromal Cells. *Stem Cells* **25,** 1627–1634 (2007).

174. Klein, D. *et al.* Vascular wall-resident CD44+ multipotent stem cells give rise to pericytes and smooth muscle cells and contribute to new vessel maturation. *PLoS One* **6,** e20540 (2011).

175. Psaltis, P. J. *et al.* Characterization of a resident population of adventitial macrophage progenitor cells in postnatal vasculature. *Circ. Res.* **115,** 364–75 (2014).

176. Zorzi, P., Aplin, A. C., Smith, K. D. & Nicosia, R. F. Technical Advance: The rat aorta contains resident mononuclear phagocytes with proliferative capacity and proangiogenic properties. *J. Leukoc. Biol.* **88,** 1051–1059 (2010).

177. Ensan, S. *et al.* Self-renewing resident arterial macrophages arise from embryonic CX3CR1+ precursors and circulating monocytes immediately after birth. *Nat. Immunol.* **17,** 159–68 (2016).

178. Nakorn, T. N., Traver, D., Weissman, I. L. & Akashi, K. Myeloerythroid-restricted progenitors are sufficient to confer radioprotection and provide the majority of day 8 CFU-S. *J. Clin. Invest.* **109,** 1579–1585 (2002).

179. Yoshida, H. *et al.* The murine mutation osteopetrosis is in the coding region of the macrophage colony stimulating factor gene. *Nature* **345,** 442–444 (1990).

180. Bjornson, C. R. Turning Brain into Blood: A Hematopoietic Fate Adopted by Adult Neural Stem Cells in Vivo. *Science (80-.).* **283,** 534–537 (1999).

181. Shih, C. C. *et al.* Identification of a candidate human neurohematopoietic stem- cell population. *Blood* **98,** 2412–2422 (2001).

182. Morshead, C. M., Benveniste, P., Iscove, N. N. & Van Der Kooy, D. Hematopoietic competence is a rare property of neural stem cells that may depend on genetic and epigenetic alterations. *Nat. Med.* **8,** 268–273 (2002).

183. Asakura, A. & Rudnicki, M. A. Side population cells from diverse adult tissues are capable of in vitro hematopoietic differentiation. *Exp. Hematol.* **30,** 1339–1345 (2002).

184. Bartlett, P. F. Pluripotential hemopoietic stem cells in adult mouse brain. *Proc. Natl. Acad. Sci. U. S. A.* **79,** 2722–5 (1982).

185. Alliot, F., Lecain, E., Grima, B. & Pessac, B. Microglial progenitors with a high proliferative potential in the embryonic and adult mouse brain. *Proc. Natl. Acad. Sci.* **88,** 1541–1545 (1991).

186. Nataf, S. *et al.* Rat Choroid Plexuses Contain Myeloid Progenitors Capable of Differentiation Toward Macrophage or Dendritic Cell Phenotypes. *Glia* **54,** 160–171 (2006).

187. Baker, M. *et al.* Use of the mouse aortic ring assay to study angiogenesis. *Nat. Protoc.* **7,** 89–104 (2011).

188. Sunderkotter, C. *et al.* Subpopulations of Mouse Blood Monocytes Differ in Maturation Stage and Inflammatory Response. *J. Immunol.* **172,** 4410–4417 (2004).

189. Bordiuk, O. L., Smith, K., Morin, P. J. & Semënov, M. V. Cell proliferation and neurogenesis in adult mouse brain. *PLoS One* **9,** e111453 (2014).

190. Göritz, C. & Frisén, J. Neural stem cells and neurogenesis in the adult. *Cell Stem Cell* **10,** 657–659 (2012).

191. Wilson, E. H., Weninger, W. & Hunter, C. A. Trafficking of immune cells in the central nervous system. *J. Clin. Invest.* **120,** 1368–1379 (2010).

192. Meeker, R. B., Williams, K., Killebrew, D. A. & Hudson, L. C. Cell trafficking through the choroid plexus. *Cell Adhes. Migr.* **6,** 390–396 (2012).

193. Anderson, K. G. *et al.* Intravascular staining for discrimination of vascular and tissue leukocytes. *Nat. Protoc.* **9,** 209–222 (2014).

194. Terashima, T. *et al.* Stem cell factor induces polarization of microglia to the neuroprotective phenotype in vitro. *Heliyon* **4,** e00837 (2018).

195. Wei, S. *et al.* Functional overlap but differential expression of CSF-1 and IL-34 in their CSF-1 receptor-mediated regulation of myeloid cells. *J. Leukoc. Biol.* **88,** 495–505 (2010).

196. Lin, H. *et al.* Discovery of a Cytokine and Its Receptor by Functional Screening of the Extracellular Proteome. *Science (80-.).* **320,** 807–811 (2008).

197. Suzumura, A., Sawada, M., Yamamoto, H. & Marunouchi, T. Effects of colony stimulating factors on isolated microglia in vitro. *J. Neuroimmunol.* **30,** 111–120 (1990).

198. Hirasawa, T. *et al.* Visualization of microglia in living tissues using Iba1-EGFP transgenic mice. *J. Neurosci. Res.* **81,** 357–62 (2005).

199. Tabrizi, M., Bornstein, G. G. & Suria, H. Biodistribution Mechanisms of Therapeutic Monoclonal Antibodies in Health and Disease. *AAPS J.* **12,** 33–43 (2010).

200. Huang, Y. *et al.* Dual extra-retinal origins of microglia in the model of retinal microglia repopulation. *Cell Discov.* **4,** 9 (2018).

201. Christensen, J. L. & Weissman, I. L. Flk-2 is a marker in hematopoietic stem cell differentiation : A simple method to isolate long-term stem cells. *Proc Natl Acad Sci U S A* **98,** 14541–14546 (2001).

202. Muzumdar, M. D., Tasic, B., Miyamichi, K., Li, L. & Luo, L. A Global Double-Fluorescent Cre Reporter Mouse. *Genesis* **45,** 418–426 (2007).

203. Elmore, M. R. P., Lee, R. J., West, B. L. & Green, K. N. Characterizing newly repopulated microglia in the adult mouse: Impacts on animal behavior, cell morphology, and neuroinflammation. *PLoS One* **10,** e0122912 (2015).

204. O'Neil, S. M. O., Witcher, K. G., Mckim, D. B. & Godbout, J. P. Forced turnover of aged

microglia induces an intermediate phenotype but does not rebalance CNS environmental cues driving priming to immune challenge. *Acta Neuropathol. Commun.* **6,** 129 (2018).

205. Hughes, P. M., Botham, M. S., Frentzel, S., Mir, A. & Perry, V. H. Expression of fractalkine (CX3CL1) and its receptor, CX3CR1, during acute and chronic inflammation in the rodent CNS. *Glia* **37,** 314–327 (2002).

206. Bennett, M. L. *et al.* New tools for studying microglia in the mouse and human CNS. *Proc Natl Acad Sci U S A* **113,** E1738-46 (2016).

207. Psaltis, P. J. & Simari, R. D. Vascular Wall Progenitor Cells in Health and Disease. *Circ. Res.* **116,** 1392–1412 (2015).

208. Droin, N. & Solary, E. CSF1R, CSF-1, and IL-34, a "ménage à trois" conserved across vertebrates. *J. Leukoc. Biol.* **87,** 745–747 (2010).

209. Kueh, H. Y., Champhekhar, A., Nutt, S. L., Elowitz, M. B. & Rothenberg, E. V. Positive feedback between PU.1 and the cell cycle controls myeloid differentiation. *Science (80-.).* **341,** 670–673 (2013).

210. Metcalf, D. The molecular control of cell division, differentiation commitment and maturation in haemopoietic cells. *Nature* **339,** 27–30 (1989).

211. De, I. *et al.* CSF1 overexpression has pleiotropic effects on microglia in vivo. *Glia* **62,** 1955–1967 (2014).

212. Wang, Y. *et al.* IL-34 is a tissue-restricted ligand of CSF1R required for the development of Langerhans cells and microglia. *Nat. Immunol.* **13,** 753–760 (2012).

213. Greter, M. *et al.* Stroma-Derived Interleukin-34 Controls the Development and Maintenance of Langerhans Cells and the Maintenance of Microglia. *Immunity* **37,** 1050–1060 (2012).

214. Erblich, B., Zhu, L., Etgen, A. M., Dobrenis, K. & Pollard, J. W. Absence of colony stimulation factor-1 receptor results in loss of microglia, disrupted brain development and olfactory deficits. *PLoS One* **6,** (2011).

215. MacVittie, T. J. & McCarthy, K. F. The Detection of In Vitro Monocyte-Macrophage Colony-forming Cells in Mouse Thymus and Lymph Nodes. *J. Cell. Physiol.* **92,** 203–207 (1977).

216. Nemzek, J. A., Bolgos, G. L., Williams, B. A. & Remick, D. G. Differences in normal values for murine white blood cell counts and other hematological parameters based on sampling site Differences in normal values for murine white blood cell counts and other hematological parameters based on sampling site. *Inflamm. Res.* **50,** 523–527 (2001).

217. Doeing, D. C., Borowicz, J. L. & Crockett, E. T. Gender dimorphism in differential peripheral blood leukocyte counts in mice using cardiac, tail, foot, and saphenous vein puncture methods. *BMC Clin. Pathol.* **3,** 3 (2003).

218. Rousseaux, J., Rousseaux-Prevost, R., Bazin, H. & Biserte, G. Tryptic cleavage of rat IgG:

A comparative study between subclasses. *Immunol. Lett.* **3,** 93–98 (1981).

219. Saunders, N. R., Ek, C. J., Habgood, M. D. & Dziegielewska, K. M. Barriers in the brain: a renaissance? *Trends Neurosci.* **31,** 279–286 (2008).

220. Mrdjen, D. *et al.* High-Dimensional Single-Cell Mapping of Central Nervous System Immune Cells Reveals Distinct Myeloid Subsets in Health, Aging, and Disease. *Immunity* **48,** 1–16 (2018).

221. Korin, B. *et al.* High-dimensional, single-cell characterization of the brain's immune compartment. *Nat. Neurosci.* **20,** 1300–1309 (2017).

222. McGrath, K. E., Fegan, K. H., Frame, J. M., Kingsley, P. D., & Palis, J. Definitive Erythro-Myeloid Progenitors (EMP) Emerge in the Yolk Sac From Hemogenic Endothelium and Share Transcriptional Regulators with Adult Hematopoiesis. *Blood* **118,** 910 (2011).

223. Yoder, M. C. & Hiatt, K. Engraftment of embryonic hematopoietic cells in conditioned newborn recipients. *Blood* **89,** 2176–83 (1997).

224. Yoder, M. C., Hiatt, K. & Mukherjee, P. In vivo repopulating hematopoietic stem cells are present in the murine yolk sac at day 9.0 postcoitus. *Proc. Natl. Acad. Sci.* **94,** 6776–6780 (1997).

225. Geissler, E. N., Ryan, M. A. & Housman, D. E. The dominant-white spotting (W) locus of the mouse encodes the c-kit proto-oncogene. *Cell* **55,** 185–192 (1988).

226. Till, J. E. & Mcculloch, E. A. A Direct Measurement of the Radiation Sensitivity of Normal Mouse Bone Marrow Cells '. *Radiat. Res.* **14,** 213–222 (1961).

227. Magli, M. C., Iscove, N. N. & Odartchenko, N. Transient nature of early haematopoietic spleen colonies. *Nature* **295,** 527–529 (1982).

228. Li, Z. *et al.* Mouse embryonic head as a site for hematopoietic stem cell development. *Cell Stem Cell* **11,** 663–675 (2012).

229. Allakhverdi, Z. *et al.* CD34+ hemopoietic progenitor cells are potent effectors of allergic inflammation. *J Allergy Clin Immunol* **123,** 472–478 (2009).

230. Mitroulis, I. *et al.* Modulation of Myelopoiesis Progenitors Is an Integral Component of Trained Immunity. *Cell* **172,** 147–161.e12 (2018).

231. Ma, Q., Ineichen, B. V., Detmar, M. & Proulx, S. T. Outflow of cerebrospinal fluid is predominantly through lymphatic vessels and is reduced in aged mice. *Nat. Commun.* **8,** (2017).

232. Raper, D., Louveau, A. & Kipnis, J. How do meningeal lymphatic vessels drain the CNS? *Trends Neurosci.* **39,** 581–586 (2016).

233. Chitu, V. *et al.* PSTPIP2 deficiency in mice causes osteopenia and increased differentiation of multipotent myeloid precursors into osteoclasts. *Blood* **120,** 3126–35 (2012).

234. Thompson, M. L. *et al.* Targeting cells of the myeloid lineage attenuates pain and disease progression in a prostate model of bone cancer. *Pain* **156,** 1692–1702 (2015).

235. Elmore, M. R. P. *et al.* Replacement of microglia in the aged brain reverses cognitive, synaptic, and neuronal deficits in mice. *Aging Cell* **17,** e12832 (2018).

236. Rice, R. A. *et al.* Microglial repopulation resolves inflammation and promotes brain recovery after injury. *Glia* **65,** 931–944 (2017).

237. Feng, X. *et al.* Colony-stimulating factor 1 receptor blockade prevents fractionated whole-brain irradiation-induced memory deficits. *J. Neuroinflammation* **13,** 215 (2016).

238. Valdearcos, M. *et al.* Microglia dictate the impact of saturated fat consumption on hypothalamic inflammation and neuronal function. *Cell Rep.* **9,** 2124–38 (2014).

239. Dai, X. M. *et al.* Targeted disruption of the mouse colony-stimulating factor 1 receptor gene results in osteopetrosis, mononuclear phagocyte deficiency, increased primitive progenitor cell frequencies, and reproductive defects. *Blood* **99,** 111–120 (2002).

240. Lawson, L. J., Perry, V. H., Dri, P. & Gordon, S. Heterogeneity in the distribution and morphology of microglia in the normal adult mouse brain. *Neuroscience* **39,** 151–170 (1990).

241. Liu, K. *et al.* In Vivo Analysis of Dendritic Cell Development and Homeostasis. *Science* **324,** 392–397 (2009).

242. Stremmel, C. *et al.* Inducible disruption of the c-myb gene allows allogeneic bone marrow transplantation without irradiation. *J. Immunol. Methods* **457,** 66–72 (2018).

243. Waskow, C. *et al.* Hematopoietic stem cell transplantation without irradiation. *Nat. Methods* **6,** 267–269 (2009).

244. Palchaudhuri, R. *et al.* Non-genotoxic conditioning for hematopoietic stem cell transplantation using a hematopoietic-cell-specific internalizing immunotoxin. *Nat. Biotechnol.* **34,** 738–45 (2016).

245. National Research Council. *Guide for the Care and Use of Laboratory Animals*. (National Academies Press, Washington, DC, 2011).

246. Galea, I. *et al.* Mannose receptor expression specifically reveals perivascular macrophages in normal, injured, and diseased mouse brain. *Glia* **49,** 375–384 (2005).

9 Acknowledgment

"Science is not only a disciple of reason but, also, one of romance and passion."

Stephen Hawking

With these words I would like to cordially thank everyone who has guided, inspired and supported me over the last years and who is passionately working in science in Würzburg and all over the world. First of all I'd like to thank my supervisors Prof. Dr. Stefanie Kürten, Prof. Dr. Rudolf Martini, Prof. Dr. Paul Lehmann, as well as Prof. Dr. Süleyman Ergün, who made it possible that I could complete this work at the Institute of Anatomy in Würzburg. I appreciate the confidence that they had in me as well as the freedom I was given to develop and pursue my own ideas. However, next to an excellent committee, a lot more people are necessary to complete such a scientific marathon. As a novice in Neuroimmunology, one needs experienced and fun colleagues such as Dr. Andrea Schampel, Dr. Marie Wunsch, Verena Schropp, and Dr. Damiano Rovituso, who know the tips and tricks and make bearable the daily struggle of experimental work. As the Kürten group moved to Erlangen in 2017, this part was seamlessly taken over by the Stem Cell Biology crowd and the legendary "lunch group", which I am very grateful for (as well as for the regular and timely mensa meal). I will not forget the kind company and excellent support of so many, who were involved in my projects and experiments in some way. First of all I would like to thank Brigitte Treffny and Alla Ganscher, but also Erna Kleinschroth, Eleonora Maier, Elke Varin, Doris Dettelbacher-Weber, Ursula Roth, Dr. Erik Henke, Berin Upcin, Tatjana Metzger, and Luisa Bell, just to name a few. I am equally grateful to Dr. Andrea Ewald, Lina Koetzner, and Franziska Veit from the FMZ animal facility, as well as Dr. Verena Pfeiffer and Dr. Heike Boemmel for the support in organizing mouse work and related bureaucracy. Likewise, the cell sorting experiments could not have been performed without the help of Christian Linden and Lisa Starick from the Institute of Immunobiology, Würzburg. I would also

like to thank the non-scientific staff of our institute, such as Roswitha Grabandt, who handled administration, Michael Christoph, who kept my computer running and introduced me to the joy of Adobe Illustrator, or Hildegard Popp, who took good care that I never slipped on a freshly wiped floor. In general, I would like to thank the whole "Anatomy family" that I could be a part of for the last 4.5 years.

I would like to thank Plexxikon Inc. (Berkeley, USA) for generously providing PLX5622 under a material transfer agreement, Prof. Dr. Bernhard Nieswandt (Institute for Experimental Biomedicine, Julius-Maximilian University, Würzburg) for sharing the GP1Bα antibody, as well as Prof. Dr. Andreas Beilhack (Medizinische Klinik und Poliklinik II & Universitäts-Kinderklinik, Julius-Maximilians-Universität, Würzburg) and Prof. Dr. Christian Schulz (Medizinische Klinik und Poliklinik I, Ludwig-Maximilians-Universität, München), who kindly provided the *Cx3cr1*$^{GFP/+}$ and *Flt3*^{Cre} x *Rosa26*$^{mT/mG}$ mice, respectively. At this point, I feel that it is appropriate to also appreciate all mice, which gave their lives for scientific advancement.

I would like to thank the members of the Graduate School of Life Sciences, especially Dr. Gabriele Blum-Oehler, for their kindness, constant support, and the opportunities that they offered in their excellent program. Due to their work, I learned a lot more than I have written down in this thesis.

Finally, I am grateful to my family and friends. Doctoral studies can be quite a challenge, and you need the right people to ground you on the way. Thank you Kathrin and Theo, the best parents I could imagine. Your support enabled me to pursue this path in the first place.

I am also grateful to my wife Irene, who went through all of this together with me (including proofreading of the thesis). I am so lucky to have you by my side.

Thank you so much.

Tobias

10 Annex

10.1 Supplementary figures

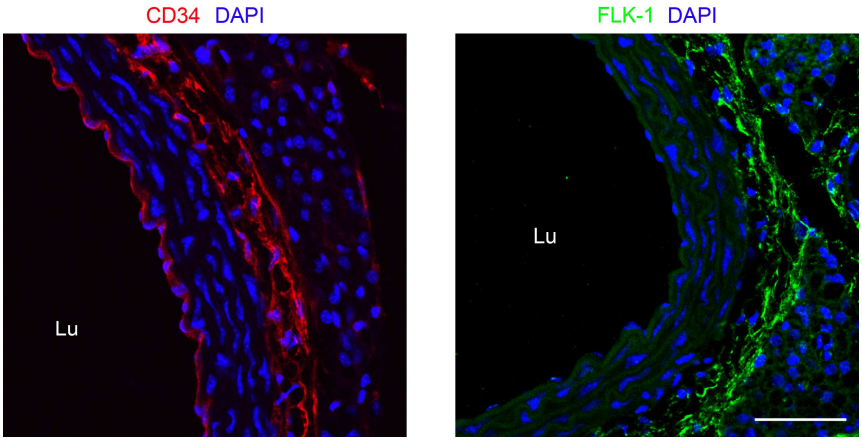

Figure S1 | Adventitial CD34 and FLK-1 staining of mouse aorta. C57BL/6 mice were sacrificed at the age of 8 weeks and 10 µm aortic cross-sections were stained via IHC-P for CD34 and FLK-1. Lu: vessel lumen. Scale bar: 50 µm

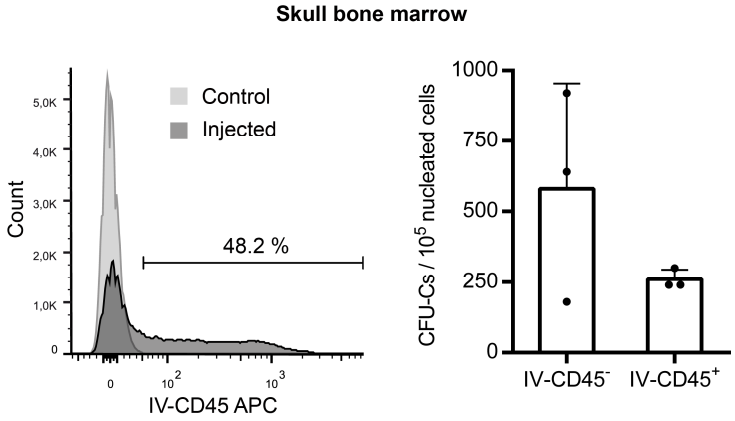

Figure S2 | BM progenitors were targeted by intravenous anti-CD45 antibody. Mice were injected i.v. with 10 µg of anti-CD45 APC antibody and sacrificed after a circulation time of 60 min. BM was prepared from the skull and sorted based on APC fluorescence. IV-CD45$^+$ and IV-CD45$^-$ cells were analyzed in collagen-based CFU assays. Results represent the means of one preliminary experiment including $n = 3$ mice. Error bars indicate SDs.

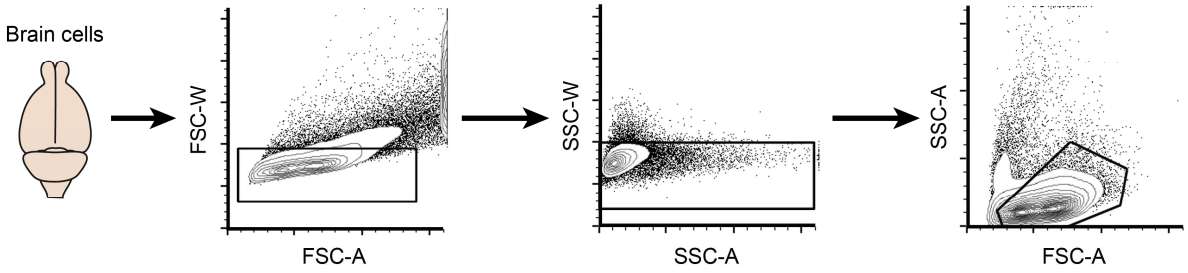

Figure S3 | Upstream gating strategy to sort brain cell suspensions. Single cells were separated from clusters and debris based on SSC/FSC characteristics. No life/dead staining was included, as viable cells were identified via trypan blue exclusion after the sort. Plots are contour plots with 5% contour levels including outliers.

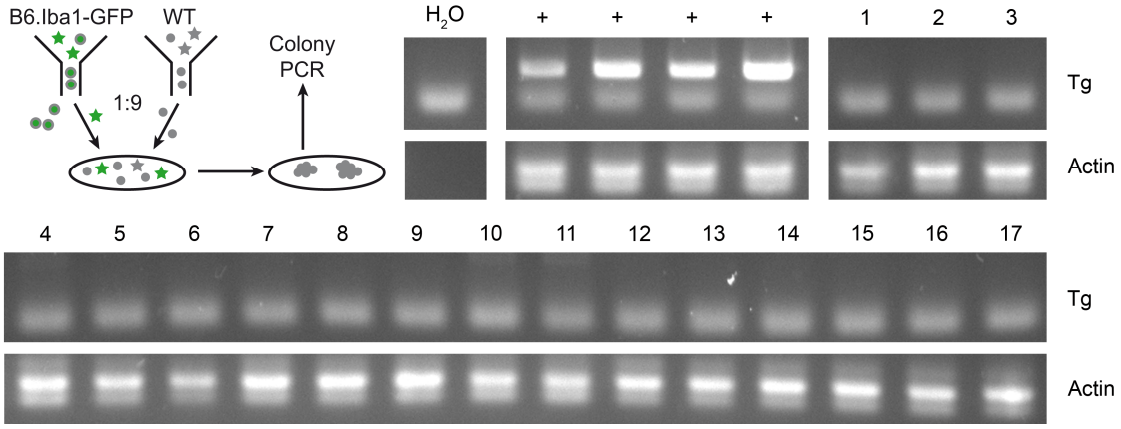

Figure S4 | CNS macrophages failed to form colonies in CFU assays even in the presence of other brain cells. 10,000 GFP^+ cells were sorted from brain homogenates of B6.Iba1-GFP mice and mixed 1:9 with pseudo-sorted WT brain cells, before analyzing the mixtures in collagen-based CFU assays. Colonies (1 - 17) were picked after 7 days of culture and examined via genomic PCR for the presence of the Iba1-GFP transgene (Tg). Colonies that arose from the GFP^- fraction of B6.Iba1-GFP brain cells were used as positive controls (+). None of the colonies that were generated in the mixed cultures were transgene-positive and therefore derived from GFP^+/*Iba1*$^+$ cells, illustrating that even in the presence of other brain cells, CNS macrophages lacked prominent clonogenicity in CFU assays. Data derived from one experiment including a total of $n = 3$ mice.

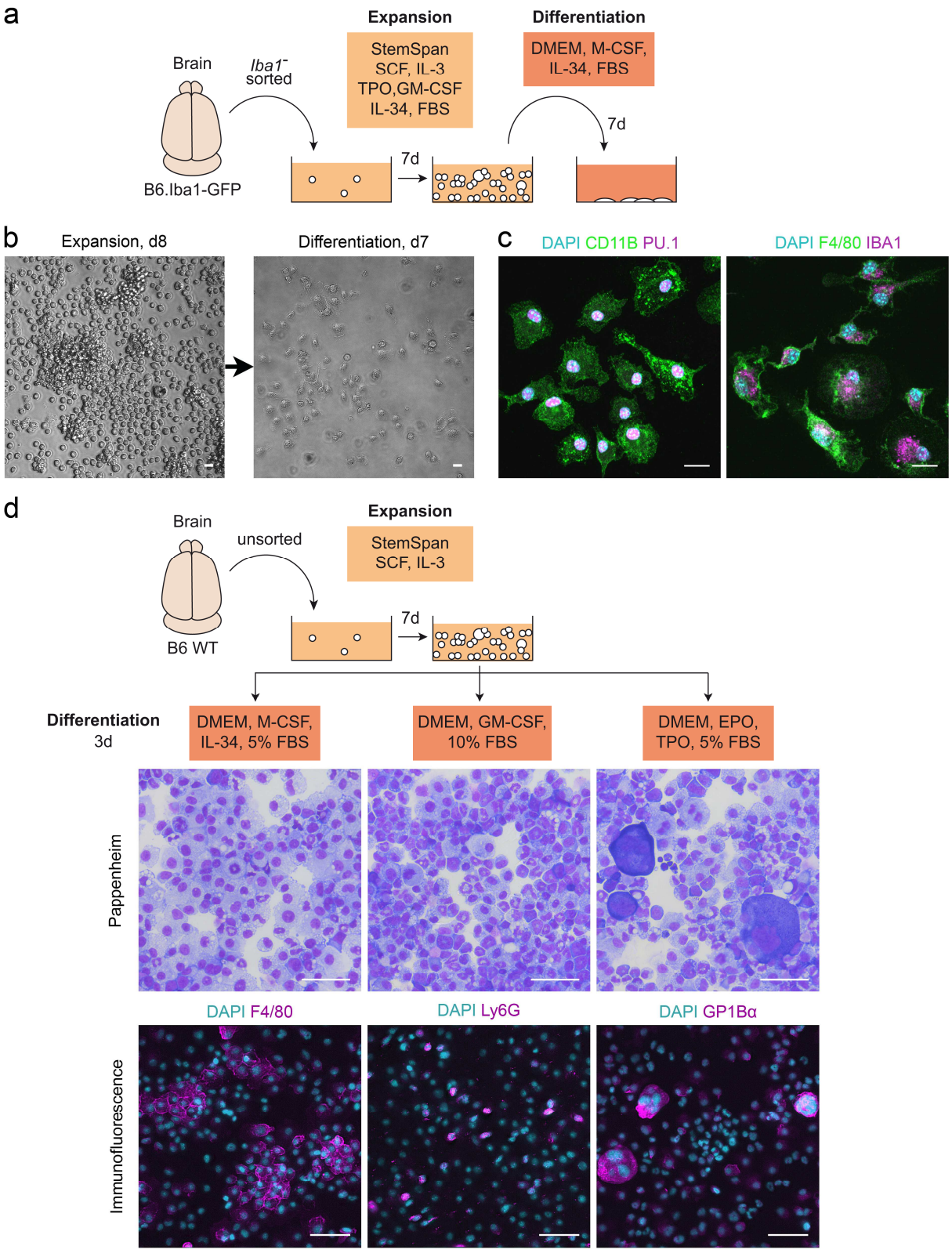

Figure S5 | Diverse myeloid cell types could be differentiated from brain suspension cultures. (**a**) Overview of the experimental procedure. GFP$^-$/*Iba1*$^-$ cells were sorted from the brains of adult

Figure S5 (continued) B6.Iba1-GFP mice and cultured in CFU assay medium without addition of collagen. After 7 days, medium was changed to DMEM plus 10 % FBS, 10 ng mL^{-1} CSF-1, 10 ng mL^{-1} IL-34 and cells were cultured for another week. (**b)** Non-adherent cells rapidly proliferated and formed free-floating clusters in expansion culture. Following medium change, cells attached to the well bottom and started to show a macrophage-like morphology. (**c**) Adherent cells stained positive for the myeloid/macrophage markers PU.1, CD11B, F4/80, and IBA1 after one week of differentiation culture. (**d**) Unsorted whole brain cells were expanded in serum-free StemSpan SFEM plus 20 ng mL^{-1} SCF and 10 ng mL^{-1} IL-3 for 7 days, followed by a short differentiation period in DMEM plus various growth factors (10 ng mL^{-1} each). Depending on the medium composition, cultures could be enriched for $F4/80^+$ monocytes/macrophages, $Ly6G^+$ neutrophils, or $GP1B\alpha^+$ megakaryocytes, which was assessed via Pappenheim and immuno-fluorescence stainings of cytospin preparations.

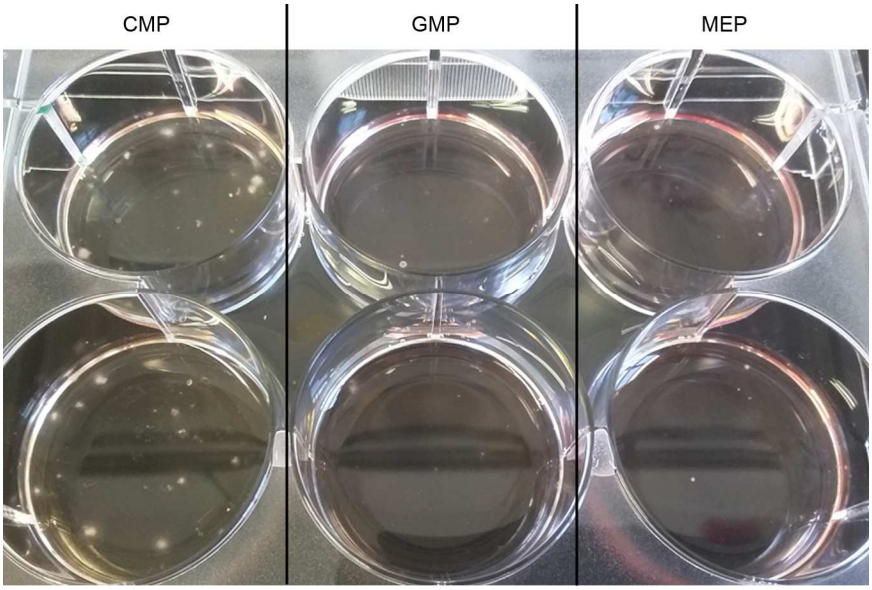

Figure S6 | CMPs frequently produced large-sized colonies in contrast to more committed progenitor fractions. BM cells were sorted into CMP, GMP, and MEP phenotypes, which were individually analyzed in methylcellulose-based CFU assays. Depicted are colonies at day 8 of culture. Although all wells contained around 100 colonies (comprising > 30 cells), many clusters in the CMP fraction were already macroscopically discernable.

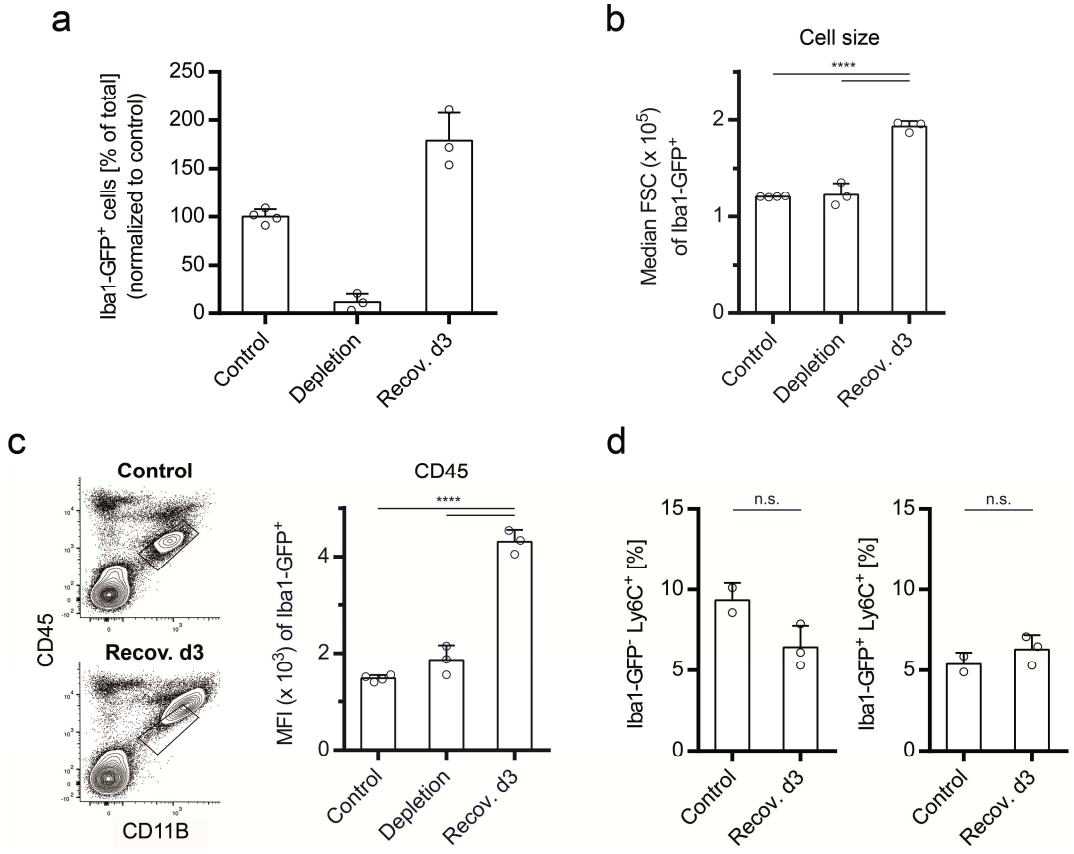

Figure S7 | Flow cytometric analysis of forced CNS macrophage repopulation. B6.Iba1-GFP mice were sacrificed following treatment with 1200 mg PLX5622 (kg chow)$^{-1}$ for 7 days (depletion) or 3 days after drug withdrawal (recov. d3). Single cell suspensions were prepared from the brains and analyzed via flow cytometry. (**a**) GFP$^+$/*Iba1*$^+$ cells were reduced by 90 % following PLX5622 treatment, but rapidly recovered within 3 days. (**b**,**c**) Repopulating GFP$^+$/*Iba1*$^+$ cells displayed increased cell size (**b**) and elevated CD45 surface expression (**c**), indicative of cellular activation. Depicted plots are contour plots with 5 % contour levels including outliers. The classical "microglia gate" (CD45^{lo} CD11B$^+$) is indicated. (**d**) The percentage of Ly6C$^+$ cells within the CD45$^+$ CD11B$^+$ myeloid population was not elevated at day 3 of recovery, arguing against infiltration of Ly6C$^+$ monocytes. Results represent the means of one experiment including a total of n = 2 - 4 mice per group/time point. Error bars indicate SDs. Statistical analyses were performed using unpaired Student's t tests or ordinary one-way ANOVAs with Tukey's multiple comparisons test. ****P < 0.0001, n.s.: non-significant, MFI: median fluorescence intensity.

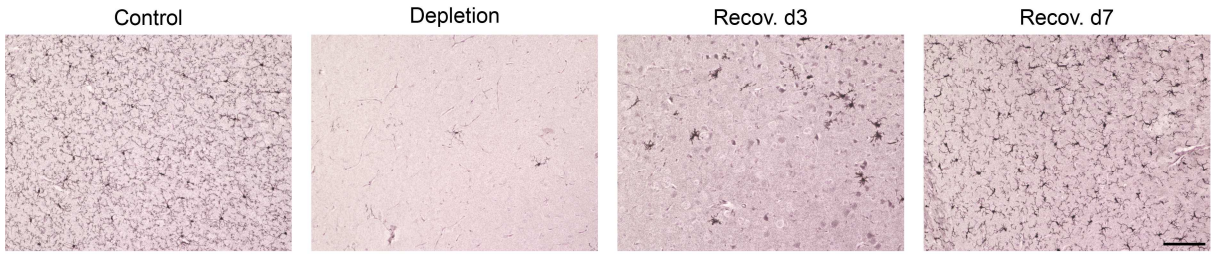

Figure S8 | Forced CNS macrophage repopulation using PLX5622 showed some degree of inter-experimental variance. Shown are representative FOVs within the neocortical region, taken from IBA1-immunostained sagittal brain sections of mice that had been fed with 1200 mg PLX5622 (kg chow)$^{-1}$ for 7 days (depletion) or had been allowed to recover (recov.) for 3 or 7 days, respectively, following withdrawal of the drug. Scale bar: 100 µm. Stainings were obtained in parallel to the qPCR data presented in Fig. 21*c* and *d*. In contrast to the analysis shown in Fig. 21*a* and *b*, repopulation occurred at a slower pace, although depletion efficiency was similar in both experiments.

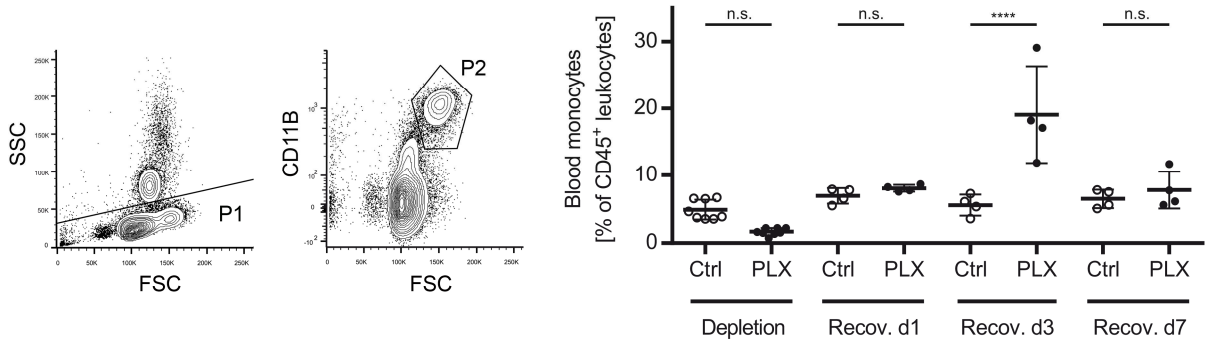

Figure S9 | The monocyte fraction expanded in blood following transient PLX5622 treatment. Mice were sacrificed after treatment with 1200 mg PLX5622 (kg chow) $^{-1}$ for 7 days (depletion) or 1, 3, and 7 days following withdrawal of the drug (recovery). Mixed PB was analyzed via flow cytometry. Blood cells were pre-gated on CD45 and monocytes were defined as the SSC^{lo} (gate P1) FSC^{hi} CD11B^{+} (gate P2) leukocyte fraction[188], as shown in the representative contour plots (5 % contour levels including outliers). Results represent the means of one experiment including n = 4 - 8 mice per group and time point. Error bars indicate SDs. Statistical analysis was performed using ordinary two-way ANOVA with Sidak's multiple comparisons test. ****P < 0.0001, n.s.: non-significant.

10.2 List of figures

Supplementary figures

10.3 List of tables

10.4 Affidavit / Eidesstattliche Erklärung

Affidavit

I herbei confirm that my thesis entitled **"The Vessel Wall and Beyond: Characterization of Myeloid Progenitors in the Adult Mouse Brain"** is the result of my own work. I did not receive any help or support from commercial consultants. All sources and / or materials applied are listed and specified in the thesis.

Furthermore, I confirm that this thesis has not yet been submitted as part of another examination process neither in identical nor in similar form.

Place, date Signature

Eidesstattliche Erklärung

Hiermit erkläre ich an Eides statt, die Dissertation **„Die Gefäßwand und darüber hinaus: Charakterisierung myeloider Vorläufer im adulten Mäusehirn"** eigenständig, d.h. insbesondere selbstständig und ohne Hilfe eines kommerziellen Promotionsberaters, angefertigt und keine anderen als die von mir angegebenen Quellen und Hilfsmittel verwendet zu haben.

Ich erkläre außerdem, dass die Dissertation weder in gleicher noch in ähnlicher Form bereits in einem anderen Prüfungsverfahren vorgelegen hat.

Ort, Datum Unterschrift

10.5 Curriculum vitae

10.6 List of publications

1. Schampel A, Volovitch O, Koeniger T, Scholz CJ, Jörg S, Linker RA, Wischmeyer E, Wunsch M, Hell JW, Ergün S, Kuerten S: “The L-type calcium channel antagonist nimodipine is neuroprotective in experimental autoimmune encephalomyelitis and induces microglia-specific apoptosis via a calcium-channel independent pathway.” (Proc Natl Acad Sci USA, 2017 114(16):E3295-E3304)

2. Bail K, Notz Q, Rovituso DM, Schampel A, Wunsch M, Koeniger T, Schropp V, Bharti R, Scholz CJ, Foerstner KU, Kleinschnitz C, Kuerten S: “Differential effects of FTY720 on the B cell compartment in a mouse model of multiple sclerosis.” (J Neuroinflammation, 2017, 14(1):148)

3. Bell L, Koeniger T, Tacke S, Kuerten S: “Characterization of blood-brain barrier integrity in a B-cell-dependent mouse model of multiple sclerosis.” (Histochemistry and Cell Biology, 2019, doi: 10.1007) [Epub ahead of print]